ROLE OF STIM IN POST EMBRYONIC DEVELOPMENT OF *DROSOPHILA MELANOGASTER*

A THESIS TO BE SUBMITTED TO

THE UNIVERSITY OF TRANS-DISCIPLINARY HEALTH SCIENCES AND TECHNOLOGY

FOR THE AWARD OF THE DEGREEOF
DOCTOR OF PHILOSOPHY

BY

MS. NANDASHREE KASTURACHARYA

UNDER THE GUIDANCE OF

PROF. GAITI HASAN

NATIONAL CENTRE FOR BIOLOGICAL SCIENCES
TATA INSTITUTE OF FUNDAMENTAL RESEARCH
BENGALURU-INDIA

JUNE 2024

THE UNIVERSITY OF TRANS-DISCIPLINARY HEALTH SCIENCES AND TECHNOLOGY

Private University Established in Karnataka by ACT 35 of 2013
BENGALURU - 560064

DECLARATION BY THE CANDIDATE

I declare that this thesis entitled "**Role of STIM in post embryonic development of *Drosophila melanogaster***" submitted for the award of Doctor of Philosophy to THE UNIVERSITY OF TRANS-DISCIPLINARY HEALTH SCIENCES AND TECHNOLOGY, Bengaluru, is my original work, conducted under the supervision of my guide Prof. Gaiti Hasan. I also wish to inform that no part of the research has been submitted for a degree or examination at any university. References, help and material obtained from other sources have been duly acknowledged

I hereby confirm the originality of the work and that there is no plagiarism in any part of the dissertation.

Place: Bengaluru

Date: 12/07/2024

Signature of the Candidate

Name of candidate: Nandashree Kasturacharya
Reg. No.: 21117020513
(November 2018)

THE UNIVERSITY OF TRANS-DISCIPLINARY HEALTH SCIENCES AND TECHNOLOGY

Private University Established in Karnataka by ACT 35 of 2013
BENGALURU - 560064

CERTIFICATE

This is to certify that the work incorporated in this thesis **"Role of STIM in post embryonic development of *Drosophila melanogaster*"** submitted by Ms. Nandashree Kasturacharya was carried out under my supervision. No part of this thesis has been submitted for a degree or examination at any university. References, help and material obtained from other sources have been duly acknowledged. I hereby confirm the originality of the work and that there is no plagiarism in any part of the dissertation.

Research Supervisor

Date: 12/7/2024

Prof. Gaiti Hasan
National Centre for Biological Sciences,
Tata Institute for Fundamental Research,
Bengaluru-India

Dadicated to

To my beloved family.....

Acknowledgement

No words can fully express the joy of achieving my dream of earning a doctorate. This success is the culmination of unwavering support from family and well-wishers at every step of journey.

I am who I am today because of the unconditional love and support from my family. The upbringing and guidance my parents provided during my younger years have been pivotal in shaping my life. I am blessed with a father who has been a constant source of support, encouraging me to dream big and pursue my passions. Meanwhile, my mother instilled in me the importance of staying realistic and grounded. I am also deeply grateful to my brother Manu, who has always been there for me whenever I needed him.

Pursuing your dreams is only possible when you have the understandable and supporting life partner and children by your side. In this, I am truly blessed to have Yoga as my life partner, and Pranav and Chiranth as my children. They've been my rock-solid support, never letting me compromise on my work and always being there for me.

My passion for research was ignited during the two years I spent working under Prof. Maneesha Inamdar at JNCASR from 2005 to 2007. Although I was quite naïve when I joined the lab, the research experience I gained there sparked a lasting enthusiasm. Moreover, this introduction to Drosophila work has made it one of my favourite models to explore.

Having immense passion and family support is invaluable, but without opportunities, they can only take you so far. For this reason, I am eternally grateful to Prof. Gaiti Hasan. When no one else was willing to give me a chance, she did. Her mentorship during my PhD extended beyond work, becoming a guiding light in my professional life. She gave me an identity for which I am forever grateful, as well as the eternal energy that brought me to her.

Constructive criticism and guidance are crucial for keeping any work on track. I would like to extend my thanks to Sunil and Arjun for agreeing to be members of my thesis committee and for ensuring that I stayed on the right path throughout the execution of my project

In the journey of a professional career, the people we meet along the way play a crucial role in helping us achieve our goals. I’m fortunate to have had

companions who made my journey worthwhile. Who I am today is the result of many people's guidance and interactions. Some were with me for a short time, others for longer, but each has had a significant impact, shaping me into a more complete person.

In Prof. Maneesha Inamdar's lab, I am especially grateful to Kavitha Siva, who exemplified what a true senior should be. The time I spent with her remains one of the most cherished and joyful periods of my life. I also extend my heartfelt thanks to Arpita, Debjani, Vaani, Ashok, Rajguru, and Shreevatsa, who made my two-year stay an unforgettable experience.

My time in Prof. Gaiti Hasan's lab has been a profound learning experience, both professionally and personally. I am especially thankful to Pragnya, Renjitha, and Dhanya, who brightened my days and were always there for both scientific and non-scientific discussions. Coffee time with Pragnya has always been memorable, and I am particularly grateful to Renjitha for encouraging me to believe in myself and pursue research. I also extend my gratitude to Dhanya (senior), Trayambak, Bipan, Siddarth, Shlesha, Steffy, Preeti Ravi, Anamika, Rishav, and Megha for their guidance with Drosophila work. A special shoutout to Rithika, Deepa, Thasneem, Raahi (my only official intern) Kavish, Mrudula, Achi, and Sameer for being fantastic young colleagues.

I extend my sincere gratitude to Prof. Vivek Jayaraman from the Janelia campus for his encouraging words and appreciation for my work. My interactions with him helped me step out of my comfort zone, for which I am truly thankful.

Collaboration and teamwork are essential factors in achieving success. Through my collaboration with Jasmine and Ashwini (from TDU), I learned the value of being a team player. I also want to thank Jasmine’s family for their assistance, which allowed me to attend the Dublin FASEB calcium meeting.

Completing any work smoothly requires financial support, and for this, I am thankful to DST-WOSA, which provided the funding that allowed me to register for my PhD. I also appreciate the Infosys travel grant for its financial support, which enabled me to attend the FASEB calcium meeting in Dublin and the Asia-Pacific Drosophila Neurobiology Conference in Tokyo. I would like to give special thanks to Deepa Agashe from the Adaptation Lab for referring me for the Infosys travel grant to attend the conference in Tokyo.

I also want to specifically thank Mr. Ravi Kumar, the Administrative Officer at TDU, for ensuring that all documentation was up to date and that we adhered to the PhD registration timelines.

Choosing to pursue my PhD at NCBS was a decision I will always value, thanks to the infrastructure that allowed me to work without any hassle. I extend my heartfelt thanks to Deepti, Hema, Yashwant and Kishore from fly facility, Sathish, Shivakumar, and everyone from Lab-Kitchen, Sharath from the travel desk, Valsala and Mayur S.P. from the academic office, Bhuvana and Teja from Dolna, the CIFF team, and all other facilities for their support.

Table of Contents

List of Figures:

List of Acronyms

AEL: After Egg Laying

BrdU: **Br**omo**d**eoxy**u**ridine

cAMP: Adenosine 3′,5′-cyclic monophosphate

CCh: Carbachol

ChAT: Choline acetyltransferase

CNS: Central Nervous System

CRAC: Calcium Release Activated Calcium

CRISPR: Clustered Regularly Interspaced Short Palindromic Repeats

CS: *Canton-S*

DA: Dopamine

DNA: Deoxyribonucleic acid

Ddc: Dopa decarboxylase

DL: Dorso Lateral

Dop1R1: Dopamine receptor 1

Dop2R2: Dopamine receptor 2

DopEcR: Dopamine/Ecdysteroid Receptor

eGFP: Enhanced Green Fluorescent Protein

ER: Endoplasmic Reticulum

FUCCI: Fluorescent Ubiquitination-based Cell Cycle Indicator

GCaMP: **G**enetically encoded **Ca**lcium binding Cal**m**odulin **P**rotein

GECI: Genetically Encoded Calcium Indicator

GMC: Ganglion Mother Cell

GPCR - G-protein Coupled Receptor

$GRAB_{DA}$: GPCR-activation-based Dopamine

HL3: Haemolymph 3

ILP: Insulin Like Peptide

InsP3: Inositol 1, 4, 5- trisphosphate

ITPR: Inositol 1, 4, 5- trisphosphate receptor

IPC: Insulin producing Cells

InR: Insulin receptor

KCl: Potassium Chloride

KO: Knock out

L-DOPA: L- 3,4-dihydroxyphenylalanine (Levodopa)

LK: Leucokinin

LNSc: Lateral Neurosecretory Cells

mCD8GFP: membrane Green Fluorescent Protein

mAChR: muscarinic Acetyl Choline Receptor

MNSc: Median Neurosecretory Cells

NB: Neuroblast

NPF: Neuropeptide F

NPY: Neuropeptide Y

RNA: Ribonucleic acid

RTK - Receptor Tyrosine Kinase

RFP: Red Fluorescence Protein

SERCA - Sarco-endoplasmic Reticulum Calcium ATPase

SEZ: Sub-Esophageal Zone

SIFa**:** Sifamide

SOCE - Store-operated Calcium Entry

sNPF: Short Neuropeptide F

STIM: Stromal Interaction Molecule

TH: Tyrosine Hydroxylase

TTX: Tetrodotoxin:

UAS: Upstream Activating Sequence

Synopsis

Calcium (Ca^{2+}), a major secondary messenger, has been shown to play a pivotal role in various phases of an organism's life cycle (Paudel et al., 2018). This is because it coordinates a diverse spectrum of cellular events in response to external signalling cues; leading to both biochemical and genetic alterations within the cell (Bagur & Hajnóczky, 2017a). The cellular internal environment exhibits robust responsiveness to fluctuations in calcium concentration, ranging from nanomolar to millimolar. The precise spatiotemporal variations in calcium concentration determine the fate of the cell (Bagur & Hajnóczky, 2017a; Clapham, 2007). Any perturbation in these events may lead to developmental defects or may even result in the lethality of the organism (Paudel et al., 2018). There are many modes of mobilization of calcium into the cytoplasm of the cells. Notably, in excitable cell types, such as neuron and muscle cells diverse proteins orchestrate distinct calcium dynamics. These includes voltage gated calcium channels, TRP channels, IP3 mediated ER calcium release and CRAC channels like the Store Operated Calcium channels (SOCs). Each one of these modes of calcium entry is highly coordinated in space, time and upstream signaling cues (Cross et al., 2010).

Store-operated calcium entry (SOCE) constitutes a specific form of calcium dynamics that takes place in response to depletion of calcium stores from the endoplasmic reticulum (ER). This depletion occurs by the activation of cell surface receptors coupled to G proteins and/or receptor Tyrosine kinases. The best studied store operated calcium channel is the calcium release activated calcium (CRAC) channel, Orai, which is activated by the ER resident calcium sensor, namely, STIM (Stromal Interaction Molecule) (Prakriya & Lewis, 2015).

SOCE has demonstrated its involvement in multiple cellular events (Prakriya & Lewis, 2015). The observation that mice carrying null mutations in either the *Orai1* or *STIM* (1and 2) genes leads to perinatal (right after the birth of the pups) lethality (Gwack et al., 2008; Oh-hora et al., 2008). This underscores the significance of SOCE not only in cell-specific functions but also in early developmental stages. However, understanding of this field is still in its nascent stages. In this context, the aim of my thesis was to comprehensively

investigate the cellular basis of SOCE in relation to the growth and development of *Drosophila melanogaster*. With STIM being a major molecular player in SOCE, I have used *dSTIM* (*Drosophila STIM*) as a molecular candidate to understand the function of SOCE in relation to early development of an organism. Here I have used the STIM null mutant (*STIM^{KO}) Drosophila melanogaster* strain, which is generated in the lab by using the CRISPR-*Cas9* gene editing technique (Pathak et al., 2017).

In-depth characterization of *STIM^{KO}* showed that even though there is a normal hatching of first-instar larvae, there is a delay of 18 h in the transition from first instar to second-instar larvae. After 72 h AEL, *STIM^{KO}* larvae exhibit retarded growth. As a result of this delay, there was inability to advance to the third instar stage. 80–86 h AEL onwards, there is a gradual decrease in the number of viable organisms. Overall, these observations suggest that cessation of *STIM^{KO}* larval growth precedes loss of viability. To figure out the underlying cause for the systemic growth arrest and loss of viability, a cell lineage assay was done to see how the cells were dividing, and a feeding assay was done to test the *STIM^{KO}* larval nutrient acquiring capacity. Cell (Neuroblast (NBs)) lineage analysis results suggested that, in *STIM^{KO}*, earlier development was normal and NBs exited from quiescence and entered the proliferative state, but subsequently, by 80–86 h, most of the neuroblasts were arrested in G2 Phase and the number of postmitotic cells decreased significantly. Since the early second instar stage is sensitive to changes in food supply, dye-laced yeast paste feeding and larval mouth hook contraction analysis were used to check the status of *STIM^{KO}* larval food intake. Both the results suggested that *STIM^{KO}* shows reduced feeding as early as 36 h AEL, and with time, acutely reduced food intake was observed. Altogether, these results suggest that consequent nutritional deficits prevent normal growth and lead to lethality (Chapter 2).

Further to understand how the loss of STIM affects the overall growth of an organism, it was important to identify the cells types which are associated for feeding and growth of an organism. To understand this, genetic screening was done. Through this, we identified a specific subset of larval dopaminergic neurons marked by *THD'GAL4*. Overexpression of the wild-type STIM gene in these neurons rescued *STIM^{KO}* larval lethality by up to 90%. To further understand how THD's neurons rescued the *STIM^{KO}*, the neuronal property of

THD’ was investigated. Characterization of dopaminergic neurons in *STIM*^{KO} showed that by 76 h AEL, these neurons are no longer able to fire or release dopamine. Lost excitability and dopamine release were rescued by overexpression of the *STIM* gene in these neurons. This suggests that STIM functions are vital in THD' neurons to maintain excitability and dopamine release for the normal growth of an organism (Chapter 3 and 4).

Since the identified cell types are neuronal in nature, it was important to identify their postsynaptic partners of THD's neurons. Optogenetic stimulation of THD’ neurons helped identify connectivity to a subset of neuropeptidergic cells, including cells that secrete insulin-like peptides, resulting in a change in the developmental profile of specific DILPs. Interestingly, overexpressing *STIM* in THD’ neurons rescued the transcriptional profiles of ilp5 and ilp3 in MNSc (ilp-producing) cells and restored them to normal levels (9). Since there was a significant upregulation of ilp3 in *STIM*^{KO}, reducing the ilp3 level partially rescued the *STIM*^{KO} larval lethality. This suggested that the ilp3 levels needs to be regulated at different phases of the development of an organism (Chapter 5).

To understand the importance of differential expression of ilp3 at different stages of development, I genetically manipulated the expression of ilp3. Knockdown of ilp3 in MNSc cells resulted in delayed pupariation, larger pupae, and overweight adults. Whereas overexpression of ilp3 showed delayed larval transition from L2 to L3 and smaller larvae. These results suggested that dopamine signals from THD’ cells are required to maintain normal expression of growth promoting ILPs (*ilp2* and *ilp5*) and repress expression of *ilp3,* which appears to function as an anti-growth signal (Chapter 6).

Overall, this work shows how the phenotypic characterization of the STIM null mutant led to the identification of a specific subset of dopaminergic neurons and the importance of STIM function in these neurons for the early development of an organism. Further, this is the first report where we have shown a functional synaptic connection between dopamine- and insulin-producing MNSc cells and ilp3 as a growth inhibitor. Also, the identification of a simple neuronal circuit where dopamine-insulin signalling regulates feeding and growth could serve as a useful model for investigating new therapeutic strategies targeted towards the

treatment of psychological disorders such as obesity and metabolic syndrome (Chapter7).

List of Publications:

1. **A STIM dependent dopamine-neuropeptide axis maintains the larval drive to feed and grow in Drosophila.**
   Nandashree Kasturacharya, Jasmine Kaur Dhall, Gaiti Hasan (https://journals.plos.org/plosgenetics/article/metrics?id=10.1371/journal.pgen.10104 35)
2. Optimized protocol for assay for transposase-accessible chromatin by sequencing (ATAC-seq) from Drosophila melanogaster brain tissue.
   Dhall JK et al., STAR Protoc. 2023 Apr 18;4(2):102153. DOI: 10.1016/j.xpro.2023.102153.

Manuscripts under preparation for following projects:

- *IP_3 receptor mediated calcium signaling shapes transcription by RNA PolII dynamics and H3K36me3 interplay*
  Authors: Jasmine Kaur Dhall, Nandashree Kasturacharya, Bharath Saravanan, Nidarshan RS, Gaiti Hasan, Dimple Notani

- *Synergism of IP_3R and parkin mutants produces oxidative stress and malfunction of flight promoting central dopaminergic neurons in Drosophila*
  Authors: Mrudula Dileep, Nandashree Kasturacharya, Anamika Sharma, Steffy B Manjila, Ashitha Bhan, Gaiti Hasan

- *Role of Brahmi as a neuroprotectant.*
  Authors: Nandashree Kasturacharya, Ashwini Thakre*, Ashwini Godbole, Gaiti Hasan*
  *Equally contributed

Chapter 1: Introduction

1.1 Role of Store Operated Ca^{2+} entry in early development of an organism

For the effective normal development, functioning, and survival of multicellular organisms, seamless coordination between individual cells, organs, and the external environment is essential (Bosch et al., 2017; Buhler et al., 2018; Fingar et al., 2002; Gilbert SF., 2000; Steinhart & Angers, 2018; Zhang & Liu, 2002). This intricate coordination hinges on a complex network of inter- and intracellular signalling mechanisms. These signalling pathways involve a diverse array of ions, small molecules, and peptides, which collectively drive cellular function in response to external cues. Molecules such as hormones and neurotransmitters that communicate between cells and organs are considered primary messengers, whereas ions and small molecule derivatives such as cAMP, Calcium, IP_3, etc. that function within the cells are considered secondary messengers (Newton et al., 2016). Among them, Calcium (Ca^{2+}), an essential divalent cation, stands out as a significant secondary messenger due to its unique chemical properties (Carafoli & Krebs, 2016; Clapham, 2007). Its pivotal role across various stages of cellular function leading to both biochemical and genetic alterations within the cell underscores its importance (Bagur & Hajnóczky, 2017; Paudel et al., 2018). Nevertheless, it's crucial to maintain suitable intracellular calcium levels because elevated concentrations can result in phosphate precipitation due to its reduced binding affinity with water, thus jeopardizing cell integrity (Clapham, 2007). In response, cells have evolved over time to compartmentalize calcium stores and developed various proteins to regulate their movement within the cell, thereby facilitating a wide range of cellular activities (Berridge et al., 2000; Carafoli & Krebs, 2016). The cellular internal environment exhibits robust responsiveness to fluctuations in Ca^{2+} concentration, ranging from nanomolar to millimolar (Berridge, 1998; Clapham, 2007; Rosenberg & Spitzer, 2011) (Fig 1.1). The precise spatiotemporal variations in calcium concentration determine the fate of the cell (Berridge et al., 2000; Clapham, 2007).

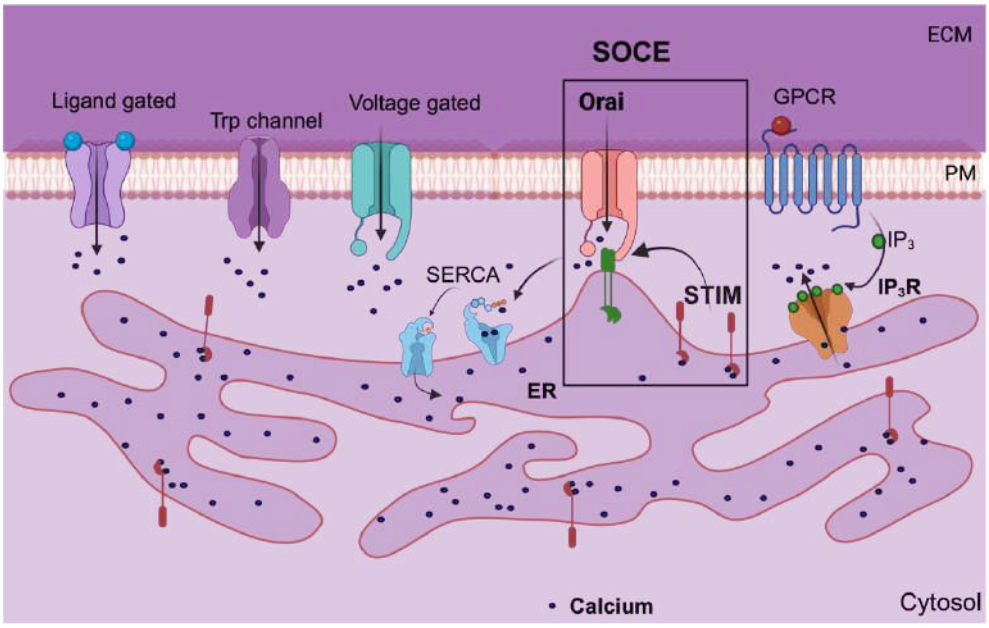

Figure 1.1: Illustration showing different modes of calcium entry and highlighting SOCE

Among multiple mode of Ca^{2+} transits, **S**tore-**O**perated **C**alcium **E**ntry (SOCE) represents a distinct mode of Ca^{2+} dynamics triggered by the depletion of calcium stores within the endoplasmic reticulum (ER), typically in response to IP_3-mediated calcium release . This depletion is initiated by the activation of cell surface receptors linked to G proteins and/or receptor tyrosine kinases, which in turn generate IP_3, a ligand for the IP_3 receptor channel (Prakriya & Lewis, 2015). Among the well-studied store-operated calcium channels is the calcium release-activated calcium (CRAC) channel, Orai (Emrich et al., 2022; Fahrner et al., 2017; Hoth & Penner, 1992; Lewis, 2001) , which is activated by the ER-resident calcium sensor, STIM (**St**romal **I**nteraction **M**olecule) (Berridge, 1998; Fahrner et al., 2017; S. L. Zhang et al., 2005). Contrary to the transient nature of calcium entry observed in voltage-gated or ligand-gated channels, SOCE channels display a distinct characteristic of sustained calcium influx lasting from minutes to hours (Prakriya & Lewis, 2015) (Fig 1.1). This enduring property of SOCE channels underscores their crucial role in modulating a range of cellular functions, including secretion, gene transcription, motility, muscle contraction, and the regulation of enzymatic activities, all of which are essential components of intricate signaling pathways (Berna-Erro et al., 2017; Gopurappilly et al., 2018; Gwack et al., 2008; Hogan et al., 2003; Mancarella et

al., 2013; Oh-hora et al., 2008; Peper & Dahl, 2015; Putney et al., 2017; Silva-Rojas et al., 2020; Somasundaram et al., 2014; Toth et al., 2016; I. Zhang & Hu, 2020).

STIM plays a crucial role in regulating SOCE across multicellular organisms, demonstrating evolutionary conservation. In invertebrates such as *Drosophila melanogaster* and *C. elegans,* there is a single isoform, while vertebrates, including mammals, possess two homologs named STIM1 and STIM2 (Prakriya & Lewis, 2015). Structurally, STIM is a transmembrane protein that spans the ER membrane. Its architecture has been thoroughly investigated, along with its capacity to precisely detect changes in ER calcium levels (S. L. Zhang et al., 2005).

Initially identified as a tumour suppressor in 1997 (Sabbioni et al., 1997), STIM's journey from its discovery to its recognized importance as a central regulator of CRAC current and its indispensable role in maintaining cellular functions has been extensively documented in numerous reviews and works (Berna-Erro et al., 2017; Berridge, 1998; Dhanya & Hasan, 2021; Mancarella et al., 2013; Maus et al., 2017b; Oh-hora et al., 2008; Peper & Dahl, 2015; Richhariya et al., 2017; Rosenberg & Spitzer, 2011; Silva-Rojas et al., 2020; Xu et al., 2019). Much of known function is directed towards adult specific mechanism. Knockout experiments have demonstrated that mice lacking both STIM1 and STIM2 do not survive beyond the prenatal stage (Oh-hora et al., 2008), while complete STIM knockout in *Drosophila melanogaster* results in lethality during the larval stage (Pathak et al., 2017). This indicates that, regardless of whether it's in vertebrates or invertebrates, these findings emphasize the crucial need for STIM during the organism's growth phase, which typically unfolds during juvenile development. However, the mechanisms underlying STIM's role in early development remain poorly understood. Given that *Drosophila melanogaster* possesses only one isoform of STIM, any phenotype observed will be closely associated with STIM-related functions. Therefore, my thesis utilized a *Drosophila* line containing a whole-body STIM knockout, which was generated in our laboratory, to explore the involvement of STIM during the initial phases of organismal development.

1.2 Drosophila larval development and feeding

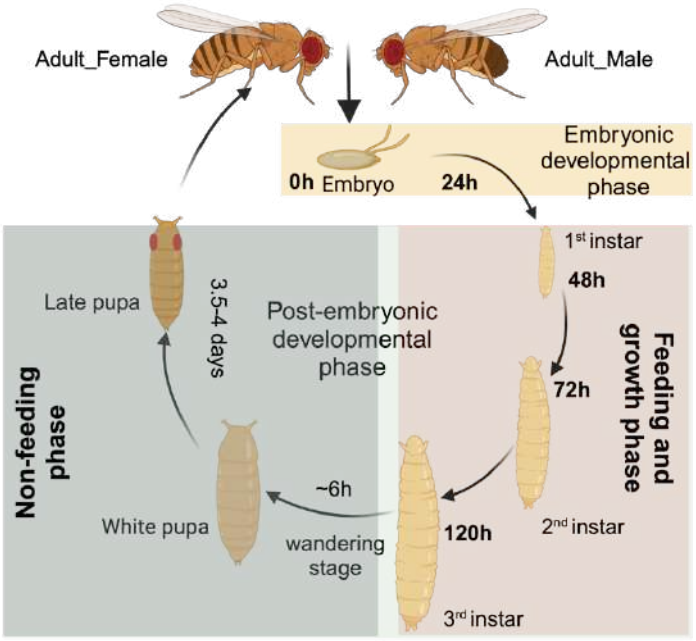

Figure 1.2: Illustration showing the various stages and phases of *Drosophila* development.

Drosophila melanogaster, undergoing complete metamorphosis as a holometabolous organism, exhibits clearly distinguishable developmental stages; Embryo, Larvae, Pupa and Adult. It's development unfolds in two phases: the embryonic phase and the post-embryonic phase (Tennessen & Thummel, 2011). The embryonic phase is a closed system, culminating with the formation of every organ, and by the end of the embryonic phase all the cells undergo a quiescent state. This quiescence arises due to limited space for further division and the absence of external nutrient supply to sustain further development. Following the 24-hour embryonic phase, the larva hatches. The larval stage of *Drosophila* spans for approximately 96 hours, progressing through three distinct instars—the first, second, and third instar—each lasting for 24, 24, and 48 hours, respectively. Within the *Drosophila* life cycle, the larval stage represents the juvenile phase of development. Post-embryonic development initiates around the late first instar stage or early second instar stage and is initiated by nutrition-sensing signals derived from the fat body (Chell & Brand, 2010; Sousa-Nunes et al., 2010, 2011). By the mid-second instar stage, every cell in the body either enters endoreplication mode or mitotic

cell division mode, resulting in an overall 200-fold increase in body size (Britton et al., 2002; Britton & Edgar, 1998; Chell & Brand, 2010).

Growth, defined as the overall increase in size through mass accumulation, is a dynamic process influenced by various external and internal factors (Guertin & Sabatini, 2008; Jacobs et al., 2020). External factors such as nutrition availability, temperature, and humidity, (Koyama et al., 2020) as well as internal factors like sensing internal energy balance and growth signaling cues such as insulin, Hippo, and Dpp signaling, play crucial roles in regulating this process (Bosch et al., 2017; Boulan et al., 2018; Brogiolo et al., 2001; Buhler et al., 2018; Delanoue et al., 2010; Okamoto et al., 2009; Robert B. Church, 1966). Any disturbance in these factors can disrupt normal development, potentially leading to severe consequences, including organismal lethality.

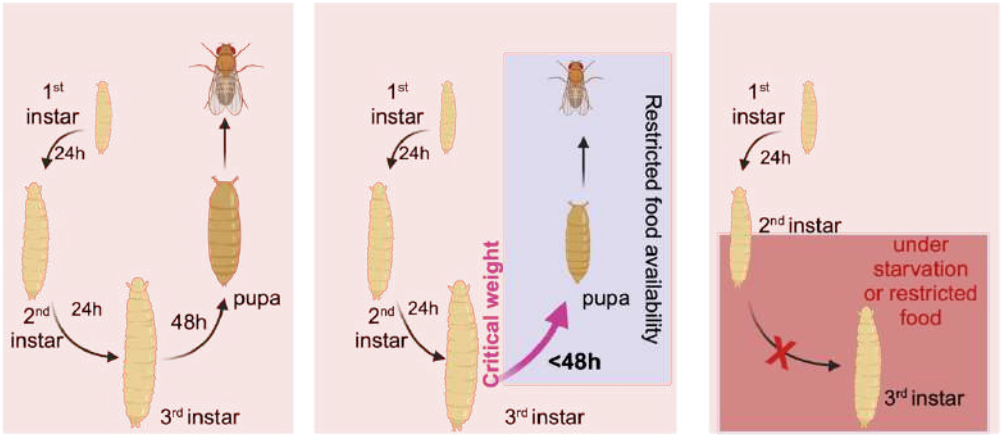

Figure 1.3: Illustration showing the impact of nutrition availability on larval development *Drosophila*

Nutrition, obtained from food, is a significant external factor impacting organismal growth (Cameron, 2022; Inzaghi et al., 2022). It serves as a vital source of both energy and the essential building blocks required for growth facilitation. Therefore, access to food is critical for the normal growth and survival of an organism. The intricate relationship between nutrition and growth is exemplified in the study of *Drosophila melanogaster* larval development (Cheng et al., 2011; Colombani et al., 2003; Delanoue & Romero, 2020; Hietakangas & Cohen, 2009; Koyama et al., 2020; Tennessen & Thummel, 2011).

It is widely acknowledged that larvae exhibit sensitivity to the availability of nutrition until they attain a critical weight (Tyson et al., 2023) (Fig 1.3). Once this critical weight is achieved, larvae proceed into pupariation, even under reduced nutrition conditions, albeit with delayed timing, resulting in the formation of smaller-sized pupae (Britton & Edgar, 1998; De Moed et al., 1999; Jayakumar et al., 2016a) (Fig 1.3).

During the larval stage, feeding is a prominent behavior exhibited by larvae. Unlike in adults, where feeding is sporadic, larval feeding is continuous and ceases as they enter the wandering stage. This distinction highlights the differing regulation of feeding between growing animals and fully developed adults. In adults, nutrition supports energy needs and overall physiological homeostasis (Chatterjee & Perrimon, 2021; Nakamura & Nakamura, 2018). The mechanism behind feeding in larvae largely stems from adult feeding regulation, which is governed by hunger and satiety signals initiating or terminating feeding (Amin & Mercer, 2016; Lin et al., 2019; Nakamura & Nakamura, 2018; Tsao et al., 2018; Wilinski et al., 2019).

1.3 Neuronal control of larval feeding

Given the continuous nature of larval feeding, it is imperative to inhibit the satiety signal responsible for terminating feeding throughout the feeding period. This is especially crucial as growing animals require heightened food intake to meet not only their energy needs but also to serve as a source of raw materials for cell growth and proliferation (Cameron, 2022; Colombani et al., 2003; Delanoue & Romero, 2020; Inzaghi et al., 2022). Additionally, they need to store nutrients for the pupal stage, which is a non-feeding developmental stage. The feeding process involves initiation, ingestion, digestion, and absorption, with various neurotransmitters and neuropeptides playing pivotal roles at each stage (Lin et al., 2019; Miroschnikow et al., 2020; Pool & Scott, 2014). Studies have indicated that in larvae, Neuropeptide F (NPF), a homolog of human NPY, acts as a motivational signal for foraging in response to appetitive odors (Pu et al., 2018; Wu et al., 2003). NPF neuron activity seems dependent on inputs from specific dopaminergic neurons receiving olfactory inputs (Y. Wang et al., 2013). Mutations affecting short neuropeptide F (sNPF), encoded by a separate gene from NPF, influence body size by regulating food

intake in larvae (Carlsson et al., 2013; Lee et al., 2004). Octopaminergic circuits regulate feeding independently of NPF signaling in 3rd instar larvae when food is restricted (T. Zhang et al., 2013). Hugin neuropeptide-secreting neurons respond to aversive gustatory signals, suppressing larval feeding upon activation (Bader et al., 2007; Hückesfeld et al., 2016). In instances of imbalanced essential amino acids, specific dopaminergic neurons are necessary for food rejection by larvae (Bjordal et al., 2014). Furthermore, serotonergic neurons from the brain project to the gut, potentially regulating feeding-related muscle movements (Schoofs et al., 2018; Schoofs, Hückesfeld, Surendran, et al., 2014).

While these studies primarily focus on the third instar stage of larval feeding, the mechanisms governing the maintenance and augmentation of feeding capacity as larvae progress through different stages, as well as the processes involved in terminating feeding, remain inadequately understood.

1.4 Aim of the thesis

In this thesis, I investigate the significance of STIM in the early developmental stages of an organism, utilizing the genetically tractable model system of Drosophila melanogaster. To accomplish this, I employed a whole-body STIM knockout (*STIM*^{KO}) model generated in the laboratory through CRISPR-*Cas9* gene editing technology (Pathak et al., 2017). The primary objective of my research was to comprehensively characterize *STIM*^{KO}, aiming to elucidate the underlying causes of lethality during the larval stage, identify cells dependent on specific STIM functions for normal development, and unravel the mechanisms involved.

Chapter 2: Growth and feeding deficit of STIM null mutants

2.1 Introduction

Stromal **I**nteraction **M**olecule (STIM), a transmembrane protein resident in the endoplasmic reticulum membrane, plays a critical role in sensing changes in calcium concentration and regulating store-operated calcium entry through the Orai calcium channel located on the plasma membrane (Liou et al., 2007) . Notably, null mutant mice lacking both STIM1 and STIM2 do not survive beyond the prenatal stage of development (Gwack et al., 2008), indicating the essential function of STIM in normal organism development. To explore this further, we turned to *Drosophila melanogaster* as a model system, given its single-copy gene and the direct impact of the specific protein on development. To study the role of STIM in development, I used a complete null mutant line of *Drosophila* that was generated using the CRISPR-*Cas9* gene editing technique (Pathak et al., 2017).

In a preliminary examination of the STIM mutant strain, lethality was observed occurring at the larval stage, with none of the organisms successfully progressing into adulthood (Pathak et al., 2017). This initial discovery underscores the critical importance of STIM in the normal developmental process of the organism. However, to gain a more comprehensive understanding of the underlying causes of this lethality, I embarked on a thorough investigation.

This chapter delves into a detailed exploration of the $STIM^{KO}$ mutant, focusing on when lethality occurs during development and the specific phenotypic traits responsible for preventing the transition into adulthood.

2.2 Materials and Methods

2.2.1 Fly rearing and Stocks

Drosophila strains were reared on standard cornflour agar media consisting of 80 g corn flour, 20 g glucose, 40 g sugar, 15 g yeast extract, 4 ml propionic acid, 5 ml *p*-hydroxybenzoic acid methyl ester in ethanol, 5 ml ortho butyric acid in 1l at 25°C, unless otherwise specified, under a 12:12 hr light : dark cycle. In all studies the *Canton S* (*CS*) strain was used as a wild-type

control and CRISPR-*Cas9* generated deficiency for *STIM* referred to as $STIM^{KO}$ served as a null mutant for the *Drosophila STIM* gene.

Other fly stocks:

InscGAL4	Marks neuroblasts of larval brain with GAL4	RRID: BDSC_8751
UASFUCCI	Marks different phases of cell cycle with fluorescent markers	RRID: BDSC_55100
UASmCD8GFP	Expresses membrane tagged GFP under UAS control	RRID: BDSC_5130

2.2.2 Staging

Synchronized larvae of the appropriate ages as described below were collected and transferred to agar less media containing yeast (4gm), sucrose (8gm), cornflour (16gm), Propionic acid (1ml) and 0.05gm of Benzoic acid in 1ml of absolute alcohol. The number of viable organisms and the developmental stage were scored at specific time points as mentioned below and in the figures and figure legends.

Figure 2.1: Genetic cross showing strategy to choose the $STIM^{KO}$ animal

Embryo and larval staging experiments were performed to obtain lethality and developmental profiles of the indicated genotypes as described previously (Joshi et al., 2004). Depending on the experiment, timed and synchronized egg-laying was done either for 6h to allow development profiling at 8-12h, 32-36h,

60-66h, 80-86h, 128-136h, 176-182h and 320-326h after egg laying (AEL) or for 2h at 35-37h (36h), 41-43h (42h), 47-49h (48h), 53-55h (54h), 59-61h (60h), 65-67h (66h), 71-73h(72h), 83-85h (84h), and 89-91h (90h) AEL for identifying a lethality window between 36-90h. Larvae were collected at either 60–66h or 35-37h AEL in batches of 25 (for developmental profile) or 10 (for lethality window). They were screened and staged subsequently. Heterozygous larvae were identified using dominant markers (*FM7iGFP*, *TM6Tb,* and *CyOGFP*) and removed (Fig 2.1). Each batch of larvae was placed in a separate vial and minimally three vials containing agar-less media were tested for every genotype at each time point. The larvae were screened at the indicated time points for the number of survivors and stage of development, determined by the morphology of the anterior spiracles and mouth hooks. Experiments to determine the viability of experimental genotypes and their corresponding genetic controls were performed simultaneously in all cases. Larval images were taken on the MVX10 Olympus stereo microscope using an Olympus DP71 camera.

2.2.3 Feeding assay

Feeding assay was performed at specific developmental time points in larvae (40-44h, 58-62h, 80-84h AEL) of the specified genotypes. Larvae were placed in a 35mm punched dish with coverslip at the base thus creating a small depression in the centre of the coverslip. In this depression a coin sized cotton swab was placed containing 4.5.% of yeast solution with 0.25% eriogluasin dye (blue dye). For scoring the number of larvae that fed, 30 larvae per plate were taken and incubated in the feeding plate for 4hrs at 25^{o}C. Larvae were removed from the paste, washed, collected and scored for presence of blue dye (Dye^{+ve}) and absence of blue dye within the gut (Dye^{-ve}).

For quantification of ingested blue dye, 12-15 larvae were incubated for 2h in yeast paste with the blue dye. Larvae were removed from the yeast paste and 10 larvae with blue dye in the gut were washed, and homogenized in 50μl of cold 1xPBS. The homogenate was spun at 5k for 2 minutes in a table top Eppendorf centrifuge. The supernatant (2μl) was taken for quantification of protein using the Thermo scientific Pierce Protein assay kit, Cat#23227. Optical density (OD) at 625nm as a measure of ingested blue dye was measured from 30μl of the homogenate. Due to variation in larval sizes between control and

experimental samples, the OD was normalized to whole larval protein concentration (μg/μl). OD was obtained using the SkanIt Software 6.1.1 RE for Microplate Readers RE, ver. 6.1.1.7. Larval imaging and processing was performed on the Olympus MVX10 stereo microscope using FIJI software.

2.2.4 Larval imaging and measurement

Staged larvae from specified genotypes were collected at specific development time points, anesthetized on ice for 1h and mounted with ice cold HL3 buffer. The mounted larvae were imaged immediately using an Olympus MVX10 stereo microscope. For measurement of larval length from mouth hook to tip of the posterior spiracle FIJI software was used. A minimum of 10-15 larvae were taken per genotype for length analysis.

2.2.5 Quantification of larval mouth hook contractions

Mouth hook contractions were measured by placing 1-3 appropriately staged larvae in a drop of 2% yeast solution in a Petri dish. Videos were taken for 30 seconds on an Olympus MVX10 stereo microscope. For each genotype a minimum of 10 animals were imaged. Mouth hook contractions were counted manually from the visualised videos.

2.2.6 Brdu uptake assay

Collect appropriate-aged larvae and dissect brains in ice-cold buffer. Until all the dissection is done, keep the brains in an ice-cold 1X PBS buffer. Remove the PBS and add the BrdU solution (75 μg/ml). Incubate for 1 hour at room temperature. Remove the solution and give it one wash for 5 minutes in 1X PBS. For 40 minutes at room temperature, fix the tissue with 4% paraformaldehyde in 1X PBS. After removing the paraformaldehyde, wash the tissues in 0.3% PTX three times for 10 minutes each at room temperature. Next, block the sample with 10% normal goat serum (NGS) in PBTx for 30 minutes at room temperature. Remove the solution, and treat the sample with a 2N HCl solution for 30 minutes at room temperature. Refix the tissue by incubating with 4% PF for 20 minutes at room temperature. Remove the fixation agent and wash the tissues with 0.3% PTX for two 10-minute periods each. In PBTx, re-block the tissue with 10% NGS for 30 minutes. Remove the blocking solution and incubate

the tissues with the anti-Brdu antibody (primary antibody) overnight at 4^{o}C. Remove the antibody solution store at 4^{o}C and this can be reused up to three times. Wash the brains three times at 10-minute intervals with PBTx, then incubated them with secondary antibodies at the dilutions described below for 2 hours at room temperature, followed by another three washes in PBTx at 10-minute intervals each. Mount the tissues in either 1X PBS with 70% glycerol or Vectashield medium. The slides should be stored in the dark at 4^{o}C until imaging.

2.2.7 Immunohistochemistry

Larval brains were dissected in ice-cold 1xPBS and fixed with 4% paraformaldehyde in 1xPBS on the shaker for 20mins at room temperature. Fixed brains were washed with PBTx (0.3% TritonX-100 in 1XPBS) 3-4 times at 10minutes intervals, blocked with 5% normal goat serum (NGS) in PBTx for 2hrs at room temperature, and incubated with primary antibodies diluted in 5%NGS+PBTx at the appropriate concentration as mentioned below, overnight at 4^{o}C. Antibody solution was removed and re-used upto three times. Brains were washed with PBTx 3 times at 10 minute intervals followed by incubation with secondary antibodies at the dilutions described below, for 2hrs at room temperature and three washes in PBTx of 10minute intervals each. Brains were mounted in 70% glycerol diluted in 1xPBS. Confocal images were acquired by using FV3000 LSM and the Fluoview imaging software.

Following primary antibodies were used: Chick anti-GFP (1:8000, Abcam Cat#13970 RRID: AB_300798), mouse anti-Prospero (1:100, DSHB Cat# Prospero (MR1A), RRID:AB_528440), Rat anti-BrdU (1:100, Cat# Abcam-ab6326; RRID: AB_305426), Rat anti-Deadpan (1:400, Cat# Abcam-ab195172; RRID:AB_2687586)

Following secondary antibodies were used: Goat anti-Chicken IgY (H+L), Alexa Fluor 488 (Thermo Fischer Scientific, Cat#A-11039; RRID: AB_2534096), Goat anti-Mouse IgG (H+L) Alexa Fluor 633 (Thermo Fischer Scientific Cat#A-21052; RRID: AB_2535719), Goat anti-Rat IgG (H+L) Alexa Fluor 594 (Thermo Fischer Scientific Cat#A-11037; RRID: AB_2534095).

2.2.8 Quantification and Statistical analysis

All bar graphs and line plots show the means and standard error of means. In boxplots, horizontal lines in the box indicate the median, box limits are from 25th-75th percentiles, and individual data points are represented by closed circles (unless otherwise specified in the figure legends). Unpaired student t-Test (for two genotypes) one way ANOVA followed by post- hoc Tukey's significance test (for data with multiple genotypes) was performed to calculate P values. All graphs were plotted using Origin 8.0 software. Ori- gin 7.5 MicroCal, Origin Lab, Northampton, MA, USA N/A, Fiji Open access (RRID: SCR_002285). Diagrammatic representative images are made with help of Biorender website (https://app.biorender.com).

2.3 Results:

2.3.1 Identification of lethality window period of *STIM^{KO}*

In previous studies, it has been shown that *STIM^{KO}* shows abnormal development compared to wild-type (*Canton-S* or *CS*). For all the studies, *STIM^{KO}* animal chosen To find out how far *STIM^{KO}* embryos develop normally, the first three batches of 25 embryos were taken and watched until they reached the first instar larval stage, and the number of embryos that hatched was estimated at 32-36h AEL. It was observed that normal hatching of larvae (24 ± 0.33) occurred. Indicated that there was no lethality at the embryonic stage of development (Fig. 2.2A). Since there was no lethality at the embryonic stage, I conducted a western blot analysis to verify the presence of STIM protein at three different time points (36h, 60h, and 74h). The results revealed that the STIM band was present in the control larvae at all three time points. However, in *STIM^{KO}* larvae, STIM was absent at all time points. Based on these findings, I selected 36–40 hours of AEL for all further studies (Fig 2.2B).

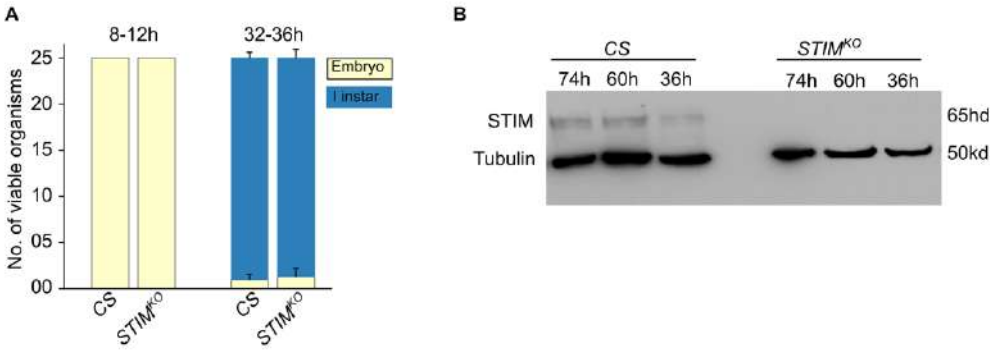

Figure 2.2: Analysis of *STIM^{KO}* embryo hatching pattern and verification for STIM protein presence.

A. Stack bar graph showing the number of viable organisms and their developmental stage at the specified hours after egg laying for *CS* and *STIM^{KO}*. Data are from three experiments, each with 25 organisms. per genotype.

Consequently, a time point of 36–42h AEL was chosen as the starting point for a comprehensive staging experiment to observe the entire developmental process up to 320 hours, where the adult eclosion occurs. A staging experiment was conducted to track the organism's development. Here, 60-66h, 80-86h, 120-128h, 168-174h, and 320-326h AEL time points are chosen for the observation of the number of viable organisms and at what stage they are present. The result of this experiment revealed that wild-type larvae of *CS* exhibited a typical developmental trajectory Out of the initial 25 first-instar larvae observed, (24±1) successfully developed into adults (Fig. 2.3A).

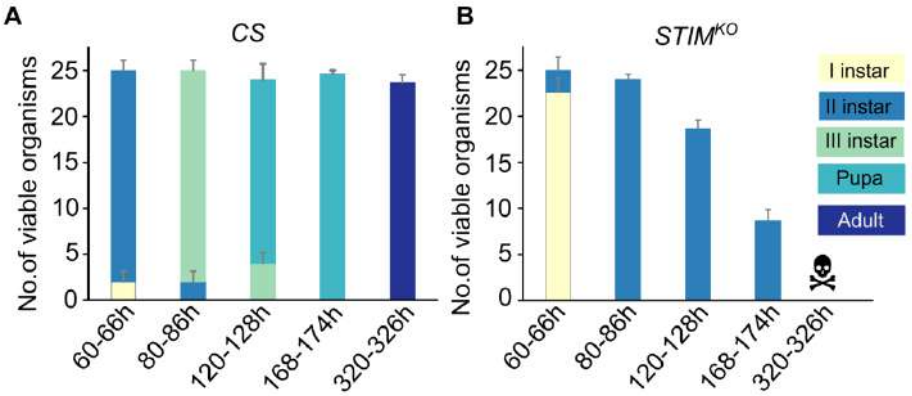

Figure 2.3: Profiling of the developmental trajectory shows larval lethality in *STIM^{KO}* animals.

A and B. Staging graph showing number of viable organisms (mean ± SEM) at the indicated developmental stage of *CS* and *STIM^{KO}* after egg laying. Number of sets (N) = 3, number of organisms per set (n) = 25.

In contrast, *STIM*^{KO} larvae exhibited a significant delay in transitioning from the first instar to the second instar stage (Figure 2.3B). Moreover, at 80–86h, all the *STIM*^{KO} larvae were still in the second instar stage. As time progressed, these second-instar *STIM*^{KO} larvae gradually decreased in number (Fig. 2.3B). In summary, the broader staging experiment highlighted a notable deviation in early larval development for *STIM*^{KO} organisms, hindering their progression beyond the second instar stage and ultimately leading to their mortality (Fig. 2.3A and B).

Next, to pinpoint the specific window of lethality, I conducted a detailed staging analysis. I observed larval development at intervals of every 6 hours, ranging from 36 hours to 90 hours AEL. The results revealed a prominent difference when compared to the *CS* larvae. In wild-type *CS* larvae, the transition from the first to the second instar typically occurs between 42 and 54h AEL. In contrast, *STIM*^{KO} larvae exhibited a delayed transition, occurring between 60 and 72 hours AEL, representing an 18-hour delay (Fig. 2.4A and B).

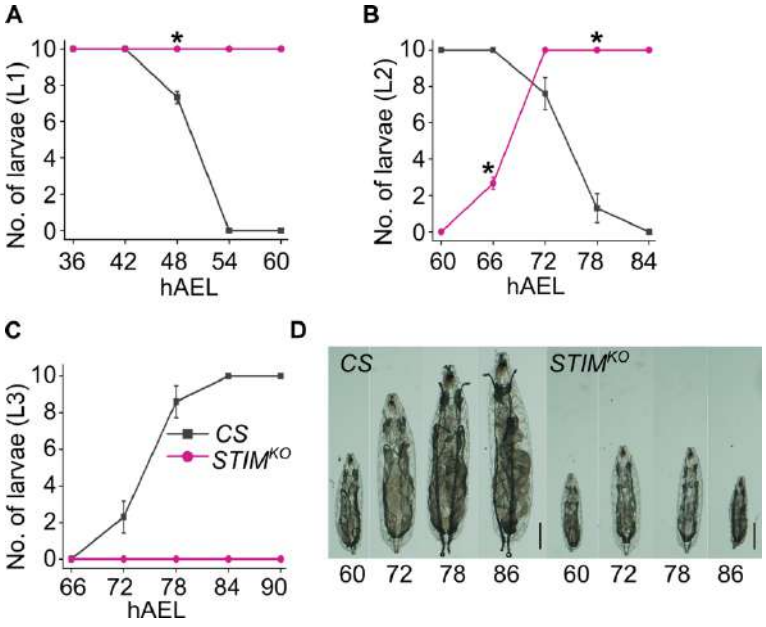

Figure 2.4: *STIM*^{KO} larvae show delayed development, and lethality starts at 78h AEL onwards.

(A-C) Number of 1st instar (L1), 2nd instar (L2) and 3rd instar (L3) larvae from *CS* (grey) and *STIM*^{KO} (magenta) measured at 6h intervals after egg laying (AEL) at the specified time points (mean ± SEM). Number of sets (N) = 3, number of larvae per replicate (n) = 10. *P < 0.05, Student's *t*-test with unequal variances.

D. Representative images of larvae from *CS* and *STIM*^{KO} at the indicated time. Scale bar = 1 mm.

Following this delay, *STIM*^{KO} larvae were unable to progress to the third instar (Fig. 2.4C). Additionally, *STIM*^{KO} larvae displayed significant growth retardation. At 72h, they resembled *STIM*^{KO} larvae at the 60-hour mark. However, beyond 72h, growth in *STIM*^{KO} larvae came to a complete halt, and there was a gradual decline in viability, particularly after 80–86h AEL (Fig. 2.4D).

This detailed analysis of the stages of development provides valuable insights into the developmental progression and the critical developmental window affected by the absence of STIM, shedding light on the underlying significance of STIM function for the early development of an organism.

2.3.2 Mitotic cell proliferation is affected in *STIM*^{KO}

Larvae, once hatched from the embryo, undergo remarkable growth, expanding to approximately 200 times their original size before transitioning into the pupal stage (Tennessen & Thummel, 2011). However, through representative larval images obtained during our staging experiment suggest that, *STIM*^{KO} larvae, once they reached 76–80h AEL **(**Fig. 2.4D), exhibited no further increase in their overall body size. To validate this observation, I meticulously measured the overall larval body size at specific time intervals: 34–38h, 58-62h, 70-74h, and 82-86h AEL (Fig. 2.5A).

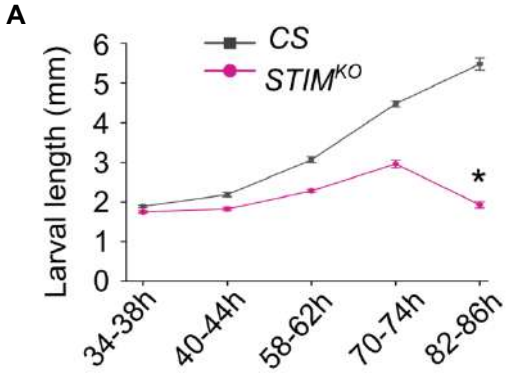

Figure 2.5: Overall body growth of *STIM*^{KO} arrests after 70-74h AEL.

A. Measurement of larval length (mean ± SEM) from *CS* (grey) and *STIM*^{KO} (magenta) larvae at the specified time points. Number of larvae per genotype per time point is (n) ≥ 12. *$P < 0.05$ for all time points, Student's *t*-test with unequal variances.

Consistently, the results pointed to a cessation of overall growth in *STIM*^{KO} larvae (Fig. 2.5A). With their size plateauing, I turned my attention to the two critical factors governing larval development during this stage, namely, cell growth and proliferation status and nutrition uptake. These two processes are

intricately linked and play a critical role in enabling larvae to expand their body size. Any deviation from the norm in these processes can have a profound impact on the overall progression of an organism's development.

As a part of this study, I did the BrdU uptake assay, which is aimed at evaluating the status of cell growth (endocycle) as well as cell proliferation. Immunohistochemistry against BrdU helps identify the cell in which active DNA synthesis happens. The momentum of larval growth predominantly relies on cell growth within endoreplication tissues (Edgar & Orr-Weaver, 2001; Fox & Duronio, 2013; Zielke et al., 2013). The fat body, a well-established tissue for studying endoreplication, served as the focal point. I conducted examinations of both wild-type and *STIM*^{KO} larvae's fat bodies at two specific time intervals: 70–74h and 82–86h. Regrettably, the delicate nature of *STIM*^{KO} fat bodies rendered them unable to withstand the necessary HCl treatment for the assay. Consequently, I shifted my emphasis towards understanding mitotic cell division.

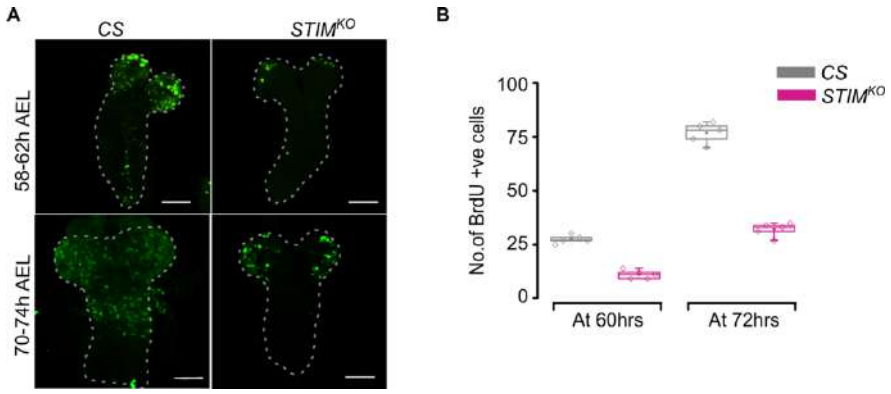

Figure 2.6: BrdU uptake assay to monitor the Neuroblast cell proliferation

A. Representative images of anti-BrdU marked larval brain from *CS* and *STIM*^{KO} animals at the indicated ages. N ≥ 3. Scale bar = 20μm.

B. Box plot showing the number of BrdU positive cells from larval brain from and *STIM*^{KO} animals at the indicated ages.

Certain organs, such as the brain and imaginal discs, undergo continuous cell division during growth. Typically, after the completion of embryonic development, mitotic cells, including the majority of neuroblasts (NBs) and imaginal disc cells, enter a quiescent state. Postembryonic larval development commences during the late first instar and early second instar stages. During this phase, cells resume growth and division in the brain and imaginal discs, but

only if adequate nutrients are available (Britton & Edgar, 1998; Homem & Knoblich, 2012). To delve into this aspect, we conducted a BrdU uptake assay on larval brains at two distinct time points: 58–62h and 70–72h.

Analysis of the *STIM*^{KO} larval brain at 58-62h revealed the marking of only few BrdU-positive cells in each lobe of the brain whereas in control, more BrdU-positive cells were seen (Fig. 2.6A). This result further confirms that at 60h, *STIM*^{KO} larvae were still developmentally at their first instar stage. It is widely documented in the literature that during the first instar stage, only mushroom body neuroblasts (four in each lobe of the brain) are in a dividing state and all others are in a quiescent state (Ito & Hotta, 1992).

Also, this agrees with the point where, in the staging experiment, *STIM*^{KO} larvae were still in the first instar stage at 58–62h, where they were supposed to be in the mid-second instar stage (Fig. 2.4A). At 70–72h, we did observe an increase in BrdU-positive cells in *STIM*^{KO} brains, although the count was lower compared to wild-type *CS* larval brains (Fig. 2.6A and B). Unfortunately, by 82–86h, the *STIM*^{KO} brain had become fragile and could not proceed with the BrdU uptake assay.

To delve deeper into the cell proliferation status of *STIM*^{KO} larvae, I adopted a genetic approach. In this method, mCD8GFP was driven under the neuroblast-specific *inscGAL4*, leading to the marking of neuroblast membranes with GFP. In each division of NB, even daughter cells, including ganglion mother cells and postmitotic cells, received mCD8GFP. By counting the number of paired postmitotic cells, we could infer the occurrence of approximately 4–5 rounds of division. Here, our focus was primarily on the well-established system of thoracic neuroblasts. Upon comparing thoracic segments of *insc>mCD8GFP* (wild-type) and *STIM*^{KO} larvae at 70-74h (Fig. 2.7A, first two columns), it was apparent that NBs in both genotypes exited quiescence and entered a proliferative state. Both the NB marker Deadpan (red) and the post-mitotic cell marker Prospero (blue) appeared normal in *STIM*^{KO} larvae aged 70-74h. However, at 82-86h, the number of postmitotic cells (Prospero-positive) decreased significantly in *STIM*^{KO} animals compared to controls, while the number of thoracic neuroblasts remained unchanged (Fig. 2.7A, compare the third and fourth columns).

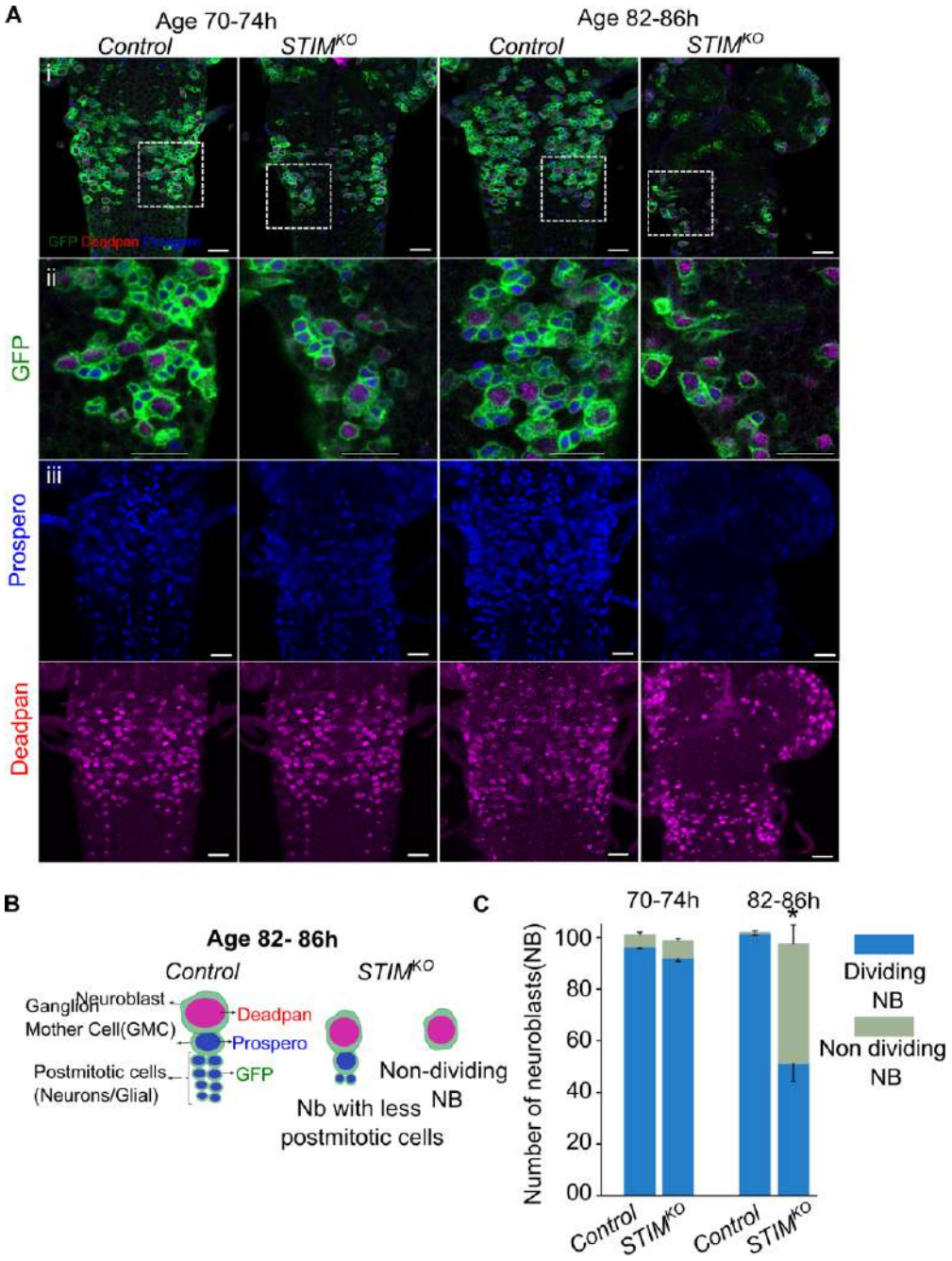

Figure 2.7: Thoracic ganglion's neuroblast proliferation is affected in *STIM^{KO}*

A. Representative images of thoracic neuroblasts marked with *Insc>mCD8GFP* (green), a neuroblast marker (anti-Deadpan, red) and a marker for post-mitotic cells (anti-Prospero, blue) from control (*Insc>mCD8GFP*). Animals at the indicated ages. N ≥ 4. Scale bar = 20μm

B. Diagrammatic summary of neuroblast proliferation in control (*Insc>mCD8GFP*) and *STIM^{KO}; Insc>mCD8GFP*.

C. Stack bar graph showing number of dividing neuroblasts to non-dividing neuroblasts.

*P < 0.05, Student's t-test with unequal variances, n = 4 animals from each genotype.

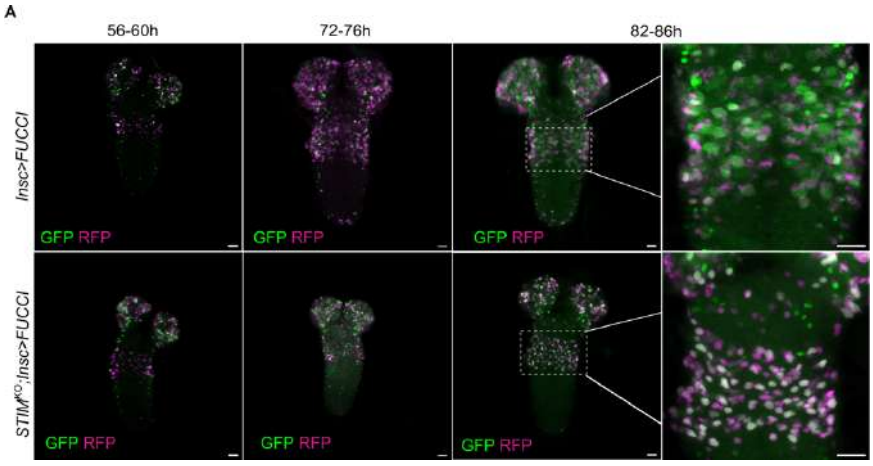

Figure 2.8: In *STIM^{KO}*, by 80–86h AEL proliferation of neuroblasts arrest in G2/M phase of cell cycle

A. Confocal images of larval brains at the indicated time points expressing the FUCCI marker. Control genotype is *Insc>FUCCI* (top row) and the mutant genotype is *STIM^{KO}*; *Insc>FUCCI* (bottom row). Here late mitosis/G1 phase, S-phase and G2/early mitosis are marked by green, red, and yellow fluorescent indicators respectively. Scale bar = 20 μm; n = 5 larval brains.

Upon quantification, the ratio of dividing neuroblasts (Deadpan surrounded by Prospero-positive cells) to non-dividing neuroblasts (Deadpan with either no or few Prospero-positive cells) changed significantly in 86-hour-old *STIM^{KO}* larvae (Fig. 2.7C and B). To elucidate the cause behind the reduced number of postmitotic cells, I analysed different phases of the cell cycle in thoracic neuroblasts of *STIM^{KO}* larval brains. For this purpose, I used genetically encoded FUCCI system (Zielke et al., 2014), which marks the G1, S, and G2 phases of interphase with green, red, and green+red (yellow) fluorescent tags, respectively. At 72-76h, both control and *STIM^{KO}* larvae exhibited an asynchronous pattern of division. However, at 82-86h, while control larvae persisted with the asynchronous pattern, the majority of thoracic neuroblasts in *STIM^{KO}* animals remained in the G2/M state (Fig. 2.8A). Cell proliferation pattern at 70-74h in *STIM^{KO}* suggests that earlier development is normal but NB later again arrested its proliferation. As it mentioned earlier, endo-cell cycle/ mitotic cell division before the attaining of critical weight, Drosophila larvae are sensitive to supply of the nutrition (Britton & Edgar, 1998). There by I went ahead to examined the nutritional uptake capacity of *STIM^{KO}* larvae.

2.3.3 *STIM*^{KO} larval lethality is associated with reduced feeding

To initiate this assessment, I introduced staged larvae to a yeast mixture containing a blue dye and monitored their food ingestion for 4hrs. Observed that even at an early stage, between 40-44h AEL, a noticeable reduction in food intake was observed in *STIM*^{KO} larvae (Fig. 2.9A**,** quantification in Fig. 2.9B). By the time they reached 80-84h AEL, two distinct classes of *STIM*^{KO} larvae emerged. One class exhibited reduced food intake, while the other class showed no food intake at all. Particularly, the proportion of *STIM*^{KO} larvae displaying no food intake reached approximately 70% by 82-86h AEL (Fig. 2.9C and D).

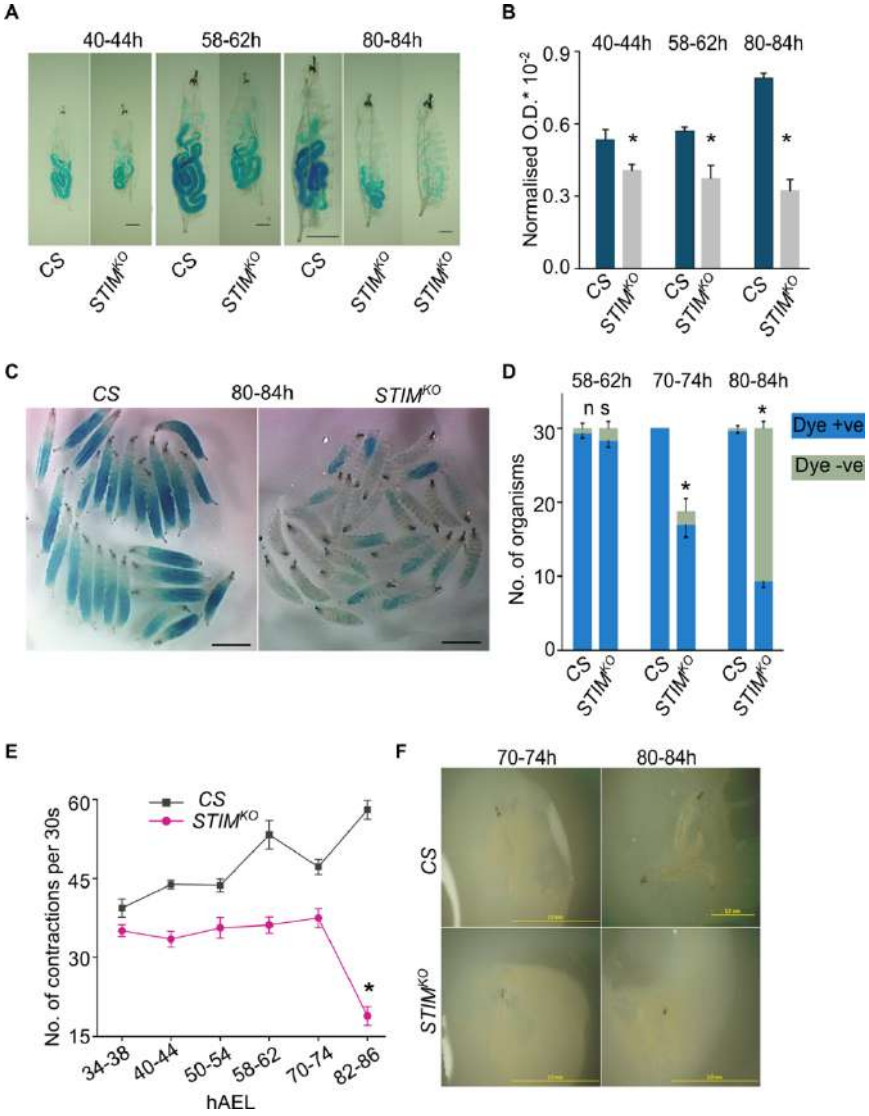

Figure 2.9: Feeding pattern is affected in *STIM*^{KO}.

A. Representative images of dye-fed larvae from *CS* and *STIM*^{KO} at the indicated times AEL, scale bar = 200µm except for *CS* (80-84h) where scale = 1mm.

B. Quantification (mean ± SEM) of ingested blue dye in *CS* and *STIM*^{KO} larvae at the indicated ages by normalizing optical density (OD) of the dye at 655nm to concentration of protein. Number of feeding plates per time point (N) = 6, number of larvae per plate (n) =10. *P < 0.05, Student's *t*-test with unequal variances.

C. Representative image of dye-fed larvae from *CS* and *STIM*^{KO} at 80-84h AEL. Scale bar: 2mm

D. Bar graph showing the average number of Dye^{+ve} (presence of blue dye in the gut) and Dye^{-ve} (absence of blue dye in the gut) *CS* and *STIM*^{KO} larvae at the indicated ages (mean ± SEM). Number of feeding plates per time point (N) = 3, number of larvae per plate (n) = 30. *P < 0.05, Student's *t*-test with unequal variances.

E. Line graph with quantification of larval mouth hook contractions per 30 seconds (mean ± SEM) from *CS* and *STIM*^{KO} at indicated developmental time points. Number of larvae per genotype per time point is (n) ≥ 10. *P < 0.05 at all time points, Student's *t*-test with unequal variances.

F. Representative images from larval mouth hook contraction video.

Further quantified the feeding ability of *STIM*^{KO} animals by assessing mouth hook contractions throughout larval development. Control larvae (*CS*) displayed a consistent increase in mouth hook contractions as they aged, except during and immediately prior to larval molts, indicating a progressively higher nutrient intake with age (Fig. 2.9E and representative images for 72 and 84h in Fig. 2.9F).

In contrast, *STIM*^{KO} larvae exhibited a slower developmental trajectory in terms of minimally increased mouth hook movements. Their growth was marked by minimal increases as they progressed from the first to the second instar larvae, followed by a cessation in mouth hook movements at 74h AEL, which was further reduced at 86h AEL (Fig. 2.9E and representative images for 72 and 84h in Fig. 2.9F) Altogether, feeding analysis, both by dye uptake and mouth hook contraction analysis, points out that *STIM*^{KO} larval lethality is caused by reduced nutrient uptake.

2.4 Discussion

The larval stage in holometabolas organisms is recognised as the juvenile phase in their life cycle. Within an organism's development, this juvenile stage holds significant importance because it marks a period of substantial growth. From the initial larval instar stage to the wandering larval stage, there is a remarkable increase in the organism's overall body size (Robert B. Church, 1966). To sustain this growth, it is imperative that the organism receive an adequate supply of nutrients to successfully complete this process. Furthermore, both the quality and quantity of food consumed during the larval stage play a pivotal role in determining the size and reproductive capacity of the

adult organism (Delanoue & Romero, 2020; May et al., 2015; Tennessen & Thummel, 2011) .

In the context of *STIM*^{KO} mutants, since it is a CRISPR-generated mutant, it specifically disrupts the zygotic transcription of the STIM gene that begins during late embryonic phases, while the maternal contribution remains unaffected. Therefore, normal embryonic development is observed. However, the absence of STIM later affects the normal development rate. Although there is a delay in early development, lethality manifests during the mid-second instar stage of the larval cycle (Fig. 2.3-2.4). After 76–80h AEL, there is a complete cessation of systemic growth in *STIM*^{KO} mutants. Extensive research has established that during the transition from the first instar stage to the early second instar stage, a fat body-dependent nutritional signal triggers the exit from a quiescent state. By mid-second instar stage, all cells, including both endoreplicative and mitotic cells, undergo growth and proliferation, respectively (Britton et al., 2002; Britton & Edgar, 1998; Chell & Brand, 2010; Shim et al., 2013). To support this cellular growth and proliferation, an adequate supply of nutrition is imperative.

The examination of mouth hook contractions provides valuable insights into this phenomenon. In wild-type larvae, between 58 and 62 hours, there is a noticeable increase in the number of contractions compared to the preceding time point. This observation suggests an active effort to enhance growth rates by increasing food intake.

In contrast, *STIM*^{KO} larvae do not exhibit an increase in mouth hook contractions resulted in limited nutrition supply (Fig. 2.9E), this limitation results in cell proliferation, where actively dividing cells enter a cell cycle arrests at G2/m phase. Existing literature has shown that until larvae reach a critical weight (De Moed et al., 1999), they are highly sensitive to both the quality and quantity of nutrients (Homem & Knoblich, 2012; Tennessen & Thummel, 2011). The occurrence of early larval developmental lethality in *STIM*^{KO}, attributed to nutritional deficits (Fig. 2.9A-F), underscores the substantial impact of altered nutrient supply on overall organismal growth. Consequently, it is important to pinpoint the specific cell type or types where the significance of STIM function becomes evident during the early stages of larval development, as elaborated in the subsequent chapters.

Chapter 3: Cellular profiling to uncover STIM-dependent requirements in larval development

3.1 Introduction

An examination of the developmental profile of *STIM*^{KO} has revealed a critical period of lethality, particularly occurring in the early 2nd instar larval stage. The investigation into the phenotypic characterization of *STIM*^{KO} has pinpointed a reduction in nutrition intake as the underlying cause of this lethality. Specifically, *STIM*^{KO} individuals exhibit a deficiency in both food intake and the frequency of mouth contraction during feeding in the larval stage, ultimately leading to systemic growth arrest. Understanding the fundamental reasons behind this altered feeding behaviour becomes crucial, given its profound impact on organismal growth.

To delve into the intricacies of this phenomenon, it is critical to identify the specific cell type or types responsible for the observed phenotype. Previous lab findings have demonstrated that the cell-specific knockout of *STIM* in Tyrosine Hydroxylase (TH)-expressing cells affects organism viability, and similarly, knocking down *TH* in TH-positive cells also affects larval viability (Pathak et al., 2017). This underscores the crucial role of TH-expressing cells in the early larval development of an organism.

Furthermore, the lab has shown that the whole-body *STIM*^{KO} can be partially rescued by overexpressing the wild-type STIM gene under *THA GAL4* (expresses in hypoderm) (Pathak et al., 2017). This suggests that TH cells require STIM function for normal development. Given that *TH* gene expression occurs in both hypoderm cells (for melanin pigment formation) and in the brain (for dopamine synthesis), it is pivotal to discern whether every TH expressing cell requires STIM function, if a specific subgroup is crucial, or also to understand the non-TH cell requirement for STIM function.

Against this background of preliminary work, this chapter provides a detailed exploration of the process involved in identifying the particular cell types essential for the early larval development of *Drosophila* and additionally demonstrates the significance of STIM function in a specific subset of dopaminergic neurons for larval growth.

3.2 Materials and Methods

3.2.1 *Drosophila* lines used

Fly strains		
Canton S	Wild type	
STIM^{KO}/FM7iGFP	Null mutant for STIM gene generated with help of CRISPR-*Cas9* gene editing technique	Generated in the lab
THGAL4 on III	Dopaminergic GAL4 driver marks TH (Tyrosine Hydroxylase) positive cells in brain and hypoderm	Serge Birman CNRS, ESPCI Paris Tech, France
THC'GAL4 on III	Marks dopaminergic cells of larval brain (Except 3 and 2 cells from DL1 and DL2 clusters respectively)	Mark N Wu, Johns Hopkins University, Baltimore (Xie et al., 2018)
THD'GAL4/CyOG	Marks subgroup of (DL1 and DL2) Dopaminergic cells in larval brain	
THGAL80 on II	Inhibits Gal4 expression in Dopaminergic cells	Toshihiro Kitamoto, University of Iowa, Carver College of Medicine.
MNScGAL4(Dilp2GAL4)/CyOG	Marks ilp (-2, -3, and -5) producing MNSc cells of larval brain	RRID: BDSC_37516
UASdsSTIM on III	UAS-RNAi against Stim gene	VDRC_47073
UASdsTH on III	UAS-RNAi against *Tyrosine hydroxylase* (*TH*) gene	RRID: BDSC_25796

UASDicer2 on X	Enhancer for RNAi	RRID: BDSC_24648
STIM^{KO}; THC'GAL4/ CyOG;+	Strains made for this study	
STIM^{KO}; THD'GAL4/CyOG;+		
STIM^{KO}; UASSTIM/CyOG;+		
STIM^{KO}; MNScGAL4/CyOG; +		
STIM^{KO}; THD'Gal4,THGAL80 /CyOG;+		
STIM^{KO}; UASDilp2/CyOG;+		
STIM^{KO}; UASDilp3/CyOG;+		
STIM^{KO}; UASDilp5/CyOG;+		

3.2.2 Fly rearing
As described in Chapter 2 (Materials and Methods).

3.2.3 Staging
As described in Chapter 2 (Materials and Methods)

3.2.4 Feeding assay
As described in Chapter 2 (Materials and Methods)

3.2.5 Quantification of larval mouth hook contractions
As described in Chapter 2 (Materials and Methods)

3.2.6 Immunohistochemistry
As described in Chapter 2 (Materials and Methods)

3.2.7 L-DOPA feeding assay

Agar-less media was prepared as mentioned in Chapter 2 (Materials and Methods). Once it gets cooled down and before solidifying, L-DOPA (1mg/mL) is added. Staged 2–6-hour old ALH-aged larvae were transferred to media with and without L-DOPA. Since L-DOPA is light-sensitive, all procedures after L-DOPA is added are performed in the dark. To avoid exposure to light, experimental media vials with larvae are wrapped in aluminum foil. Larvae were observed at 80-86h AEL (or 60-66h ALH) and scored for the number of viable organisms and respective developmental stages.

3.2.8 Adult fly weight measurement

For weight measurement of adult flies, 10 flies (5 females and 5 males) of the appropriate genotype were taken 6 – 10 hr post-eclosion and weighed after placing them in a small Eppendorf tube. Thereafter, the weight of the same empty tube was measured. Fly weights were calculated by subtracting the weight of the tube from the total weight of flies + tube. A minimum of five such measurements were performed for each genotype.

3.2.8 Quantification and Statistical analysis

All bar graphs and line plots show the means and standard error of means. In boxplots, horizontal lines in the box indicate the median, box limits are from 25th-75th percentiles, and individual data points are represented by closed circles (unless otherwise specified in the figure legends). Unpaired student t-Test (for two genotypes) one way ANOVA followed by post- hoc Tukey's significance test (for data with multiple genotypes) was performed to calculate P values, given for all figures in **Table-1**. All graphs were plotted using Origin 8.0 software. Ori- gin 7.5 MicroCal, Origin Lab, Northampton, MA, USA N/A, Fiji Open access (RRID: SCR_002285). Diagrammatic representative images are made with help of Biorender website (https://app.biorender.com).

3.3 Results

3.3.1 STIM function in dopaminergic neurons is crucial for normal larval development

Considering the growth defects observed in $STIM^{KO}$, speculation arose regarding the potential involvement of insulin signaling, with literature pointing to the crucial role of insulin signaling (specifically regulated by ilp2 and ilp5) in systemic organismal growth (Britton et al., 2002; Ikeya et al., 2002; Rulifson et al., 2002; Semaniuk et al., 2021). Concurrently, prior research in our lab demonstrated that cell-specific knockout of *STIM* in TH expressing cells affects organism viability. To explore this, I used the UAS/GAL4 system (Brand & Perrimon, 1993) to identify the cells that require STIM-specific functions for the early development of an organism. Here I used the 2 different GAL4s, which expresses in MNSc cells, where they produces insulin-like peptides -2, -3, and -5, and *THGAL4* (Friggi-Grelin et al., 2003), which expresses in all TH^{+ve} cells. Staging experiments showed that under both $MNSc>STIM^{+}$ and $TH>STIM^{+}$ expressions, the rescue of $STIM^{KO}$ was achieved (Fig 3.1A). However, the TH-specific rescue showed a more significant $STIM^{KO}$ rescue compared to *MNScGAL4* (19.4±0.62 and 11.6±0.8 viable adults eclosed under *THGAL4* and *MNScGAL4* respectively from batches of 25 larvae) (Fig 3.1A Green and Blue arrows; *THGAL4* and *MNScGAL4* respectively**)**. Given this observation and the limited understanding of the role of dopamine in early growth regulation, the study decided to prioritize the investigation of the dopaminergic system over the insulin system for further exploration.

Considering the expression of *THGAL4* in both the brain and hypoderm regions and the previous findings indicating partial rescue through hypodermal-specific *STIM* overexpression (Pathak et al., 2017), I sought to investigate whether overexpressing *STIM* specifically in TH^{+ve} cells within the brain could also lead to a rescue of $STIM^{KO}$.

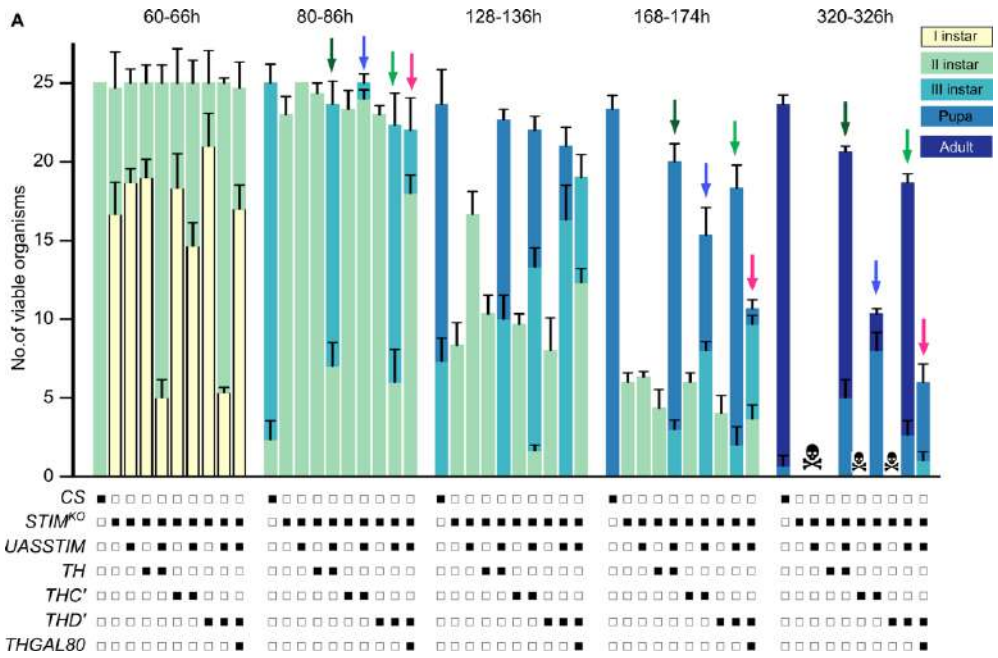

Figure 3.1: STIM function in TH positive cells crucial for normal development of an organism.

A. Stack bar graph showing the number of viable organisms (mean ± SEM) and their developmental stage at the specified hours after egg laying for the indicated genotypes. Coloured arrows mark bars that exhibit rescue of *STIM*^{KO} upon expression of STIM^{+} driven by *THGAL4* (dark green) and *MNScGAL4 (*also known as *Dilp2GAL4)* (Green), with all appropriate genetic controls as indicated. Number of sets (N) = 3, number of organisms per set (n) = 25.

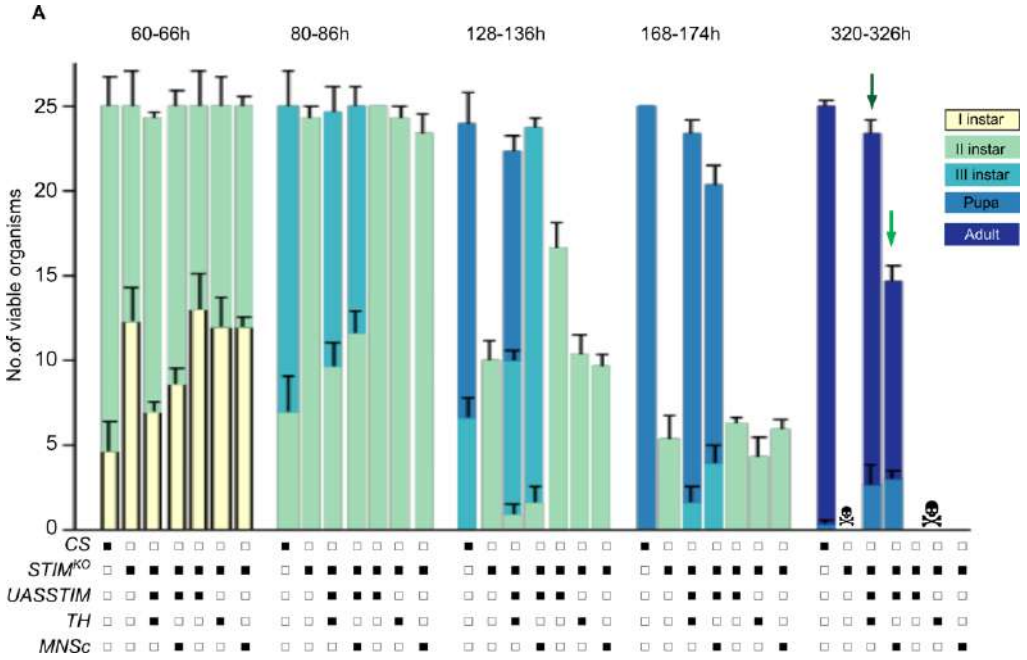

Figure 3.2: Developmental profile of *STIM*^{KO} under different genetic rescue condition

A. Stack bar graph showing the number of viable organisms (mean ± SEM) and their developmental stage at the specified hours after egg laying for the indicated genotypes. Coloured arrows mark bars that exhibit rescue of *STIM*^{KO} upon expression of STIM^{+} driven by *THGAL4* (dark green), *THC'GAL4* (blue), *THD'GAL4* (green) and restricted

rescue in presence *of THGAL80* (red) with all appropriate genetic controls as indicated. Number of sets (N) = 3, number of organisms per set (n) = 25.

The *Drosophila* larval brain, consisting of approximately 10,000 neurons, hosts around 74 dopaminergic neurons (Budnik et al., 1986; Friggi-Grelin et al., 2003). Given the clustering of dopaminergic cells in the brain, I employed subset-specific dopaminergic *GAL4* drivers *THC'GAL4* and *THD'GAL4* (Xie et al., 2018) with distinct expression patterns (Bjordal et al., 2014). *THC'GAL4* marked all dopaminergic cells in the central nervous system (CNS) and ventral ganglia, excluding a few cells in the DL1 and DL2 clusters, which were labelled by *THD'GAL4* (refer to Figs. B) (Bjordal et al., 2014; Xie et al., 2018).

Staging experiment under *THD'>STIM*$^{+}$ exhibited a significant rescue of *STIM*^{KO} larvae from the 2nd to the 3rd instar, reaching an approximately 90% rescue rate (Fig. 3.2A; green arrow and Fig. 3.3A and B). This rescue was comparable to the *THGAL4* driven rescue (Fig 3.1A and 3.2A; Dark green), with both yielding a notable number of viable adults (20±1.5 and 18±2 viable adult eclosed respectively from batches of 25 larvae.

In contrast, the rescue achieved by *THC'>STIM*$^{+}$ (Fig 3.2A; Blue arrow, out of batches of 25 animals 5±1 adults eclosed) marked neurons was substantially lower, indicating a higher requirement for STIM function in THD'-marked dopaminergic neurons. This observation reinforces the essential role of STIM in dopaminergic neurons rather than in hypoderm, as confirmed by the survival rate of *STIM*^{KO} animals.

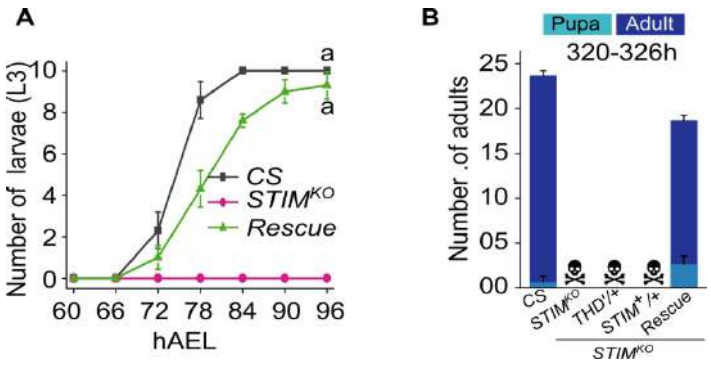

Figure 3.3: *STIM*^{KO} development profile under *THD'>STIM*$^{+}$ rescue condition

A. Number (mean ± SEM) of 3rd instar larvae (L3) are restored close to wildtype (CS) levels by expression of *STIM*$^{+}$ in *THD'* cells of *STIM*^{KO} larvae (rescue). Larvae were monitored

at 6h intervals from 66h to 96h AEL. Number of sets (N) = 3, number of larvae per set (n) = 10. Letters represent statistically similar groups for the 90h and 96h time point.

B. Stack bars with the number of adults (mean ± SEM) that eclosed at 320 to 326h AEL from the indicated genotypes. The genotype of rescue larvae is *STIM^{KO}; THD'>STIM^{+}*. Number of sets (N) = 3, number of organisms per set (n) = 25.

Given the observed impact of *STIM^{KO}* on feeding, dye feeding and mouth hook contraction assays were conducted. Under the *THD'>STIM^{+}* rescue condition, both assays demonstrated a rescue in dye uptake and mouth hook contractions, confirming improvements in food ingestion and increased mouth hook contraction frequency resulted in the rescue of the *STIM^{KO}* larval growth defect (Fig. 3.6 A-C).

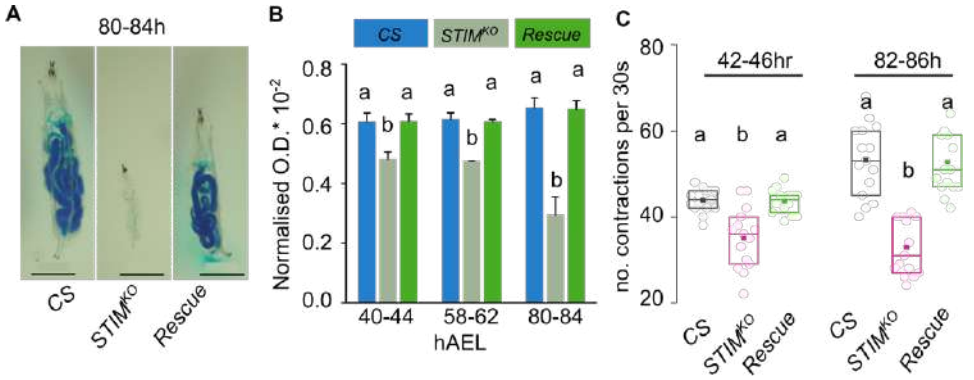

Figure 3.4: Overexpression of *STIM^{+}* in THD' cells rescues *STIM^{KO}* feeding defect

A. Representative images of dye-fed larvae of *CS, STIM^{KO}* and rescue (*STIM^{KO}; THD'>STIM^{+}*) genotypes at 80-84h AEL Scale bar = 1mm.

B. Bar graph with quantification of ingested food containing a blue dye in larvae of the indicated genotypes (*CS, STIM^{KO}* and *STIM^{KO}; THD'>STIM^{+}* rescue) at the indicated developmental times. Mean (mean ± SEM) optical density (655nM) of blue dye in larval lysates after normalizing to larval protein concentration (OD/Protein conc. X 10^{-2}) was obtained from 6 feeding plates (N) each containing 10 larvae (n). Different alphabet represent statistically significant groups.

C. Expression of *STIM^{+}* in THD' cells rescues the feeding behaviour deficit of *STIM^{KO}* larvae. Box graph with quantification of larval mouth hook contractions of the indicated genotypes (*CS, STIM^{KO}* and *STIM^{KO}; THD'>STIM^{+}* rescue). Circles represent single larvae in the box graph of 25th and 75th percentiles with the median (bar), and mean (square). Number of larvae per genotype per time point is (n) ≥10. Different alphabet represent statistically significant groups.

3.3.2: STIM function in THD' dopaminergic neurons is essential to regulate the overall growth rate of an organism.

Following the significant rescue observed with THD', next I investigated its expression pattern throughout the larval body under *THD'>mCD8GFP*. Examination of GFP positive cells revealed that *THD'GAL4* expresses in the

brain, posterior, and anterior spiracles, with no other tissues expressing GFP. In the brain, GFP-positive cells were observed in both the CNS and ventral ganglia, with each lobe containing two clusters (3 and 2 cells) of GFP-positive cells and 3 to 4 GFP-positive cells in the ganglia (Fig. 3.4A)

Further to verify the dopaminergic identify, immunohistochemistry against the TH protein was done. IHC revealed two classes of GFP-positive cells were identified in the larval brain: all GFP-expressing cells in DL1 and DL2 cluster of in the central brain were positive for tyrosine hydroxylase (TH), while a pair of THD' cells in the ventral ganglion were TH^{-ve} (Fig.3.4A, II).

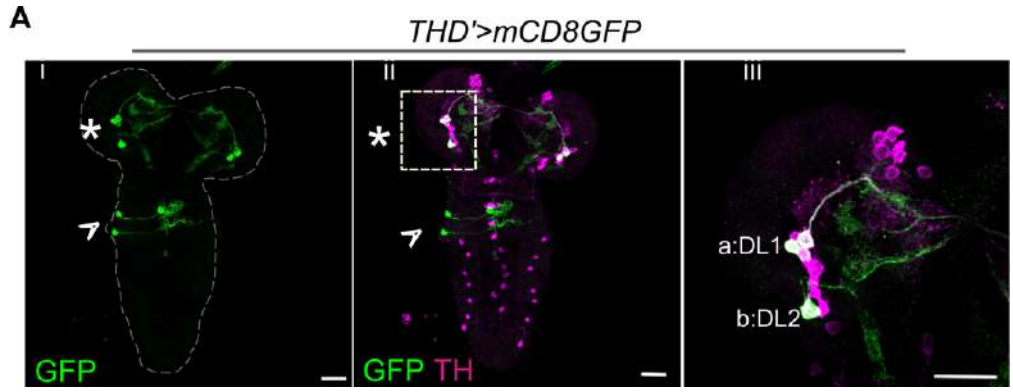

Figure 3.5: Expression profile of THD'GAL4 showing two different cellular identity.

A. Representative confocal images of the larval brain from animals of the genotype *THD'>mCD8GFP*. Anti-GFP (green) indicates the expression of *THD'GAL4* and anti-TH (magenta) marks all dopaminergic cells. Asterisks mark TH^{+ve} cells in CNS whereas arrowheads mark non-TH positive cells in ventral ganglia of larval brain (i and ii). DL1 and DL2 clusters in the central brain of three and two dopaminergic cells respectively are marked (iii). Scale bars = 20µm.

To evaluate the significance of TH^{-ve} cells localized in the ventral ganglia in the rescue of $STIM^{KO}$ animals by *THD'*>$STIM^{+}$, the UAS/GAL4/GAL80 tri system was utilized. Through the use of *THGAL80* (Sitaraman et al., 2008), the expression of *THD'GAL4* was restricted to THD' neurons in the ventral ganglia (Fig. 3.5A). Staging experiments demonstrated a notable decrease in the rescue of $STIM^{KO}$ larvae, which persisted into adulthood (Fig. 3.2A; red arrow, Fig3.5B and C). This underscores the essential involvement of brain-specific THD's dopaminergic neurons in the viability rescue of $STIM^{KO}$ animals. Following the cell screening, a specific subset of dopaminergic neurons within the central nervous system (CNS) was identified, where the *THD',THGAL80>*$STIM^{+}$ proved TH^{+ve} cells are sufficient to rescue the larval

lethality associated with *STIM*^{KO} (Fig. 3.5B and C). This finding shows how important STIM-dependent function is for an organism's normal growth, especially in dopaminergic neurons that have been marked with THD'.

To further validate the significance of STIM function in THD'-marked dopaminergic neurons, I employed the RNAi method to knock down STIM using a previously characterized *UASSTIMRNAi* (*dsSTIM*) (Venkiteswaran & Hasan, 2009). Staging experiments were conducted to assess the normal developmental pattern, scoring for the number of viable organisms and their developmental stage at specified times

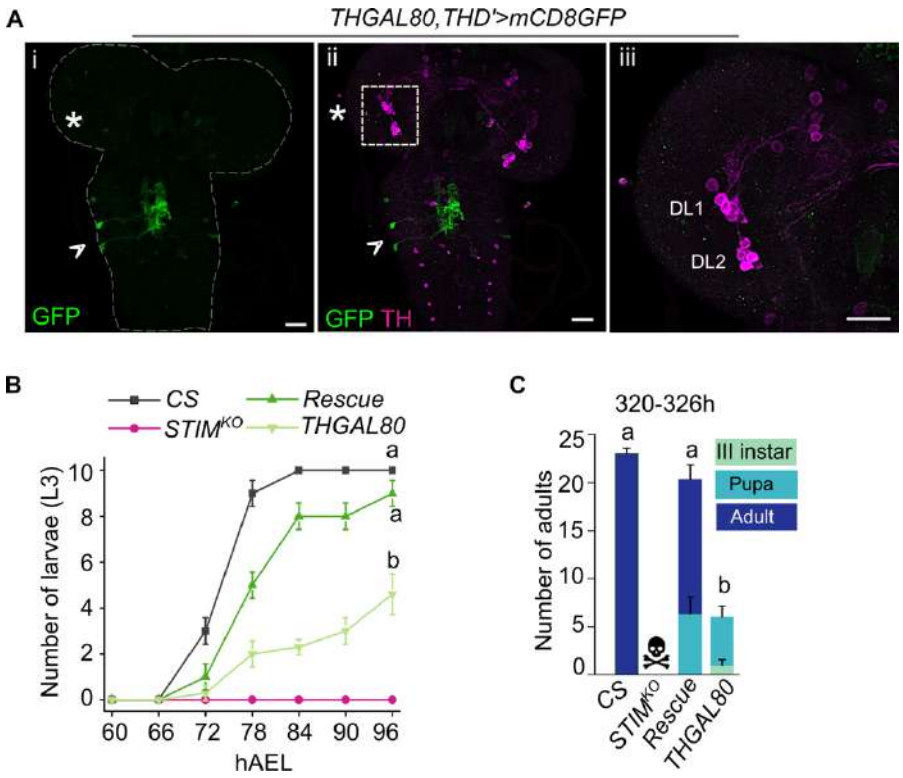

Figure 3.6: *STIM*^{KO} rescue under restrictive *THD'GAL4* expression is reduced.

A. Representative confocal images of the larval brain from animals of the genotype *THGAL80,THD'>mCD8GFP*. *THD'GAL4* driven GFP expression (green) is suppressed in DL1 and DL2 clusters in the CNS (asterisk) by *THGAL80* but not in the ventral ganglia (arrowheads). Scale bar = 20µm.

B. Line graph shows the number (mean ± SEM) of 3rd instar larvae from *CS, STIM*^{KO}, *STIM*^{KO}*;THD'>STIM*$^{+}$ *and STIM*^{KO}*;THGAL80,THD'>STIM*$^{+}$ at 6h intervals between 60 to 96h AEL. Number of sets (N) = 3, number of larvae per set (n) = 10. Different alphabet represent statistically significant groups for 84h, 90h and 96h.

C. Stack bar graph showing the number of adults eclosed (mean ± SEM) at 320 to 326h AEL from *CS (*wildtype*), STIM*^{KO} (mutant), *STIM*^{KO}*;THD'>STIM*$^{+}$ (rescue) and *STIM*^{KO}*;THGAL80,THD'>STIM*$^{+}$ (THGAL80 - restrictive rescue) genotypes. Different alphabet represent statistically significant groups. Number of sets (N) = 3, number of organisms per set (n) = 25.

. A comprehensive staging analysis revealed a developmental delay in *THD'>dsSTIM* animals compared to the controls (Fig. 3.7A), although no larval lethality was observed. Close monitoring of larval development at six-hour intervals from 60 to 96 hours indicated a 12-hour delay in moulting from the 2nd instar to the 3rd instar in *THD'>dsSTIM* animals, impacting the subsequent developmental phases (Fig. 3.7B).

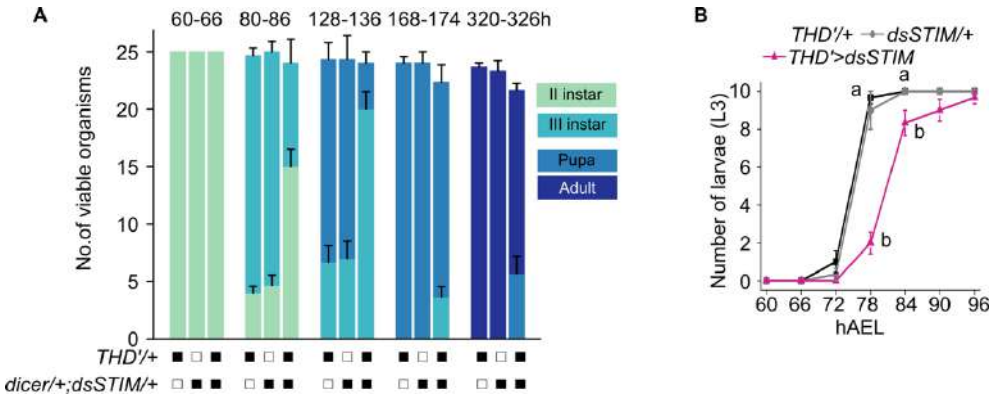

Figure 3.7: Developmental profile of *Drosophila melanogaster* under *THD'>Dicer,dsSTIM* genetic condition

A. Stack bar graph showing the number of viable organisms (mean ± SEM) and their developmental stage at specified hours after egg laying for the indicated genotypes; *THD'/+, dicer;+;dsSTIM/+* (controls) and *THD'>dicer,dsSTIM*. Number of sets (N)=3, number of organisms per set (n)=25.

B. Number of 3rd instar larvae (mean ± SEM) from RNAi knockdown of STIM+ in THD' neurons (*THD'>dsSTIM*) along with control genotypes *THD'/+* and *dsSTIM/+* at 6h intervals between 66h to 96h AEL. Number of sets (N) = 3, number of larvae per set (n) = 10. Different alphabet represent statistically significant groups.

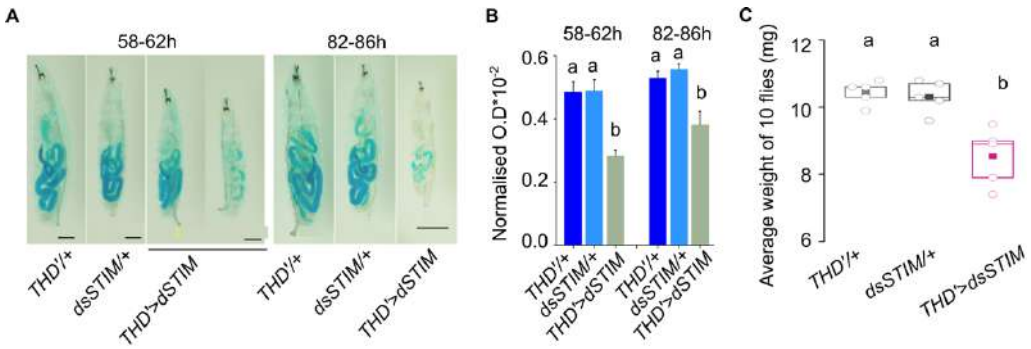

Figure 3.8: *THD'>dsSTIM* affects normal larval feeding

A. Representative images of dye-fed larvae of the indicated genotypes at 58-62h and 82-86h AEL. Scale bar = 200µm.

B. Quantification (mean ± SEM) of blue dye containing ingested food (OD/Protein concentration X 10^{-2}; similar to panel D above) in larvae of the indicated genotypes at 58-62h and 82-86h AEL. No. of plates for each time point, (N) = 3, number of larvae per plate (n) = 10.

C. Quantification of weight of 10 flies from indicated genotypes. Box plots show the 25th and 75th percentiles with median (bar), mean (square) and each circle represents one set. Each set consists 10 flies of which 5 are females and 5 are male adult flies collected at 6-8h after eclosion. Number of set (N) ≥5. Alphabets indicate different statistical groups.

Taking into account that *STIM^{KO}* affects food ingestion, coupled with the observed developmental delay in *THD'>dsSTIM* (Fig. 3.8A and B), I proceeded to assess the feeding capacity of *THD'>dsSTIM* larvae at 58–62h and 82–86h AEL. As anticipated, both time points revealed a noticeable decrease in food intake in *THD'>dsSTIM* larvae compared to the genetic controls (Fig. 3.8A and B). Given the established connection between larval food intake and adult size and fecundity, I measured the weight of adult flies aged 6–10h post-eclosion (a total of 10 flies per set: 5 males and 5 females). The results of this experiment revealed a reduction in the overall body weight of the flies (Fig. 3.8C**)**.

3.3.3: THD' neurons tune larval growth by enhancing the feeding frequency

The specific rescue of *STIM^{KO}* by THD' neurons and the knockdown of *STIM* in THD' neurons cells highlight the crucial role of THD' neurons in normal larval development. As these neurons are dopaminergic, I further investigated whether the reduced feeding observed in *STIM^{KO}* larvae is a result of impaired dopamine signaling. To confirm this, in wild-type larvae, I reduced dopamine levels by silencing the key dopamine-synthesis enzyme Tyrosine Hydroxylase (TH) in THD's cells.

The knockdown of *TH* resulted in a notable decrease in mouth hook contractions in larvae at 80–86h AEL, indicating reduced feeding (Fig. 3.9C). This was accompanied by a slower progression through larval moults and some mortality at each larval stage (Fig. 3.9A). Ultimately, out of 25 larvae, only 20±1.2 successfully reached the third instar stage and pupated, with 15 adults emerging (Fig 3.9A). Consistent with lower nutrient intake during the larval stages, third-instar larvae exhibited smaller size and gave rise to adults with significantly reduced body weight (Fig 3.9B, D and E).

The results obtained from the *THD'>dsTH* experiment unequivocally highlighted the involvement of dopaminergic signaling in the observed phenotypes. Subsequently, the investigation sought to ascertain whether rescuing the lethality associated with *STIM^{KO}* could be achieved by restoring

the dopamine signaling pathway. This was pursued through both genetic and pharmacological approaches.

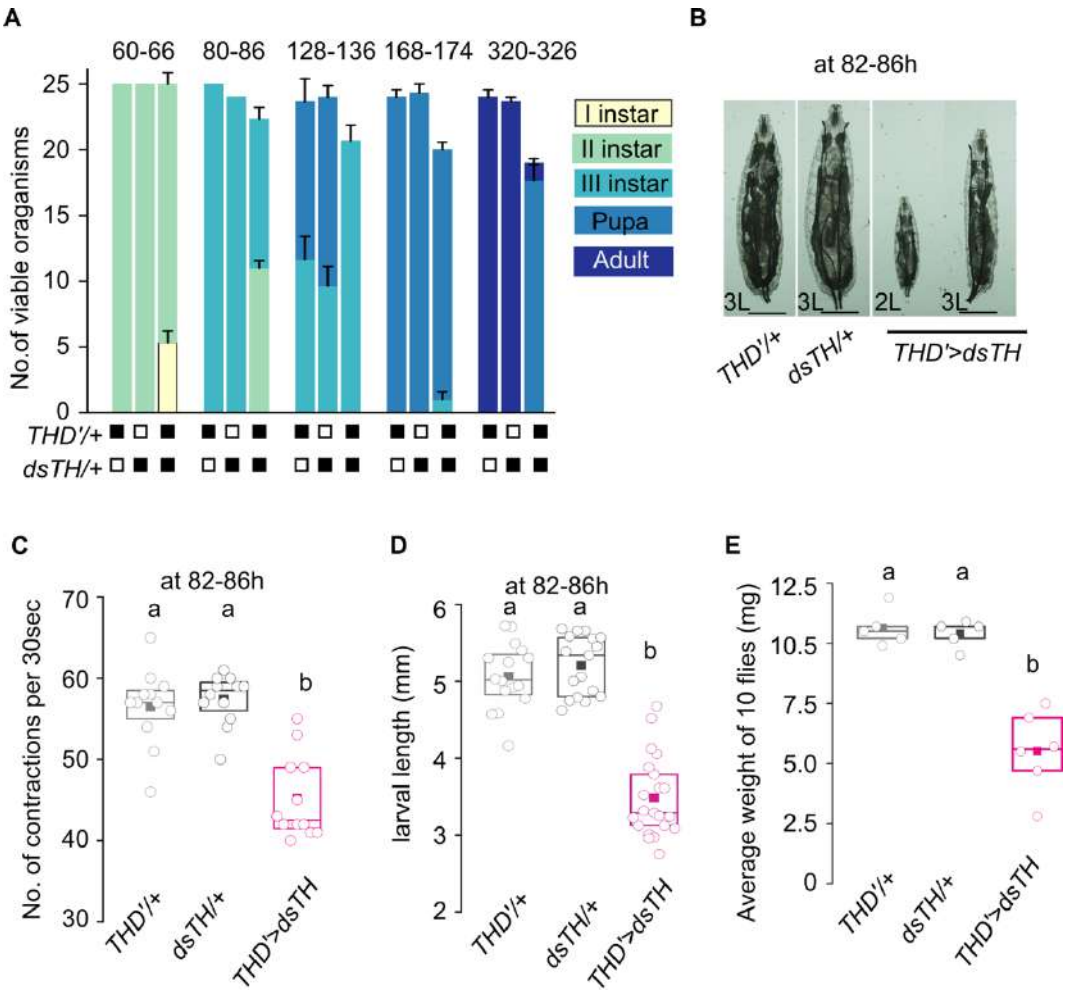

Figure 3.9: Dopamine signaling from THD' cells regulates larval development by modulating the feeding rate

A. Stack bar graph showing the number of viable organisms (mean ± SEM) and their developmental stage at specified hours after egg laying for the indicated genotypes *THD'/+, dsTH/+* (controls), and *THD'>dsTH*. Number of sets (N)=3, number of organisms per set (n)=25. Significant changes were calculated by one way ANOVA followed by post-hoc Tukey's test.

B. Representative images of larvae with knockdown of Tyrosine Hydroxylase (*THD'>dsTH*) and controls (*THD'/+, dsTH/+*) at 82-86h. Scale bar = 1mm.

C. Larval mouth hook movements that correlate with feeding are reduced in larvae with reduced dopamine synthesis in THD' neurons. Box graph with quantification of mouth hook contractions in larvae with knockdown of Tyrosine Hydroxylase (*dsTH*) in THD' neurons and appropriate control genotypes. Number of larvae per genotype per time point is (n) ≥10.

D. Quantification of larval length from the indicated genotypes. n≥15.

E. Quantification of weight of 10 flies from the indicated genotypes. Each circle represents one set of adult flies consisting of 5 females and 5 males, 6-8h post-eclosion. A minimum of 5 sets were measured for each genotype.

In the genetic rescue attempt, I sought to bring back dopamine synthesis by overexpressing tyrosine hydroxylase (TH) in THD's neurons. TH, being a rate-limiting enzyme in the dopamine synthesis pathway, was expected to play a key role. However, the overexpression of *UASTH1cDNA* (*TH1*$^{+}$) (Friggi-Grelin et al., 2003) in THD' neurons did not result in the rescue of *STIM*^{KO} larval lethality (Fig. 3.10A). This outcome suggested that the potential rescue might lie downstream in the dopamine synthesis pathway.

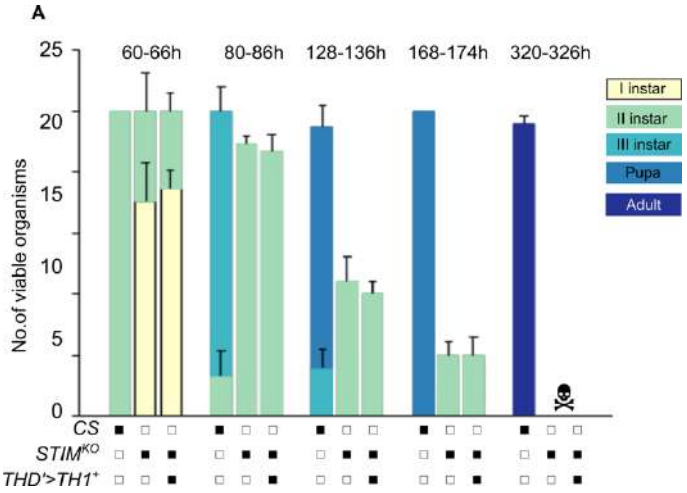

Figure 3.10: Overexpression of *TH* in THD' neurons fails to rescue *STIM*^{KO}

A. Stack bar graph showing the number of viable organisms (mean ± SEM) and their developmental stage at specified hours after egg laying for the indicated genotypes *THD'/+, dsTH/+* (controls), and *THD'>dsTH*. Number of sets (N)=3, number of organisms per set (n)=25. Significant changes were calculated by one way ANOVA followed by post-hoc Tukey's test.

Given the lack of rescue with *THD'>TH1*$^{+}$, the next approach involved external administration of the dopamine precursor L-DOPA. This well-established treatment is known to elevate endogenous dopamine levels (Cha et al., 2005; Szczypka et al., 1999). In this experiment, along with control (*CS*) and *STIM*^{KO} larvae, a positive control, *TH>dsTH*, was included to validate the effectiveness of L-DOPA feeding. Larvae aged 6–10h AEL were transferred to media containing L-DOPA, and assessments were conducted at 92-96h AEL. The number of viable larvae and their developmental stages were recorded.

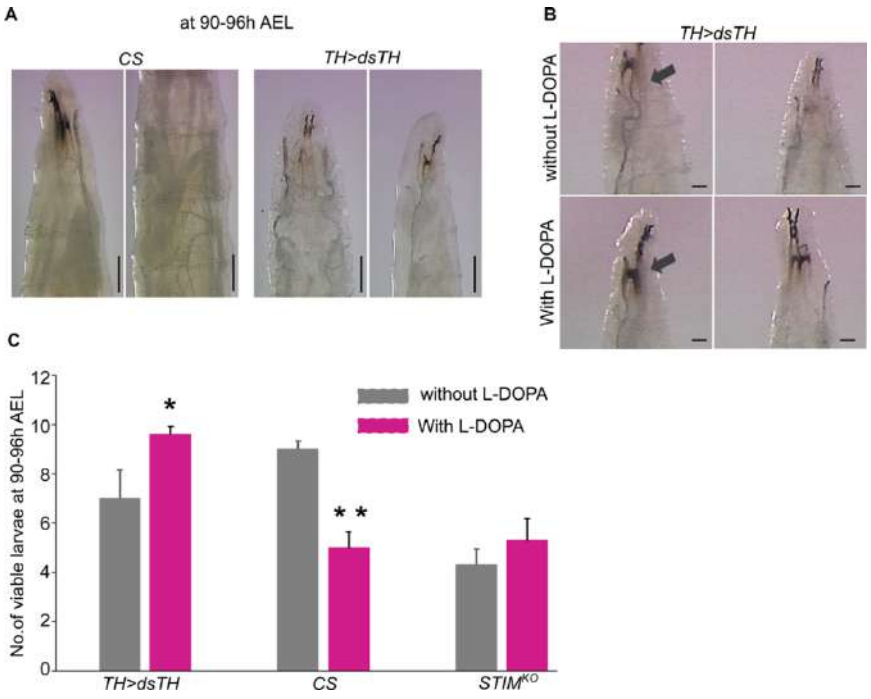

Figure 3.11: L-DOPA feeding does not rescue *STIM^{KO}*.

A. Representative image of larvae from *CS* and *TH>dsTH* at 90-96h AEL. Scale bar:1mm
B. Representative images of *TH>dsTH* larval mouth hook under with and without L-DOPA feeding. Arrow mark shows the melanin coloration at mouth hook. Scale bar: 200μm
C. Bar graph showing number of viable 3rd instar larvae at 90-96h AEL after feeding with and without L-DOPA feeding.

Results revealed a reduction in the number of L-DOPA-fed control (*CS*) larvae (9.1±0.33 and 7±1.2 viable larvae under with and without L-DOPA feeding respectively, Fig. 3.11B). possibly attributed to the toxicity of high dopamine levels. Particularly, no discernible rescue was observed in *STIM^{KO}* larvae subjected to L-DOPA feeding (5.3±0.63 and 4.3±0.55 viable *STIM^{KO}* larvae under with and without L-DOPA feeding respectively Fig. 3.11B). This observation was linked to the persistent feeding defect exhibited by *STIM^{KO}* larvae since the first instar, possibly rendering them unresponsive to L-DOPA later in development.

In contrast, *TH>dsTH* larvae exhibited a significant increase in survival compared to their non-fed counterparts (9.6±0.55 and 7±1.3 viable *TH>dsTH* larvae under with and without L-DOPA feeding respectively, Fig. 3.11B). Additionally, L-DOPA-fed *TH>dsTH* larvae displayed enhanced melanin pigmentation in the hypoderm and increased mouth hook coloration when

compared to non-fed *TH>dsTH* larvae, which had a paler appearance (Fig 3.11A and B**)**.

Further genetic experiments demonstrated that, apart from STIM overexpression, other genetic manipulations failed to rescue $STIM^{KO}$ (Table1), reinforcing the notion that STIM-dependent function is downstream of dopamine synthesis.

3.4 Discussion

It is widely recognized that the quality and quantity of nutrition acquired during the larval stage significantly impact the overall size and fecundity of adult Drosophila. Unlike the sporadic feeding pattern observed in adults, larval feeding is continuous and ceases upon entry into the wandering stage. This implies that the continuous feeding observed in larvae must override satiety signals, allowing them to continuously acquire nutrition to support robust larval growth and store nutrients for the pupal stage.

The significant rescue of $STIM^{KO}$ by THD' dopaminergic cells, along with the understanding that the primary cause of $STIM^{KO}$ larval lethality is a reduction in feeding, aligns with the phenotype exhibited by mouse pups with dopamine mutations. These pups perish due to starvation, highlighting the critical role of dopamine in regulating feeding behavior across species.

This study presents the first evidence indicating that dopamine (DA) regulates feeding in early-stage *Drosophila* larvae, building upon the well-established influence of DA on feeding in mice as well as in adult *Drosophila* (Boekhoudt et al., 2017; Kleinridders & Pothos, 2019; Landayan et al., 2018; Missale et al., 1998; Sharma & Hasan, 2020; Szczypka et al., 1999; Volkow et al., 2011; G.-J. Wang et al., 2011; Wise, 2006; Yamamoto & Seto, 2014). Specifically, in third-instar larvae, a dopaminergic-NPF circuit originating from central dopaminergic DL2 neurons, marked by *THD'GAL4*, has been shown to stimulate feeding in the presence of appetitive odors (Y. Wang et al., 2013). This highlights the necessity of THD' neuronal function throughout larval feeding.

Moreover, the observed mean frequency of mouth hook contractions in *THD'>dsTH larvae*, occurring at 82-86h AEL (Fig. 3.9C), resembles the mouth hook frequency observed in *CS* late first/early second instar larvae (Chapter 2,

Fig. 2.8E) This suggests that *THD'>dsTH* larvae consume a similar amount of food as first instar larvae, which is insufficient to support the robust growth initiated from the mid-second instar stage. Thus, dopamine from THD' neurons appears crucial for enhancing feeding frequency at later larval stages. These findings parallel previous studies where prenatal mice genetically deficient in dopamine were unable to feed and succumbed to starvation, a condition that could be ameliorated by enforced supplementation or injection with L-DOPA.

Notably, unlike mice rescued with L-DOPA feeding, both genetic approaches (overexpression of *TH* in THD') and L-DOPA feeding failed to rescue $STIM^{KO}$. This suggests that STIM function may be required downstream of dopamine synthesis and that the feeding defect in $STIM^{KO}$ larvae could affect L-DOPA availability.

In addition to the dopaminergic rescue, a significant restoration of $STIM^{KO}$ was observed under *MNScGAL4*, (Fig. 3.1) where it marks insulin producing cells (IPCs). This mirrors previous rescue patterns observed in *itpr* mutants. Notably, as demonstrated by Agrawal et al., (2009) the rescue of *itpr* mutants is particularly significant in $DdcGAL4>itpr^{+}$ (which marks both dopaminergic and serotonergic cells) compared to $MNScGAL4>itpr^{+}$.

Insulin signaling is known to govern various aspects of organismal development, growth, metabolism, feeding, and aging (Erion & Sehgal, 2013; Nässel & Zandawala, 2019, 2020). In the context of *Drosophila*, Ilp2 and Ilp5, two of the eight recognized insulin-like peptides (ILPs), play crucial roles in post-embryonic development and systemic growth. Dysfunction in either the biosynthesis or release of Ilp2 and Ilp5, or downstream insulin signaling, results in delayed development or lethality during the larval stage. Moreover, the release of Ilp2 and Ilp5 depends on the presence of sufficient nutrition in the hemolymph; otherwise, vesicles containing these peptides accumulate at presynaptic terminals (Britton et al., 2002; Brogiolo et al., 2001; Erion & Sehgal, 2013; Ikeya et al., 2002; Nässel & Broeck, 2016; Okamoto & Nishimura, 2015; Semaniuk et al., 2021). Studies have indicated that STIM is involved in both transcriptional regulation and exocytosis (Dhanya & Hasan, 2021; Richhariya et al., 2017).

The observed rescue of $STIM^{KO}$ under $MNSc>STIM^{+}$ suggests a potential rescue mechanism at the synthesis or release of ILPs into the system.

However, insights from the developmental profiles and feeding behavior of *STIM*^{KO} larvae reveal that acute feeding defects primarily contribute to systemic larval growth arrest and lethality. Study by Zhao et al, (2012) in *Drosophila* larvae have demonstrated that insulin signaling in the mushroom body affects feeding (Zhao & Campos, 2012). Therefore, the rescue by overexpression of *STIM* in MNSc cells implies that STIM may regulate either the synthesis or release of ILPs, subsequently rescuing the feeding defect.

Overall, these findings underscore the intricate relationship between STIM, dopaminergic, and insulin signaling pathways, which collectively regulate larval development. They emphasize the necessity for further investigation into the underlying mechanisms to fully comprehend the complexity of these interactions.

Chapter 4: The importance of THD' neuronal function in *Drosophila* larval development

4.1 Introduction

The preceding chapter established that THD' neurons are adequate for rescuing $STIM^{KO}$ larval lethality to a larger extent. Understanding how the function of THD' neurons is affected in the absence of STIM becomes imperative for deciphering the intricate network governing larval development. examination to elucidate the functional alterations within THD' neurons under the context of $STIM^{KO}$. This endeavour aims to provide critical insights into the sequence of changes leading to the observed rescue. By providing a thorough account of these mechanisms, this chapter aims to contribute crucial knowledge to the broader understanding of the intricate interplay between STIM, THD' neurons, and the developmental processes in *Drosophila* larvae.

4.2 Materials and Methods

4.2.1 Fly stocks

Fly strains		
THD'GAL4	Marks subgroup of Dopaminergic cells in larval brain	Mark N Wu, Johns Hopkins University, Baltimore
UASGCaMP6m	Ca^{2+} Sensor with intermediate kinetics expresses under UAS	RRID: BDSC_42748
UASSyt-eGFP,Denmark	Syt-eGFP marks presynaptic terminals and Denmark (mCherry) marks post synaptic part of the neuron.	RRID: BDSC_33065
$UASGRAB_{DA}$	A Genetically Encoded Fluorescent Sensor for Dopamine	Yulong Li, Peking University School of Life Sciences, Beijing, China
UASERGCaMP-210	ER specific Ca^{2+} sensor	Cahir O'Kane, Can University, UK
UASNaChBac	Increases sodium conductance and therefore activates the neuron	RRID: BDSC_9468

dsSTIM (III)	UAS-RNAi against Stim gene	VDRC_47073
UASKir2.1	Prevents membrane depolarization	RRID: BDSC_6595
UASmCD8GFP	Expresses membrane tagged GFP under UAS control	RRID: BDSC_5130
UASSTIM+	*Stim* wildtype cDNA under UAS control	Generated in the lab
$STIM^{KO}$; THD'GAL4/CyOG; +	Strains and recombinant lines made for this study	
$STIM^{KO}$; UASGCaMP6m/CyOG; +		
$STIM^{KO}$;THD'GAL4,GCaMP6m /CyoG;+		
$STIM^{KO}$; UASmCD8GFP/CyOG; +		
UAS-STIM+/CyOG; $UASGRAB_{DA}$/Tb		
UAS-STIM+/CyOG; UASERGCaMP-210/Tb		

4.2.2 Fly rearing

As described in chapter 2

4.2.3 Staging

As described in chapter 2

4.2.4 Immunohistochemistry

As described in chapter 2.

4.2.5 Ex-vivo imaging of the larval brain

GCaMP signals were obtained from appropriately aged larval brains dissected from the specified genotypes and dissected in hemolymph like saline (HL3) (70mM NaCl, 5mM KCl, 20mM MgCl2, 10mM NaHCO3, 5mM trehalose, 115mM sucrose, 5 mM HEPES, 1.5mM Ca2+, pH 7.2). Dissected brains were transferred to a 35mm punched dish with a cover slip adhered to the bottom. Brains were embedded in ~5µl of 0.8-1% ultrapure low

melt agarose (Invitrogen, Cat#16520-100) and bathed in 86µl of HL3. Images were acquired as a time series on an XY plane at an interval of 2sec using a 20X-oil objective on an Olympus FV3000 inverted confocal microscope (Olympus Corp., Japan). For KCl stimulation, at the 40th frame, 7µl of HL3 was added and at the 80th frame 7µl of 1M KCl was added. The final concentration of KCl in the solution surrounding the brain was 70mM. For stimulation with Carbachol (Sigma Aldrich Cat# C4382), 10µl of HL3 was added at the 40th frame followed by 10µl of 100mM Carbachol at the 80th frame. Final carbachol concentration was maintained at 1mM and Ca^{2+} responses were acquired till the 300th frame (600sec).

Changes in ER-Ca^{2+} were measured using an ER-GCaMP-210 strain (Oliva et al., 2020). The brain sample was prepared as above. Images were acquired as a time series on an XY plane at an interval of 1 sec using a 20X oil objective on an Olympus FV3000 inverted confocal microscope (Olympus Corp., Japan). For Carbachol stimulation, 10µl of HL3 was added at the 50th frame and 10µl of 100mM of Carbachol was added at the 100th frame. Final carbachol concentration was maintained at 1mM. Images were obtained for 600 frames (600 secs).

4.2.6 Quantification and Statistical Analysis

All bar graphs and line plots show the means and standard error of means. In boxplots, horizontal lines in the box indicate median, box limits are from 25th-75th percentiles, and individual data points are represented by closed circles (unless otherwise specified in the figure legends). Unpaired student t-Test (for two genotypes) and one way ANOVA followed by post-hoc Tukey's significance test (for data with multiple genotypes) was performed to calculate P values, given for all figures in **S2 Table.** All graphs were plotted using Origin 8.0 software. Origin 7.5 MicroCal, Origin Lab, Northampton, MA, USA N/A, Fiji Open access (RRID:SCR_002285).

4.3 Results

4.3.1 THD’ neuronal activity requires STIM function.

In this chapter, I investigated how THD' neurons exert regulatory effects and contribute to the rescue of *STIM*^{KO} larval lethality. As an initial step, I scrutinized the physical status of the cells to ascertain whether any neurodegeneration had occurred. For analysis, *STIM*^{KO} larval brains at 80–84h AEL were chosen, considering the presence of a few viable organisms despite the cessation of growth and feeding. Here, cells were marked with the fluorescence protein GFP, followed by staining the brain tissues with anti-TH sera. Confocal imaging of both DL1 and DL2 cells of THD' central brain dopaminergic cell clusters from control (*THD’>mCD8GFP*), *STIM*^{KO} larvae (*STIM*^{KO};*THD'>mCD8GFP*), and *STIM*^{KO} rescue (*STIM*^{KO}*;THD’>mCD8GFP, STIM*$^{+}$) revealed that *THD'>mCD8GFP* cells displayed no noticeable differences in *STIM*^{KO} and *STIM*$^{+}$ rescued animals at 80–84h AEL, compared to controls at either 58–62h or 80–84h AEL (Fig. 4.1A). Additionally, the numbers of THD' GFP cells and TH^{+ve} cells in the central nervous system remained consistent (Fig. 4.1B). These findings show that the loss of STIM does not lead to the loss of dopaminergic neurons in the larval brain.

Imaging of THD' cells made it evident that the cellular integrity remained intact. Given the inability of genetic means, specifically the overexpression of *TH1*$^{+}$, to rescue *STIM*^{KO} lethality (as discussed in Chapter 3), it strongly suggests that the functional impairment lies downstream of dopamine synthesis. Drawing insights from literature highlighting the impact of altered STIM function on neuronal activity and exocytosis (Dhanya & Hasan, 2021; Richhariya et al., 2017), I aimed to analyse both the excitability property and dopamine release in THD' neurons. Subsequently, I proceeded to examine the neuronal excitability of THD’ neurons.

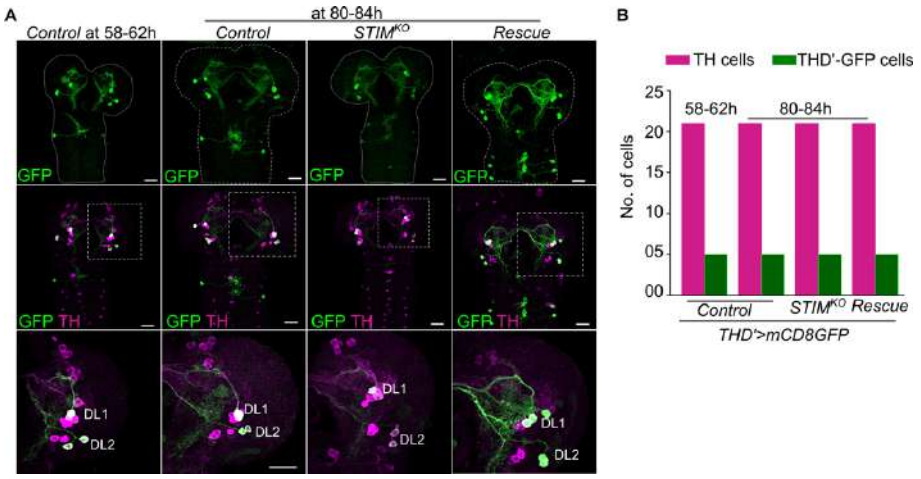

Figure 4.1: Absence of STIM does not affect cells integrity.

A. Representative confocal images of larval brains showing THD' neurons marked with anti-GFP (green) and anti-TH (red) from control (*THD'>mCD8GFP*), *STIM^{KO}* (*STIM^{KO}*; *THD'>mCD8GFP)* and rescue (*STIM^{KO};THD'>mCD8GFP, STIM^{+}*) animals at the indicated developmental time points. Scale bars = 20µm.

B. Numbers of TH positive cells (magenta) and THD' cells (green) in the larval CNS of the indicated genotypes. Cells were quantified from *THD'>mCD8GFP* (control) at 58-62h and 80-84h and from *STIM^{KO};THD'>mCD8GFP* (*STIM^{KO}*) and *STIM^{KO};THD'>mCD8GFP, STIM^{+}* (rescue) at 80-84h. The numbers of TH^{+ve} and GFP^{+ve} cells were counted manually and were no different among four hemi-lobes from four brains of a single genotype and among all brain hemi-lobes of all genotypes. Hence the absence of error bars.

Due to the minute size of *Drosophila* larval neurons, conventional electrophysiological methods presented challenges in measuring neuronal excitability. Instead, I employed the well-established genetic tool *UASGCaMP6m* to monitor cytoplasmic Ca^{2+} dynamics. GCaMP6m, a genetically encoded calcium indicator (GECI), was utilised to observe changes in cytoplasmic calcium levels. Under the *THD'>GCaMP*, potassium chloride (KCl, 70 mM)-induced cytosolic calcium transients were measured in the ex vivo preparation of larval brains as explained in (Jayakumar et al., 2016b) from similarly staged control (58-62h AEL) and *STIM^{KO}* (70-74h AEL) larvae. At 70-74h AEL, the *STIM^{KO}* larvae exhibited a healthy appearance and were developmentally comparable to the mid-second larval instar stage observed in the control larvae at 58-62h AEL (Chapter 2, Fig. 2.3D and Fig. 2.4A-B)

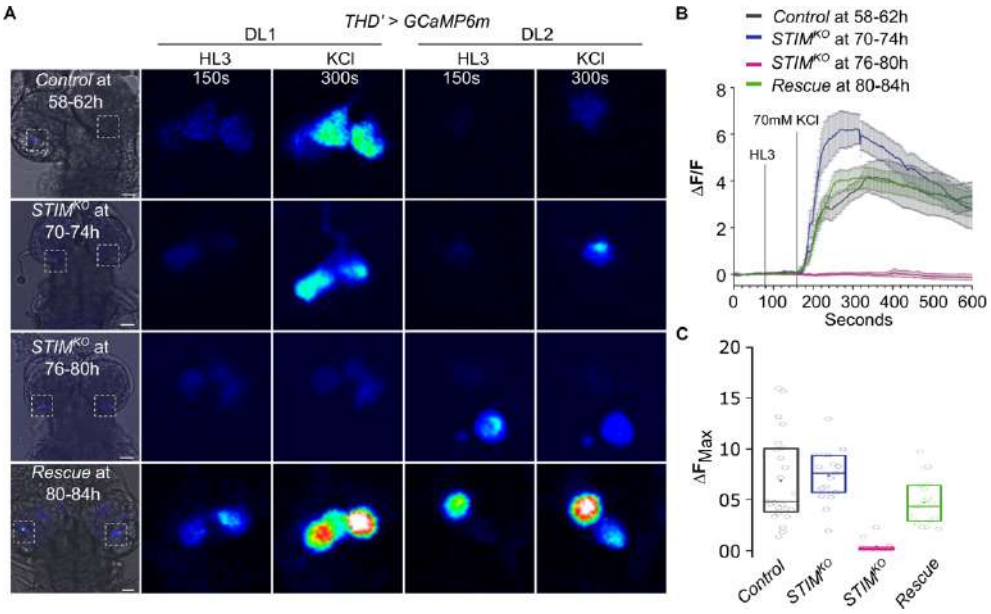

Figure 4.2: STIM modulates the activity of THD' neurons.

A. Representative images of the central brain (left panels) indicating the region of focus (boxed), followed by images of DL1 and DL2 clusters of THD' cells from two lobes of same brain with Ca^{2+} transients at the indicated time points before and after addition of a depolarizing agent (KCl – 70mM). Ca^{2+} transients were measured by changes in the intensity of GCaMP6m fluorescence from *THD'>GCaMP6m* (control), *$STIM^{KO}$; THD'>GCaMP6m*, *$STIM^{KO}$;THD'>GCaMP6m, $STIM^{+}$* (rescue). Scale bar 20µm

B. Changes in GCaMP6m fluorescence (mean ± SEM of ΔF/F) from THD' neurons of the indicated genotypes. Number of brains, (N) ≥ 5, number of cells, (n) ≥ 15.

C. Peak intensities of GCaMP6m fluorescence (ΔF) in THD' cells from the indicated genotypes. Box plots show 25th and 75th percentiles, the median (bar), and mean (square) of ΔF of each cell (small circles).

Results indicated that both DL1 and DL2 cells of *THD'GAL4* responded similarly in terms of changes in GCaMP intensity (Fig. 4.2A; representative image in second row and Fig. 4.2 B and C). Subsequent analysis at 76-80h AEL, a time point when *$STIM^{KO}$* larvae still appeared healthy, demonstrated a loss of the ability to evoke and maintain cytosolic Ca^{2+} transients both in the DL1 and DL2 cells of *$STIM^{KO}$* larvae (Fig. 4.2A; representative image in third row). To validate this STIM-dependent phenomenon, calcium dynamics were examined under the *$STIM^{+}$* rescue condition. Overexpressing STIM in these neurons effectively restored the calcium dynamics in DL1 and DL2 neurons (Fig. 4.2A; representative image in fourth row and quantifications are in Fig. 4.2B and C).

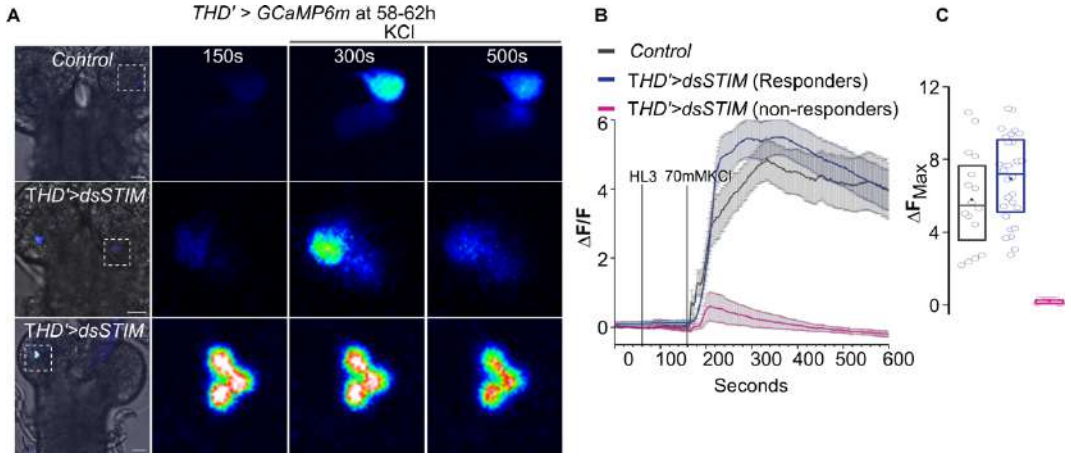

Figure 4.3: Neuronal activity requires STIM-dependent function.

A. Representative images of the central brain (left panels) indicating the region of focus (boxed), followed by images of THD' cells with Ca^{2+} transients at the indicated time points after addition of a depolarizing agent (KCl, 70mM). Ca^{2+} transients were measured in the indicated genotypes: *THD'>GCaMP6m* and *THD'>dicer;dsSTIM,GCaMP6m* by measuring changes in the intensity of GCaMP6m fluorescence. Scale bar = 20µm
B. Quantified changes in GCaMP6m fluorescence (mean ± SEM of ΔF/F) from THD' neurons of the indicated genotypes. Number of brains, (N) ≥ 6, number of cells, (n) ≥11.
C. Peak intensities of GCaMP6m fluorescence (ΔF) in THD' cells from the indicated genotypes. Box plots show 25th and 75th percentiles, the median (bar), and mean (square) of ΔF of each cell (small circles).

To ascertain the dependence of membrane excitability on STIM, I conducted experiments under the *THD'>dsSTIM* condition and measured KCl-induced cytosolic calcium transients in larval brains aged between 58-62h AEL. This time point was selected based on the observation that larvae remained visibly healthy, and deviations in developmental patterns were noted after 66 hours onward. The results revealed the presence of two distinct classes of calcium transients.

In 70% of cells, there was a normal or enhanced change in intensity compared to control cells upon KCl stimulation (Fig 4.3A; second row, and quantification in 4.3C). However, in 30% of cells, KCl failed to evoke a calcium transient (Fig. 4.4A; third row and quantification in 4.3C). This observed heterogeneity in response could be attributed to variations in the extent of STIM knockdown by RNAi within individual THD' cells. These findings contribute valuable insights into the impact of STIM on membrane excitability, underscoring the importance of individual cellular responses in the context of STIM function. All together, these findings suggest that the impact on membrane

excitability properties and the responsiveness of THD' neurons to stimuli is indeed dependent on the presence of STIM.

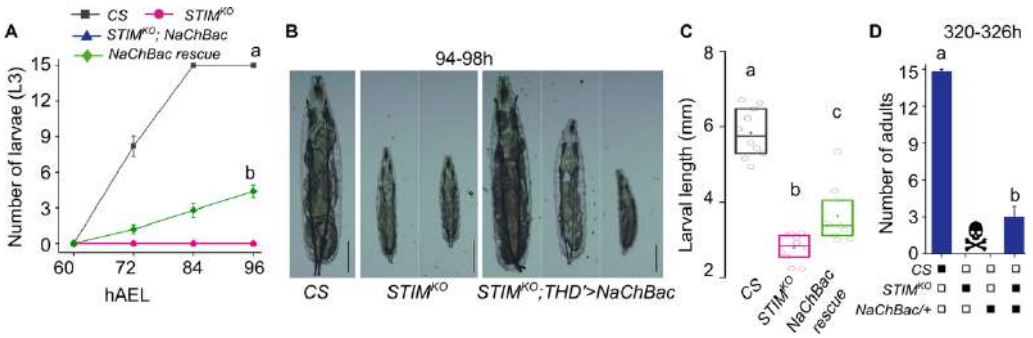

Figure 4.4: Restoring the neuronal activity of THD' neurons partially rescues *STIM^{KO}*.

A. Representative images of larvae from *CS, STIM^{KO}* and *STIM^{KO}; THD'>NaChBac* at 94-98h AEL, scale bar = 1mm.
B. Quantification of larval length from the indicated genotypes. n=10.
C. Number of adults eclosed at 320h AEL (mean ±_SEM) from wildtype (*CS),* mutant (*STIM^{KO}*) and NaChBac rescue (*STIM^{KO}; THD'>NaChBac*) animals. Numbers were obtained from three experiments (N = 3), number of organisms per experiment, n = 15.

Subsequently, the question was posed regarding whether the activity of THD' neurons, when restored in *STIM^{KO}*, could rescue larval lethality. To address this, the bacterial Na+ channel NaChBac (Nitabach et al., 2006) was overexpressed in THD' neurons of *STIM^{KO}* larvae. The introduction of NaChBac in THD' neurons of *STIM^{KO}* larvae revealed a modest rescue of developmental deficits, including a transition to third instar larvae (4.4±0.4) and adult viability (out of batches of 15 animals, 2.4±0.6) (Fig. 4.4 A-D). Despite its weak nature, the rescue by NaChBac remained consistently observed.

4.3.2 Dopamine release and ER-Ca^{2+} homeostasis are affected in the *STIM^{KO}*

Neuronal excitability plays a crucial role in neurotransmitter release at presynaptic terminals. Given the complete abolition of neuronal activity in *STIM^{KO}*, I hypothesized that this would likely impact neurotransmitter release. To explore this, first, the pre- and post-terminals of THD' neurons were identified using SyteGFP and Denmark, where they mark the pre-synaptic (green) and post-synaptic (red) terminal regions, respectively (Fig. 4.5A, panel a and b). Analysis of pre-synaptic regions revealed three distinct areas in the CNS: one at the centre corresponding to the mushroom body, a branched form in the

basomedial protocerebrum, and punctae spread across the esophageal regions (Fig. 4.5A, panel c and d).

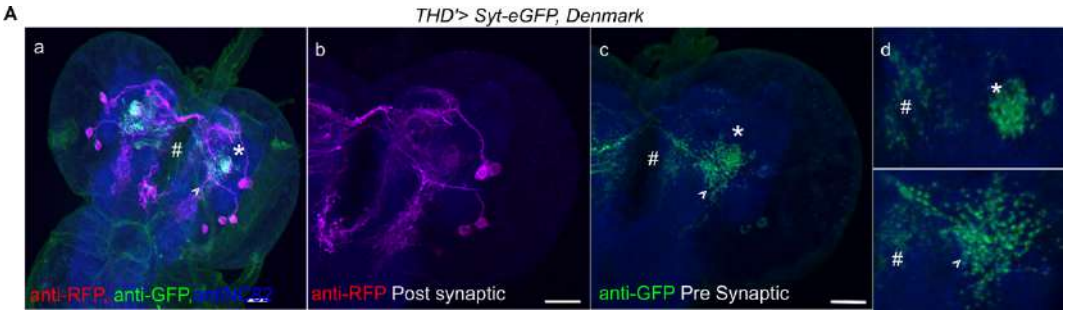

Figure 4.5: Pre- and post-synaptic terminals' anatomic patterns of THD' neurons.

A. Axonal and dendritic projections of THD' neurons visualized by expression of SyteGFP (green) and Denmark (anti-RFP, magenta) respectively in a representative brain immunostained for anti-Brp (blue). Panels marked as (d) contain magnified images from (c) of presynaptic terminals (green) located at the base of the mushroom body in the CNS (asterisk), as branches extruding into basomedial protocerebrum of the CNS (arrowhead) and as punctae near the oesophageal region (hash).

With this information, the genetically encoded fluorescent GPCR-activation-based Dopamine sensor ($GRAB_{DA}$) (Sun et al., 2018)was used to measure the dopamine release at prominent presynaptic areas (corresponding to the mushroom body and basomedial protocerebrum) of THD' neurons. Dopamine release in $STIM^{KO}$ larvae at 76-80h (This time point was selected because at this juncture, the KCl-evoked GCaMP transients were found to be abolished (Fig. 4.2A, 3rd row)) was significantly reduced compared to controls (Fig 4.6A and B); this attenuated dopamine release was rescued by the overexpression of $STIM^{+}$, though with altered dynamics (Fig. 4.6B).

Since dopamine (DA) release was stimulated by carbachol (CCh), an agonist for the muscarinic acetylcholine receptor (mAChR), that links to Ca^{2+} release from ER-stores through the ER-localised IP_3 receptor (Luo et al., 2001) and is expressed on THD' neurons (Sharma & Hasan, 2020). CCh-induced changes in ER-Ca^{2+} were tested directly by introducing an ER-Ca^{2+} sensor (Oliva et al., 2020) in THD' neurons. Though ER-Ca^{2+} release in response to CCh could be measured in just 7 out of 23 cells, the subsequent step of ER-store refilling, presumably after store-operated Ca^{2+} entry into the cytosol through the STIM/Orai pathway, could be observed in all control THD' cells (58–62h AEL), whereas it was absent in THD' neurons from $STIM^{KO}$ brains (76–80h AEL).

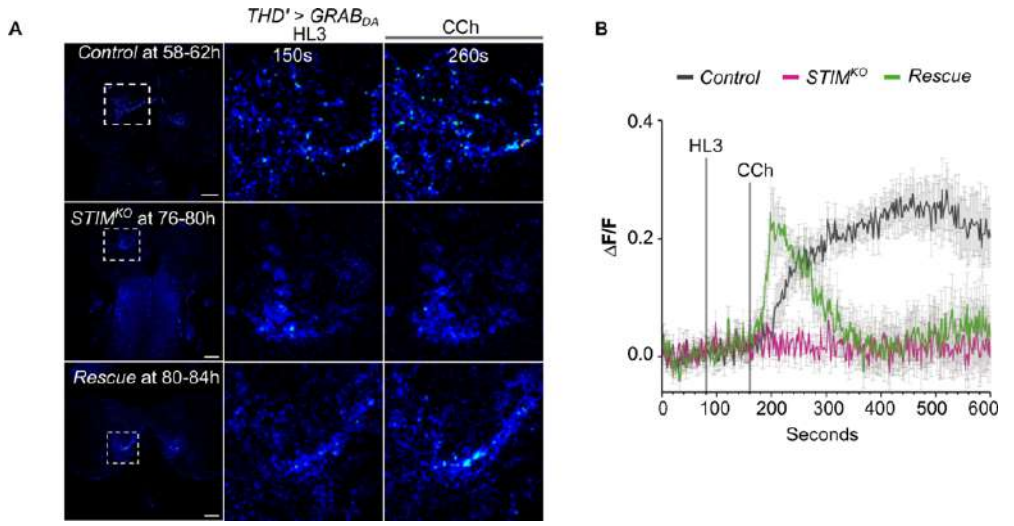

Figure 4.6: At the presynaptic terminals of the neurons, dopamine release requires STIM function.

A. Representative images of dopamine release before and after addition of Carbachol (CCh) as measured by changes in intensity of $GRAB_{DA}$ at the presynaptic terminals of THD' neurons of control (*THD'>GRAB$_{DA}$*), *STIM^{KO}* (*STIM^{KO};THD'>GRAB$_{DA}$*) and rescue (*STIM^{KO};THD'>GRAB$_{DA}$, STIM^{+})* genotypes. Scale bar = 20mm

B. Normalized changes in fluorescence (ΔF/F) of $GRAB_{DA}$ measuring dopamine release from THD' neurons of control (*THD'>GRAB$_{DA}$*), *STIM^{KO}* (*STIM^{KO};THD'>GRAB$_{DA}$*) and rescue (*STIM^{KO};THD'>GRAB$_{DA}$, STIM^{+})* genotypes. Traces show the average change in $GRAB_{DA}$ florescence (mean ± SEM of (ΔF/F)) measured from individual presynaptic regions of interest (≥10) taken from N ≥ 6 brains of each genotype.

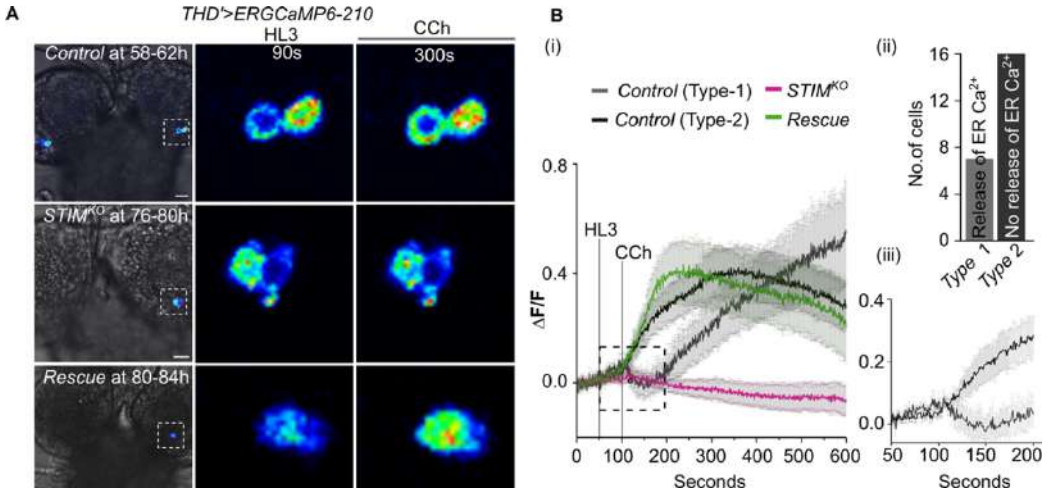

Figure 4.7: In *STIM^{KO}*, ER calcium homeostasis is affected.

A. Representative time series images of ER calcium transients as measured by changes in intensity of ER-GCaMP in THD' neurons of control (*THD'>ER-GCaMP-210*), *STIM^{KO}* (*STIM^{KO};THD'> ER-GCaMP-210)* and rescue (*STIM^{KO};THD'> ER-GCaMP-210, STIM^{+}*) genotypes.

B. (i) Traces of normalized ER-GCaMP (ΔF/F) responses (mean ± SEM) from THD' neurons of the indicated genotypes. Control (*THD'>ER-GCaMP-210*) Type 1, indicates cells that exhibit ER-Ca^{2+} release upon CCh addition followed by refilling of ER-stores. Control Type 2 indicates cells where ER-Ca^{2+} release was not evident. Rescue indicates *STIM^{KO}*;

THD'>ERGCaMP-210,STIM^{+}. For each genotype, number of cells (n) ≥ 15 and N ≥ 5 brains.

(ii) Quantification of control cells that exhibit ER Ca^{2+} release (Type 1) and cells where ER Ca^{2+} release was not observed (Type 2). (iii) Boxed region from (i) enlarged to show ER Ca^{2+} response of Type 1 and Type 2 control cells.

The ER-Ca^{2+} response was rescued by over-expressing *STIM*$^{+}$ in THD' neurons (Fig. 4.7A and B). The absence of an ER-GCaMP response in *STIM*^{KO} indicates a potential disruption in ER-Ca^{2+} homeostasis due to the lack of STIM. Consequently, under STIM deficiency, there may be a loss of IP_3-mediated Ca2+ release. Rescuing *STIM*^{KO} partially through NaChBac overexpression implies the significance of sustaining THD' neuron activity in larval development. To validate the impact of altered THD's neuronal activity on normal larval growth, I genetically manipulated neuronal function by employing Kir2.1 (Nitabach et al., 2002) and NaChBac channels for reducing and increasing membrane excitability, respectively.

4.3.3 THD' activity undergoes stage-specific regulatory changes during development

Rescuing *STIM*^{KO} partially through *NaChBac* overexpression implies the significance of sustaining THD' neuron activity in larval development. To validate the impact of altered THD's neuronal activity on normal larval growth, I genetically manipulated neuronal function by employing Kir2.1 (Nitabach et al., 2002) and NaChBac channels for reducing and increasing membrane excitability, respectively.

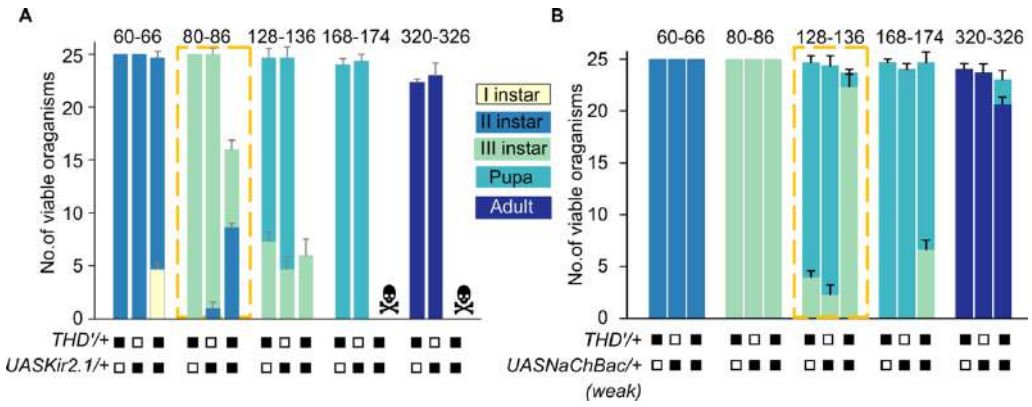

Figure 4.8: THD' activity is differentially regulated at different stages of development.

(A-B) Altered excitability in THD' neurons by expression of either a mammalian inward rectifying potassium channel (Kir2.1) or a bacterial sodium channel (NachBac) affects larval developmental progression and viability. Stack bar graphs show the number of

viable organisms (mean ± SEM) and their developmental stage at the indicated hours after egg laying (top) for the indicated genotypes. Number of sets (N) = 3, number of organisms per set (n) = 25. P values calculated after one way ANOVA followed by post-hoc Tukey's test are given for relevant stages.

Staging experiment of *THD'>UASKir2.1* pointed out developmental delays and eventual lethality in second and third instar larvae (Fig. 4.8A). Conversely, employing *THD'>NaChBac* led to delayed pupariation for 12-16h AEL (Fig. 4.8B). This shows that THD' neuronal activity is essential for larvae to develop normally.

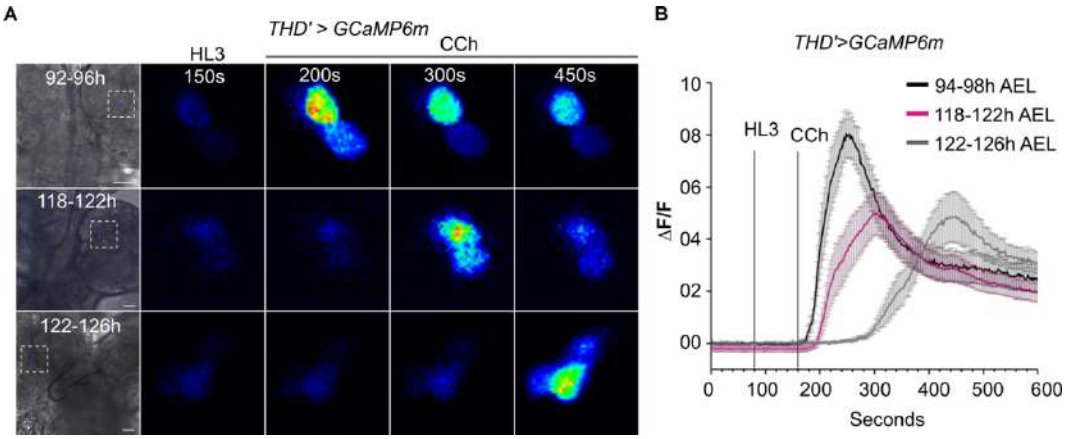

Figure 4.9: The neuronal activity of THD' exhibits dynamic characteristics at different stages of development.

A. Representative images of the central brain (left panels) indicating the region of focus (boxed), followed by images of THD' cells with Ca^{2+} transients at the indicated time points after addition of mAChR agonist (CCh 100μM). Ca^{2+} transients were measured in the indicated genotype by measuring the changes in the intensity of GCaMP6m fluorescence. Scale bar = 20μm

B. Quantified changes in GCaMP6m fluorescence (mean ± SEM of ΔF/F) from THD' neurons of the indicated genotypes. Number of brains, (N) ≥ 4, number of cells, (n) ≥12.

The examination of the larval developmental profile under varying THD' neuronal activities implies the crucial role of maintaining THD' neuronal activity throughout the larval growth period. Nevertheless, the observed delayed pupariation in *THD'>NaChBac* (Fig. 4.8B) indicates the necessity to reduce this activity as larvae transition into the pupariation stage. To test this hypothesis, I investigated the CCh-induced change in GCaMP intensity at three specific developmental stages: 94–98h AEL (mid-third instar stage; larval growth and feeding period), 118–122h AEL (early wandering; no growth stage and entering a non-feeding state), and 124–128h AEL (late wandering stage; complete cessation of feeding and entering pupariation). As expected, the transition of

larvae into the non-growth and non-feeding states revealed a noticeable alteration in the activity pattern of THD' neurons during these stages (Fig. 4.9). This observation suggests that the activity of THD' neurons is subject to differential regulation at different stages of organismal development.

4.4 Discussion:

4.4.1 STIM and cellular homeostasis

The assessment of THD' neuronal property in *STIM^{KO}* has effectively revealed the functional connection between STIM and dopamine (DA) signaling. The clear distinction in THD's neuronal activity, marked by its complete loss (Fig. 4.2), precisely aligns with the onset of reduced feeding and lethality as shown in Chapter 2, emphasizing the critical role of STIM during the mid-second instar stage of development. Despite the apparent dependence on activity, the rescue of *STIM^{KO}* larval lethality through *NaChBac* overexpression (only the rescue observed other than *THD'>STIM^{+})* did not match the efficacy achieved with STIM-dependent rescue (Fig. 4.4 and Fig.3.3). This suggests that, besides its involvement in maintaining neuronal activity, STIM is also implicated in other cellular functions like intracellular calcium homeostasis (Prakriya & Lewis, 2015), transcriptional regulation (Dhanya & Hasan, 2021; Maus et al., 2017a; Richhariya et al., 2017) and exocytosis (Richhariya et al., 2017), as previously demonstrated .

Moreover, the observed impairment in CCh-induced IP_3-mediated calcium release in *STIM^{KO}*, as depicted in (Fig. 4.7), highlights a substantial interplay between IP_3R-mediated cellular processes and STIM-dependent functions. This interplay may contribute to the incomplete rescue of *STIM^{KO}* observed under *THD'>NaChBaC*.

4.4.2 THD' activity, feeding, and larval development

The developmental profile observed under *THD'>Kir2.1* and *THD'>NaChBaC* (Fig. 4.8 A and B) highlights the essential role of THD' neuron activity in normal larval development and the timing of pupariation. Subsequently, monitoring *THD'>GCaMP* neuronal activity during different feeding states of larval development emphasizes (Fig.4.9) the critical role of THD' neuron activity in sustaining feeding persistence. However, data from

THD'>NaChBaC and delayed *THD'>GCaMP* responses observed during both early and late wandering stages indicate the necessity of inhibiting this neuronal activity as larvae transition into the non-feeding state.

Furthermore, the observed modulation in THD' activity induced by CCh, an acetylcholine agonist, suggests that cholinergic input precedes the activation of THD' neurons. While the specific cells responsible for acetylcholine production were not identified in this study, previous research has implicated a subset of Kenyon cells, particularly those expressing Choline acetyltransferase (ChAT) and part of the mushroom body, in the regulation of appetitive olfactory memories during early larval stages (Barnstedt et al., 2016; Pauls et al., 2010). Additionally, silencing *mAChR* on THD' neurons in starved flies resulted in a noticeable decrease in food-seeking behavior (Sharma & Hasan, 2020; Tsao et al., 2018). Moreover, Hartenstein et al., (2017) demonstrated that larval dopaminergic neurons, which develop during embryonic neurogenesis, persist and integrate into the adult brain. This suggests the continued presence of cholinergic inputs to THD' neurons for sensing nutritional state and hunger, potentially extending across both larval and adult stages. A recent review on the role of muscarinic receptors neurotransmission in the energy homeostasis of organisms, both directly and indirectly (Falk et al., 2020) further supports the observations made here.

Further given the insights into the role of THD' neurons in larval development, it has now become crucial to identify the downstream synaptic partners of THD' neurons and comprehend how dopamine signaling contributes to this intricate relationship, highlighting the multifaceted role of STIM in cellular functionality. This adds depth to our understanding of its contributions to larval development, as detailed in the subsequent chapters.

Chapter 5: THD' neurons regulate the function of a specific subset of neuropeptidergic cells

5.1 Introduction:

In the preceding chapter, the pivotal role of THD' neuronal activity in regulating larval development was clearly demonstrated. Although the larval dopaminergic circuitry is well established at the single-cell level (Hartenstein et al., 2017; Selcho et al., 2009), DA exerts its influence over a broader effector zone. This extends beyond direct synaptic partners, encompassing a larger subset of neurons through diffusion-aided volumetric transmission (Birman, 2005; Wiencke et al., 2020). Consequently, it becomes crucial not only to identify the physical synaptic partners but also to unravel the downstream functional partners that actively engage with THD' neurons. This chapter delves comprehensively into the establishment of both physical and functional synaptic partnerships involving THD' neurons.

5.2 Materials and methods

5.2.1 Fly stocks

Fly strains		
THD'GAL4 /CyOG	Marks subgroup of Dopaminergic cells in larval brain	Mark N Wu, Johns Hopkins University, Baltimore(Xie et al., 2018)
Trans-TANGO (*UAS myrGFP, QUAS TdTomato; Trans - Tango)*	Marks post-synaptic neurons with RFP	Michael Rosbash Brandies University, USA
UASTANGO (UAS myrGFP, QUAS TdTomato)	*trans*-TANGO genetic control	
UASCsChrimson	Optogenetically encoded cation channel that is activated at 625nm	RRID: BDSC_55136
LexAopGCaMP6f	Ca^{2+} Sensor with faster kinetics	

	expresses under LexAop	
c929LexA (DimmLexA)	Marks neuropeptidergic cells	Michael Texada, Janelia Farms, USA (Jayakumar et al., 2016a)
THD'GAL4,UASChrimson/CyOG	Recombinant line made for this study	
C929LexA,LexAopGCaMP6f, LexAopmCherry/Tb		

5.2.2 Fly rearing

As described in chapter-2

5.2.3 Immunohistochemistry

As described in chapter-2

5.2.3 Preparation of larval brain for Ex-vivo imaging

GCaMP signals were obtained from appropriately aged larval brains dissected from the specified genotypes and dissected in hemolymph like saline (HL3) (70mM NaCl, 5mM KCl, 20mM MgCl2, 10mM NaHCO3, 5mM trehalose, 115mM sucrose, 5 mM HEPES, 1.5mM Ca2+, pH 7.2). Dissected brains were transferred to a 35mm punched dish with a cover slip adhered to the bottom. Brains were embedded in *5µl of 0.8-1% low melt agarose (Invitrogen, Cat#16520– 100) and bathed in 100µl of HL3.

5.2.4 Analysis of Optogenetic signals

Larvae from the specified genotypes were reared in fly media containing 0.2mM ATR (All- trans retinal Sigma-Aldrich Cat#R2500). Brain samples were prepared as mentioned above. Images were acquired as a time series on an XY plane at an interval of 2 sec/frame using a 20X oil objective on an Olympus FV3000 inverted confocal microscope (Olympus Corp., Japan). For optogenetic stimulation of *CsChrimson*, a 633nm LED (from Thor labs) was used and GCaMP6f fluorescent images were obtained simultaneously using a 488nm

laser line so as to measure changes in cytosolic Ca^{2+} upon CsChrimson activation. Image acquired till 200th frames (400 secs).

A minimum of 6 independent brain preparations were used for all live imaging experiments and the exact number of cells imaged are indicated in the figures. Raw fluorescence data were extracted from the marked ROIs using a time series analyser plugin in Fiji. ΔF/F was calculated using the following formula for each time point (t): $\Delta F/F = (F_t/F_0)/F_0$, where F_0 is the average basal fluorescence obtained from the first 40 frames.

5.3 Result

5.3.1 THD' neurons are trans-synaptically connected with neurons across the CNS of the larval brain.

Building upon the SyteGFP pattern elucidated in Chapter 4 and the detailed anatomical insights into larval dopaminergic circuitry at the single-cell level, as presented by Pauls et al., (2010) the suggestion emerges that three cells of DL1 within THD' cells correspond to DL1-2, DL1-5, and DL1-6. Additionally, two cells of DL2 align with DL2-2 and DL2-3 within their respective clusters.

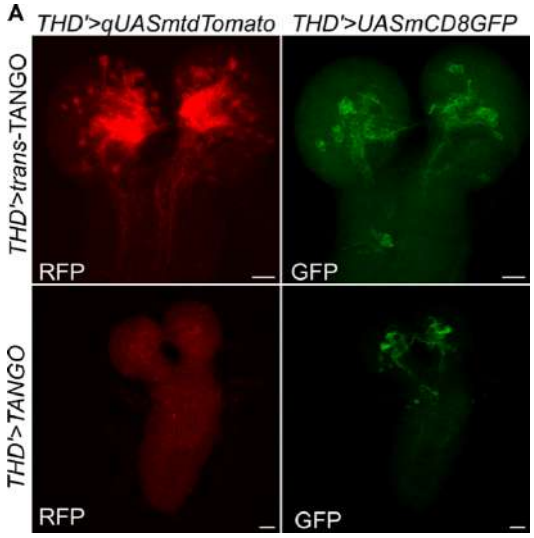

Figure 5.1: THD neurons make postsynaptic connections with multiple neurons.

A. Representative confocal images of the larval brain from animals with the *THD' > trans*-TANGO genotype (first row) exhibit tdTomato expression in the presence of TANGO signaling pathway molecules. In this context, post-synaptic neurons are labelled with anti-RFP (red) and anti-GFP (green), illustrating the expression profile of THD' neurons. The second row shows *THD' > qUAStdTomato, UASmyrGFP*, a genetic control for *trans*-TANGO, where TANGO signaling molecules are not expressed. Scale bar = 20μm.

In the pursuit of uncovering the downstream synaptic partners of *THD'GAL4,* the widely used *trans*-TANGO (Talay et al., 2017) genetic method was initially employed. This tool facilitated the identification of neurons anterograde to THD' neurons, with the reporter gene expressing only when the proximity between pre- and postsynaptic membranes allows binding between the membrane-tethered form of glucagon (ligand expressed in the presynaptic terminals of THD' neurons) and the Tango signaling pathway (*UASmyrGFP*, hGCGR::TEVcs::QF and hArr::TEV (TANGO), and *qUAStdTomato*) expressed pan-neuronally, respectively. Simultaneously, among the postsynaptic neurons expressing the reporter gene tdTomato, some may not be synaptically functional with our target neurons. This is because, regardless of whether they carry the respective receptor for the neurotransmitter or not, if the glucagon ligand and its respective Trans receptor come into contact, the receptor activates the expression of the reporter gene (RFP). Nevertheless, this method provides an overview of the postsynaptic partners of the neurons of interest. The results from *THD'>trans*-TANGO identified multiple neurons with extensive axonal projections throughout the brain as postsynaptic partners of THD' cells, as indicated by RFP fluorescence in the figure (Fig. 5.1A; first row).

In the UAS control (*THD'> UASmyrGFP,QUAStdTomato*), no leaky expression was observed (Fig. 5.1A; second row)., supporting the likelihood that RFP-positive cells under *THD'>trans*-Tango are indeed genuine. However, while this method revealed the spatial orientation of RFP cells, it fell short of determining their cellular identity. To identify the identity of RFP-positive cells, a speculative inference was made based on the observed spatial orientation.

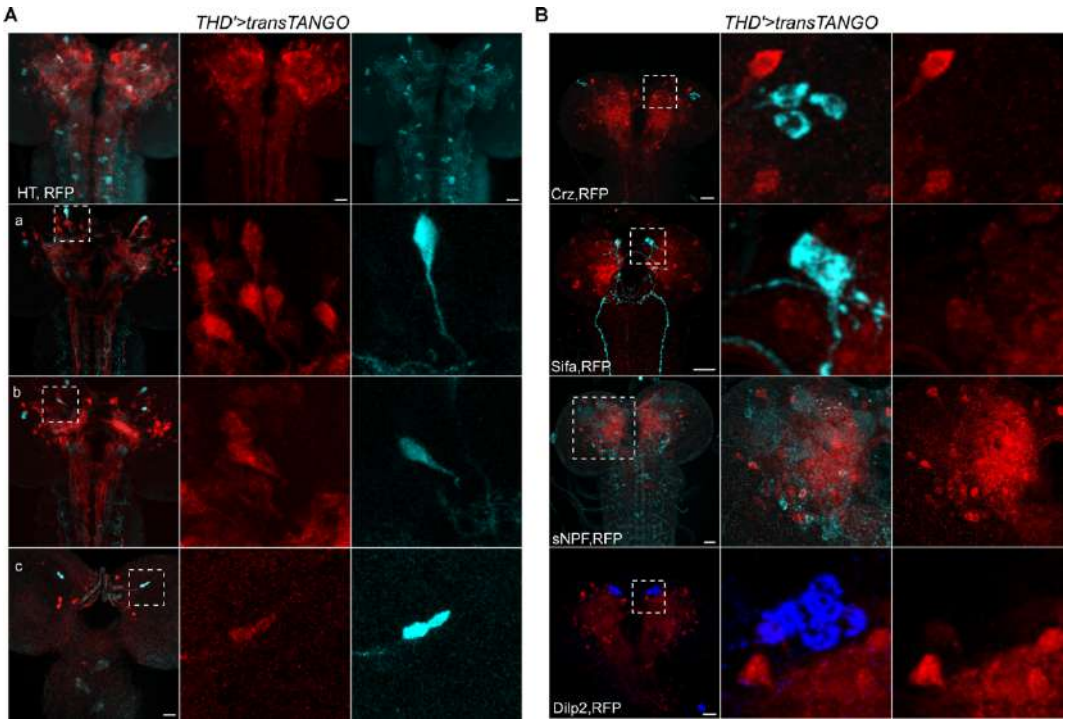

Figure 5.2: Subset of serotonergic neurons colocalize with post-synaptic neurons of *THD'>trans*-TANGO.

A. Representative confocal images of the larval brain from animals of the genotype *THD'>trans*-TANGO. Anti-RFP (Red) indicates marker for post-synaptic neurons of THD' neurons. Anti-HT (Cyan) marks serotonergic neurons. (a), (b) and (c) showing the subset of serotonergic neurons colocalized with RFP^{+ve} cells. 2nd and 3rd column represents the blow up of highlighted area of first column. Scale bars = 20µm.

B. Representative confocal images of the larval brain from animals of the genotype *THD'>trans*-TANGO. Anti-RFP (Red) indicates marker for post-synaptic neurons of THD' neurons. First row; IHC for neuropeptide Corazonin (Crz), Second row; IHC for neuropeptide Sifamide (Sifa), Third row; IHC for neuropeptide Short neuropeptide F (sNPF), and fourth row; IHC for neuropeptide for Dilp2. 2nd and 3rd column represents the blow up of highlighted area of first column. Scale bars = 20µm.

To validate this hypothesis within the context of *trans*-Tango results in the background of *THD'>trans*-TANGO, immunohistochemistry was conducted for endogenous neurotransmitters and some neuropeptides known for larval growth and feeding. The IHC results indicated that, apart from subset of serotonergic neurons (as shown in the in the Fig. 5.2A (a,b, and c) , none of the neuropeptides used here colocalized with the RFP cells (Fig. 5.2B).

5.3.2 THD’ neurons differentially activate subset of neuropeptidergic cells

In the context of addressing the *STIM*^{KO} feeding defect and its rescue by THD'-dopaminergic neurons, recent literature has emphasized the expression of diverse dopamine receptors in specific neuropeptidergic cells (Sareen et al., 2021). Alterations in the levels of these dopamine receptors have been demonstrated to influence feeding preferences, particularly in distinguishing between sweet and bitter tastes (Sareen et al., 2021). Simultaneously, extensive research has underscored the regulatory role of numerous neuropeptides in larval development and growth (Nässel & Zandawala, 2019, 2020). Furthermore, dopamine (DA) has been acknowledged for its ability to function as a neuromodulator, diffusing into a broader effector zone to regulate signaling in downstream neurons, even those not in immediate post-synaptic proximity (Wiencke et al., 2020).

In light of these findings, I sought to investigate potential functional synaptic interactions between THD’ neurons and neuropeptidergic cells. To address this hypothesis, I employed an optogenetic approach utilizing a well-established two-binary system (*GAL4>UAS* combined with *LexA>LexAop*).

This strategy involved the expression of an optogenetically activable red-shifted Channelrhodopsin (CsChrimson) (Klapoetke et al., 2014) in THD’ (*THD’>Chrimson*). For monitoring calcium transients, GCaMP6f was expressed in c929 positive neuropeptide cells (Park et al., 2008) with mCherry, a fluorescent protein, as an internal control (*C929LexA>LexAopGCaMP6f,LexAopmCherry*).

Recognizing the challenge of imaging only one focal plane at a time under confocal LSM and the dispersed distribution of c929 cells throughout the central nervous system (CNS), there was a potential risk of losing crucial information. To overcome this limitation, the light source was externally applied, as depicted in the figure (Fig. 5.3A). By dorsal mounting of the brain, THD’ cells were exposed to red light, allowing flexibility in identifying c929 cells, which are present across various focal planes.

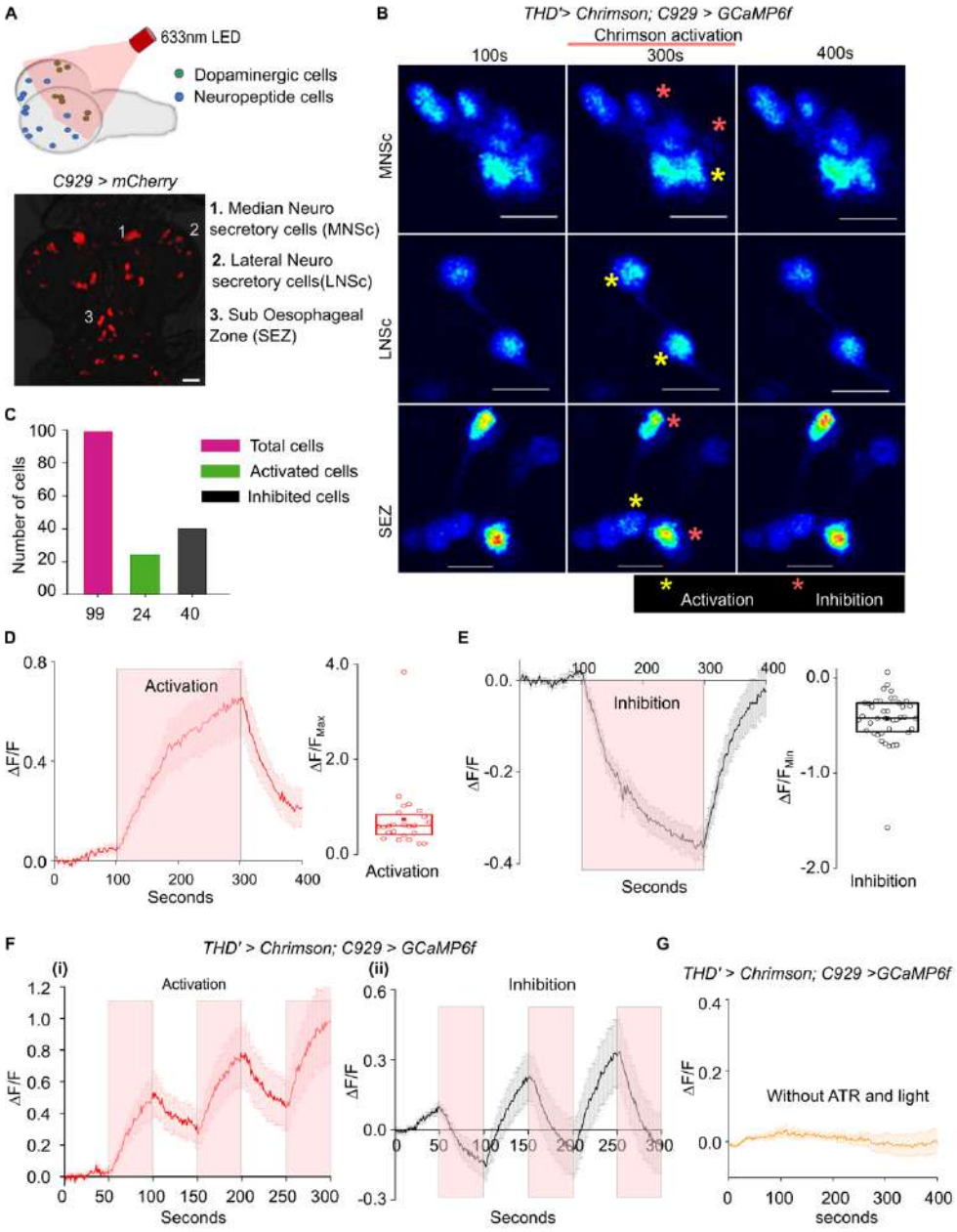

Figure 5.3: Differential regulation of neuropeptidergic cell activity by THD' neurons.

A. Pictorial representation of an experimental setup for testing functional connectivity of dopaminergic (THD') and peptidergic (c929) cells in organisms of the genotype *THD'>Chrimson, C929LexA>LexAopGCaMP6m.* The lower panel shows the peptidergic neurons containing regions 1-3 in which change in Ca^{2+} transients were observed upon activation of THD' cells.

B. Ca^{2+} transients in peptidergic Median Neurosecretory cells (MNSc, top), lateral neurosecretory cells (LNSc, middle) and suboesophageal region (SEZ, bottom) as measured by the intensity of GCaMP6m before Chrimson activation (100s) and after Chrimson activation (300s and 400s) of THD' cells. Activated cells (red asterisks) and inhibited cells (yellow asterisks) are marked. Scale bar = 20um.

C. Quantification of total C929 marked cells from 9 brains that were either optogenetically activated or inhibited.

D. Average GCaMP6m responses (mean ± SEM of ∆F/F) across time in C929 marked cells that were activated upon Chrimson activation of THD' neurons at 633nm. The box plot shows 25th and 75th percentiles of peak responses measured by change in GCaMP6m of individual activated peptidergic cells (circles), with the median (bar), and mean (square). n = 24 cells from (N) = 9 brains

E. Average GCaMP6m responses (mean ± SEM of ∆F/F) across time in C929 marked cells that were inhibited upon Chrimson activation of THD' neurons at 633nm. The box plot shows 25th and 75th percentiles of peak responses measured by change in GCaMP6m of individual inhibited peptidergic cells (circles), with the median (bar), and mean (square). n = 40 cells from (N) = 9

F. (i) Pulsed activation of THD' neurons produce corresponding pulses of activation in certain peptidergic neurons as evident from their GCaMP6m responses (mean ± SEM). Red panels indicate the time intervals (50s each) of *THD'>Chrimson* activation. n = 21 cells from N = 11 brains.
(ii) Pulsed activation of THD' neurons produce corresponding pulses of inhibition in certain peptidergic neurons as evident from their GCaMP6m responses (mean ± SEM). Red panels indicate the time intervals (50s each) of *THD'>Chrimson* activation. n = 19 cells from N = 9 brains.

G. GCaMP6m responses (mean ± SEM) are absent in C929 cells in the absence of red light and in larvae that were not fed with All-trans Retinol (ATR). n = 50 cells from N=9 brains.

Under the specified genetic condition and imaging setup, imaging was conducted on a total of nine brains. It was observed that upon optogenetic activation of THD' neurons, some c929 cells exhibited changes in GCaMP intensity. Based on the spatial orientation analysis of the responsive cells revealed consistent alterations in GCaMP intensity among c929 cells from lateral neurosecretory cells (LNCs), median neurosecretory cells (MNCs), and the suboesophageal zone (SEZ) (Fig. 5.3B) (Nässel & Zandawala, 2020). Specifically, in the LNSc region, 2 cells were activated, while cells with both activation and inhibition were observed in the MNSc and SEZ regions. Out of the 99 cells examined, 64 cells displayed changes in GCaMP intensity, with 24 exhibiting elevated GCaMP intensity and 40 displaying reduced intensity signals (Fig. 5.3B and C). Conversely, the remaining 35 cells showed no change in basal GCaMP intensity (Fig. 5.3C). Upon cessation of optogenetic activation of THD' neurons, calcium levels promptly returned to baseline in these 64 cells (Fig. 5.3B and 5D-E).

To scrutinize the specificity of the observed changes in calcium dynamics, further GCaMP dynamics observed with pulses of red light. This confirmed individual cells manifested either activatory or inhibitory responses upon repeated optogenetic stimulation with pulses of red light (Fig. 5.3F,(i) and (ii)). This indicates that THD' cells evoke specific responses of either stimulation or inhibition based on the class of neuropeptide cells. The specificity of the

THD'>Chrimson-evoked response was further authenticated by testing brains from larvae reared without all-trans-Retinal (ATR), a cofactor necessary for the function of Channelrhodopsin (Fenno et al., 2011), and by imaging in the absence of light (Fig. 5.3G).

5.4 Discussion

The recent delineation of the larval synaptic connectome (Winding et al., 2023), along with insights from other studies (Aso et al., 2014; Eichler et al., 2017; Eschbach et al., 2020; Saumweber et al., 2018; Selcho et al., 2009) examining the syt-GFP expression pattern outlined in Chapter 4 (Fig 4.5d; asterisk), lends additional support to the existence of a synaptic connection between THD' neurons and the mushroom body. The mushroom body plays a pivotal role in olfactory learning and memory formation (Eichler et al., 2017) and has been demonstrated to integrate signals related to hunger and satiety, thereby influencing innate food-seeking behavior (Tsao et al., 2018). The attenuation of THD' neuronal activity in $STIM^{KO}$ may have disrupted this neuronal circuit, consequently affecting feeding behavior. Moreover, the expression patterns of both presynaptic terminals and axonal dendrites reveal extensive arborization of THD' neurons across the central nervous system (CNS) and the neurohemal releasing site of the larval brain. This extensive branching likely contributes to the notable abundance of RFP-positive cells observed in *THD'>trans*-TANGO. Although the precise cellular identity remains undisclosed, the distinctive arrangement of RFP-positive cells in *THD'>trans*-TANGO has facilitated the identification of synaptic connections with a subset of serotonergic neurons.

Recognizing serotonergic neurons as post-synaptic partners of THD' neurons offers an alternative explanation for the feeding behavior manifested by $STIM^{KO}$. This finding aligns with prior research by Schoofs et al., underscoring the pivotal role of serotonergic neurons in the gustatory pathway and their involvement in regulating feeding behavior (Schoofs et al., 2018; Schoofs, Hückesfeld, Surendran, et al., 2014). The significance of serotonergic neurons in feeding behavior is further emphasized by the successful rescue of *itpr* mutants using *DdcGAL4*, which marks both serotonergic and dopaminergic

neurons (Agrawal et al., 2009). While this study support the idea of THD' influencing serotonergic neurons, the presence of dopamine receptors on these neurons remains uncertain. The well-established roles of both dopamine and serotonin in normal eating behavior underscore the importance of comprehending the intricate interplay between these two neuromodulators.

In spite of there is no evidence of a direct synaptic connection between central dopaminergic neurons and the neuropeptidergic cells, the result from the optogenetic method has unequivocally established that function of certain neuropeptidergic cells present in the MNSc, LNSc, and SEZ regions of larval brain are regulated by DA signaling. However, it is noteworthy that this method did not provide specific cell identity information. In parallel, the work presented by Kasturacharya et al., (2023) utilizing RNA sequencing data from *STIM*^{KO} larval brains, revealed changes in the transcripts of neuropeptides such as ilp2, ilp3, ilp5, and Sifa (Kasturacharya et al., 2023). In particular, alterations in ilp transcripts (-2, -3, and -5) in *STIM*^{KO} explains the lower rescue under *MNSc>STIM*$^{+}$ and significant rescue under *THD'>STIM*$^{+}$, indicating the role of DA signaling in regulating the transcription of ilps in MNSc cells. Interestingly, transcripts of neuropeptides like NPF, sNPF, LK, AstA, DH44 and Hugin, known for their involvement in feeding regulation (Hückesfeld et al., 2016; Nässel & Zandawala, 2019, 2020; Sareen et al., 2021; Schoofs, Hückesfeld, Schlegel, et al., 2014), remained unchanged (Kasturacharya et al., 2023). This suggests that DA signaling in these neurons might regulate their activity.

Further the investigation into the functional relevance of dopamine-insulin signaling with respect to larval growth has become a focal point of this work, as detailed in the preceding chapter. This line of inquiry holds promise for uncovering the intricate interplay between neurotransmitter signaling pathways and hormonal regulation in the context of larval development and growth.

Chapter 6: Dopamine modulates larval growth by regulating the transcription of MNSc insulin-like peptides (ilps)

6.1 Introduction

In earlier sections, it has become apparent that reducing dopamine signaling, achieved through either *TH* or *STIM* knockdown in THD' cells, significantly alters the rate of feeding. This, in turn, exerts an influence on nutritional uptake, thereby impacting the normal systemic growth rate of larvae. Despite the establishment of postsynaptic connections through *trans*-TANGO and optogenetic methods with various neurons and neuropeptidergic cells, respectively, the cellular details remain elusive. However, valuable insights gleaned from RNA-seq data obtained from $STIM^{KO}$ larval brains, the successful rescue of ilp3 and ilp5 transcript levels under $STIM^{KO}$*;THD'>*$STIM^{+}$*,* (Kasturacharya et al., 2023) and findings from optogenetic experiments (Chapter 5, Fig. 5.2B; first row) have shed light on a functional connection between THD' cells and insulin-like peptide (ilp)-producing median neurosecretory cells (MNSc). Importantly, in *Drosophila*, ilp-2,-3 and -5 are temporally regulated at different stage of the development of an organism (Okamoto & Nishimura, 2015). This temporal regulation is notably disrupted in $STIM^{KO}$, though ilp5 and ilp3, barring ilp2, return to normal levels under *THD'>*$STIM^{+}$ rescue (Kasturacharya et al., 2023). This strongly indicates that dopamine plays a crucial role in regulating the temporal expression of ilps, particularly ilp5 and ilp3. While the early-stage function of ilp5 in larval development is well-established (Britton et al., 2002; Nässel & Broeck, 2016; Rulifson et al., 2002; Semaniuk et al., 2021), the reasons behind the distinctive expression pattern of ilp3 during larval development remain elusive (Hu et al., 2017).

This chapter guides through a series of genetic experiments designed to uncover the significance of ilp3 in the developmental stages of larvae. It also delves into the intricate influence of dopamine signaling in MNSc cells, specifically in relation to larval growth.

6.2 Materials and methods

6.2.1 Fly rearing

As described in Chapter 2 (Materials and Methods).

6.2.2 Fly stocks

Fly strains		
Canton S	Wild type	
$STIM^{KO}$/FM7iGFP	Null mutant for STIM gene generated with help of CRISPR-Cas9 gene editing technique	Generated in the lab
$STIM^{KO}$;UASdsilp3/CyOG	Strain made for this study	
MNScGAL4 (Dilp2GAL4)	Marks ilp (-2, -3, and -5) producing MNSc cells of larval brain	RRID: BDSC_37516
UAS$ilp3^{+}$	Over expression of wildtype ilp3 gene	Ernst Hafen's lab
UASdsilp3	RNAi for ilp3 gene	RRID: BDSC_33681
UASDop1R1RNAi	RNAi for Dop1R1 receptor	RRID: BDSC_62193
UASDopEcR RNAi	RNAi for DopEcR receptor	RRID: BDSC_31981
UASDop2R2RNAi	RNAi for Dop2R receptor	RRID: BDSC_36824
UASGCaMP6m	Ca^{2+} Sensor with intermediate kinetics expresses under UAS	RRID: BDSC_42748

6.2.3 Staging

As described in Chapter 2 (Materials and Methods)

6.2.4 Quantification of larval mouth hook contractions

As described in Chapter 2 (Materials and Methods)

6.2.5 Adult fly weight measurement
As described in Chapter 3 (Materials and Methods)

6.2.6 Larval imaging and measurement
As described in Chapter 2 (Materials and Methods)

6.2.6 Live imaging

Larval brain expressing *MNSc>GCaMP* is used for DA (Sigma, Cat#H8502) stimulation. Dissected brains were transferred to a 35mm punched dish with a cover slip adhered to the bottom. Brains were embedded in ~5µl of 0.8% low melt agarose (Invitrogen, Cat#16520-100) and bathed in 80µl of HL3 having 1uM of TTX. Images were acquired as a time series on an XY plane at an interval of 1.5sec using a 20X-oil objective on an Olympus FV3000 inverted confocal microscope (Olympus Corp., Japan). At the 30^{th} frame, 10µl of HL3 was added and at the 60^{th} frame 10µl of 1mM DA was added. Ca^{2+} responses were imaged till the 250^{th} frame (450sec).

6.2.7 Quantification and Statistical Analysis

All bar graphs and line plots show the means and standard error of means. In boxplots, horizontal lines in the box indicate median, box limits are from 25^{th}-75^{th} percentiles, and individual data points are represented by closed circles (unless otherwise specified in the figure legends). Unpaired student t-Test (for two genotypes) and one way ANOVA followed by post-hoc Tukey's significance test (for data with multiple genotypes) was performed to calculate P values**.** All graphs were plotted using Origin 8.0 software. Origin 7.5 MicroCal, Origin Lab, Northampton, MA, USA N/A, Fiji Open access (RRID:SCR_002285).

6.3 Result

6.3.1 Reducing ilp3 level in *STIM^{KO}* partially rescues *STIM^{KO}* larval lethality.

The temporal expression profile of ilp3 reveals that, expression is highly regulated and expression is suppressed during the larval growth period, which coincides with the active feeding phase (Chapter 2, Fig. 2.8E). However, in *STIM^{KO}*, ilp3 is significantly upregulated during the second instar stage

(Kasturacharya et al., 2023). This led to the hypothesis that rescuing *STIM*^{KO} might be achievable by reducing ilp3 levels. To investigate this, *ilp3* was knocked down in MNSc cells of *STIM*^{KO}, and the developmental profile was observed. Staging experiments confirmed a partial rescue of *STIM*^{KO}, evidenced by the rescue of larval lethality in the second instar larvae, followed by their transition to the third instar larvae (5±0.5). Among three batches of 25 animals, a few of the rescued third instar larvae grew to full size, pupariated, and some even eclosed as adults (2.3±0.3) (Fig. 6.1A-C).

The observed partial rescue via *ilp3* knockdown could be attributed to the roles of additional dopamine-modulated neuropeptides, coupled with the lower expression of ilp2 and ilp5 in *STIM*^{KO} animals (Kasturacharya et al., 2023). Since both ilps serve as growth signals in the second and third instar larvae (Okamoto & Nishimura, 2015), the limited rescue may be due to their involvement. Notably, a small proportion of *STIM*^{KO} larvae rescued by ilp3 knockdown exhibited a significant increase in size compared to control larvae

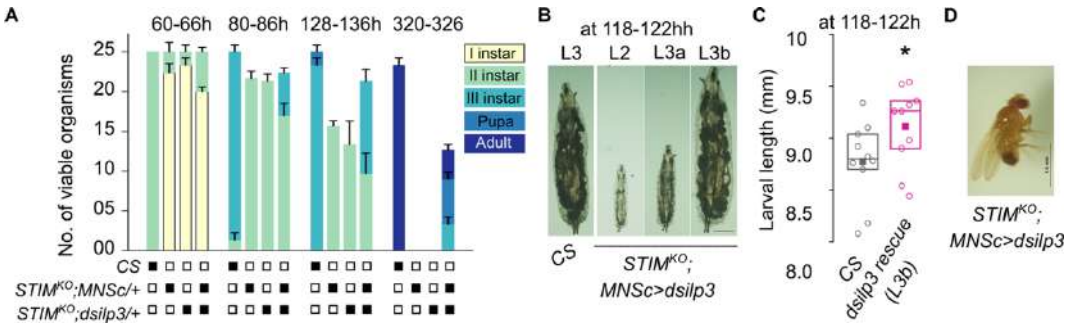

(Fig. 6.1B), suggesting that reducing ilp3 can indeed regulate the growth of animals.

Figure 6.1: Reducing the expression of ilp3 in MNSc cells provides partial rescue in *STIM*^{KO}.

A. Knockdown of *ilp3* partially rescues viability in *STIM*^{KO} larvae. Stack bar graph showing the number of viable organisms and their developmental stage at the specified hours after egg laying for *CS, STIM*^{KO}*; MNScGAL4/+, STIM*^{KO}*; dsilp3/+* (control) genotypes followed by *STIM*^{KO}*;MNScGAL4>dsilp3*. Data are from three experiments, each with 25 organisms per genotype.

B. Representative images of larvae from *CS* and *STIM*^{KO}*; MNSc>dsilp3* at 118-122h AEL, scale bar = 1mm.

C. Quantification of larval length from *CS* and *STIM*^{KO}*; MNSc>dsilp3* (rescue, L3b) genotypes. Box plots show the 25th and 75th percentiles with median (bar), mean (square) and sizes of individual larvae (circles), n=10. *P<0.05 (unpaired t-test).

D. Representative image of an adult *STIM*^{KO} mutant fly rescued by knockdown of *ilp3* (*STIM*^{KO}*; MNScGAL4>dsilp3*). Scale bar = 1mm.

6.3.2 ilp3 is a negative regulator of larval growth

The larvae rescued in *STIM*^{KO} (*MNSc>dsilp3*) exhibited a larger size compared to the control larvae (Fig. 6.1B). To investigate the role of ilp3 in larval growth in a wild-type background, I monitored the developmental profile under both knockdown and overexpression of *ilp3* in MNSc cells.

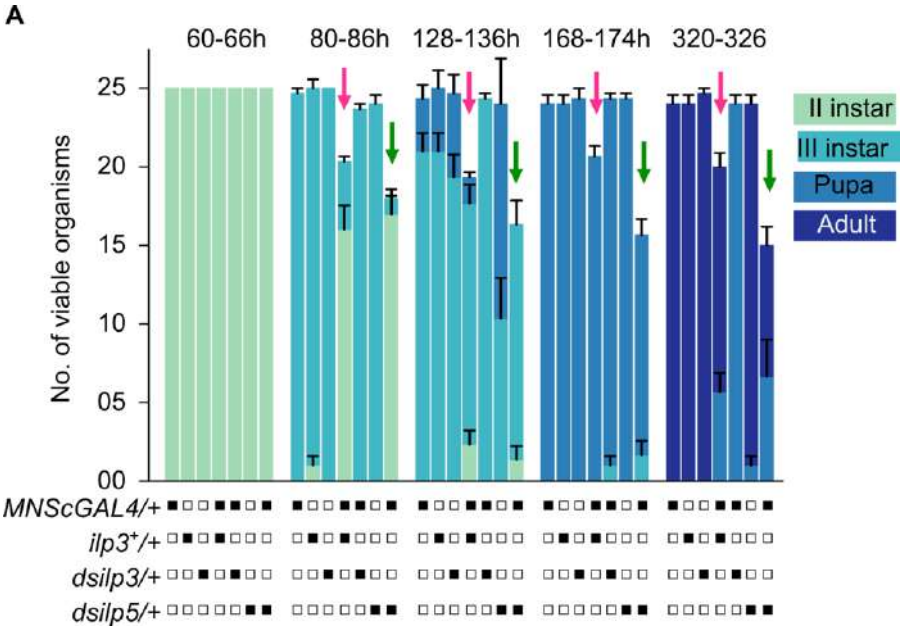

Figure 6.2: Change in temporal expression of ilp3 affects normal development of an organism

A. Larval developmental profile with overexpression of ilp3 in MNSc (red arrow) appears similar to knockdown of ilp5 (green arrow). Stack bar graph showing the number of viable organisms and their developmental stage at the specified hours after egg laying for the indicated genotypes. N=3 sets with 25 larvae in each set.

Given that ilp3 expression is temporally regulated, examining both knockdown and overexpression helps elucidate the reasons for ilp3 regulation at specific developmental stages. A comprehensive staging experiment revealed distinct differences in the developmental profiles of *MNSc>dsilp3* and *MNSc>ilp3*$^{+}$ compared to the control (Fig. 6.2A). Under the 12-hour staging, *MNSc>dsilp3* animals pupariated between 132-156h AEL, indicating a delay of approximately 48 hours compared to the control (Fig. 6.3A). This delayed pupariation resulted in larger pupae and overweight adults (Fig. 6.3B and C, 6.3H). Conversely, overexpression of *ilp3* in MNSc cells led to a delayed larval

transition from L2 to L3, resulting in smaller-sized larvae (Fig. 6.3D-F), similar to the delayed larval development observed in ilp5 knockdown animals (Fig. 6.2A).

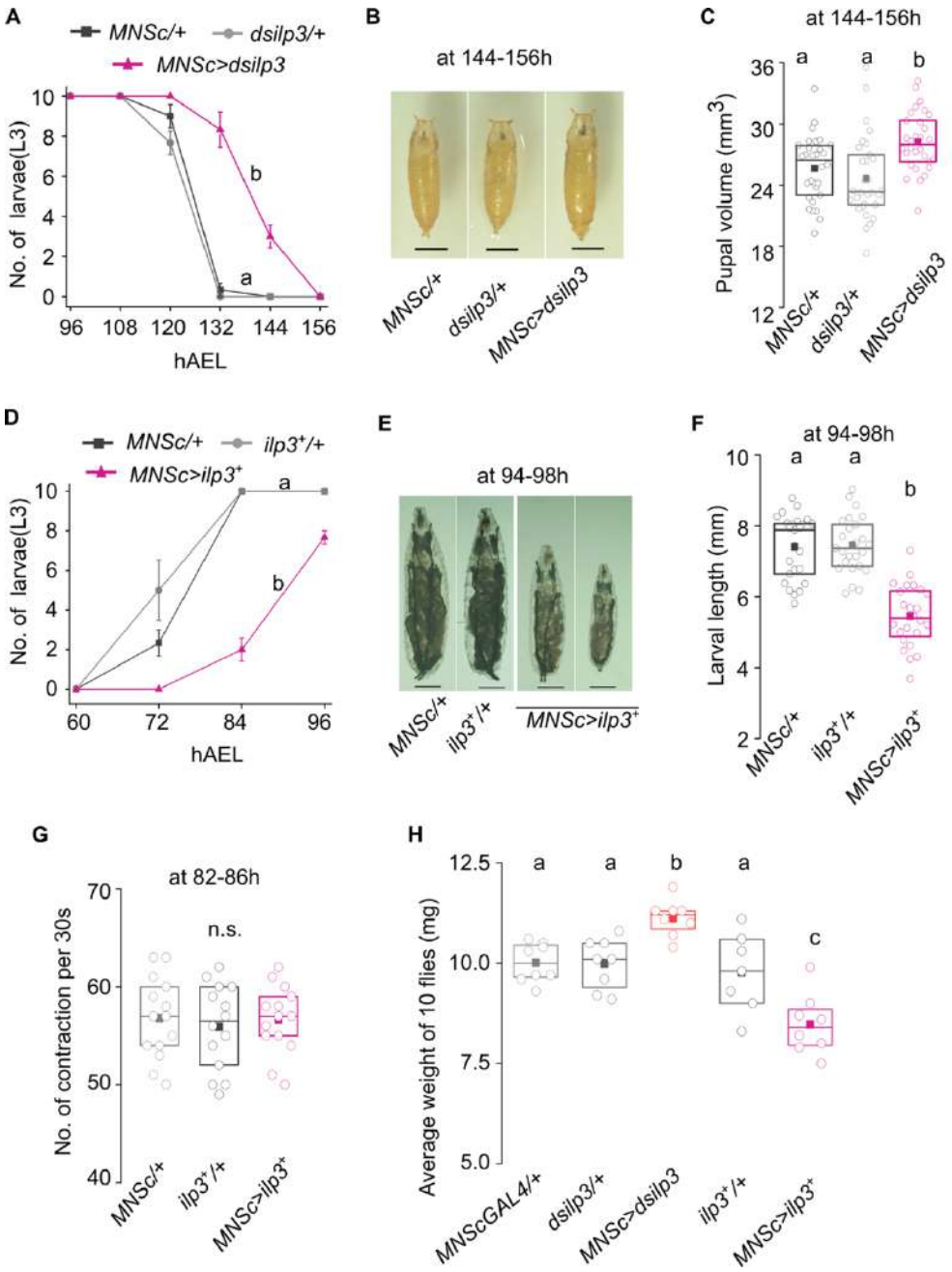

Figure 6.3: Ilp3 negatively regulate larval growth.

- **A.** Number of 3rd instar larvae at the indicated times AEL (mean ± SEM) from the indicated genotypes with knockdown of *ilp3* in the MNSc (*MNSc>dsilp3*) and of controls (*MNSc/+ and dsilp3/+*). Alphabets indicate statistically different groups at 132h and 144h. Number of sets (N) = 3 and number of larvae per set (n) = 10.
- **B.** Representative images of pupae with knock-down of *ilp3* (*MNSc> dsilp3*) at 144-156h AEL and appropriate controls (*MNSc/+* and *dsilp3/+*). Scale bar = 1mm.
- **C.** Quantification of pupal volume from the indicated genotypes. Box plots show the 25th and 75th percentiles with median (bar), mean (square) and sizes of individual pupa (circles), n=30

D. Number of 3rd instar larvae obtained by over-expression of *ilp3* (*MNSc>ilp3^{+})* and in appropriate control genotypes (*MNSc/+, ilp3^{+}/+*) at the indicated time AEL (mean ± SEM). (N) = 3 and (n) = 10. Alphabets indicate statistically different groups.

E. Representative images of larvae with over-expression of *ilp3* (*MNSc>ilp3^{+}*) and appropriate controls (*MNSc/+* and *ilp3^{+}/+*) at 94-98h AEL, scale bar = 1mm.

F. Overexpression of ilp3 results in smaller sized larvae. Quantification of larval length from the indicated genotypes. Box plots show the 25th and 75th percentiles with median (bar), mean (square) and sizes of individual larvae (circles), n ≥24.

G. Overexpression of ilp3 does not affect feeding. Box graph showing 25th and 75th percentiles, the median (bar), and mean (square) of number of larval mouth hook contraction per 30 seconds, where each circle represents a single larva of the indicated genotype. Number of larvae per genotype is (n)≥10.

H. Knockdown and overexpression of ilp3 in the MNSc affects adult weights in opposing directions. Quantification of weight of 10 flies from the indicated genotypes. Box plot shows the 25th and 75th percentiles with median (bar), mean (square). Each circle represents one set consisting of 10 flies in each of which 5 females and 5 males were collected at 6-8h post- eclosion. A minimum of 5 sets were quantified for each genotype.

For all graphs and box plots, alphabets represent distinct statistical groups as calculated by one way ANOVA followed by post-hoc Tukey's test, n.s. indicates non-significant groups.

Additionally, when quantifying mouth hook contraction in *MNSc>ilp3^{+},* it was observed that the frequency of mouth hook contraction closely resembled that of its genetic controls (Fig. 6.3H). This implies that the slower growth and smaller size observed in *MNSc>ilp3+* larvae and adults (Fig. 6.2A and 6.3D-F and H) may not be attributed to nutrition.

6.3.3 Insulin producing cells of median neurosecretory cells (MNSc) responds to DA signaling

In *Drosophila*, DA signaling exerts its effects through four known specific dopamine receptors, namely Dop1R1, Dop1R2, DD2R and a non-canonical DopEcR (Karam et al., 2020). Despite the absence of a direct synaptic connection between THD' and MNSc cells (Eschbach et al., 2020; Miroschnikow et al., 2020), both optogenetic experiments (Chapter 5, Result 4.3.2) and RNA-seq data from *STIM^{KO}* (Kasturacharya et al., 2023) larval brains suggest the involvement of DA signaling in MNSc cells. To validate this, I conducted knockdown experiments targeting Dop receptors (Dop1R1, Dop2R2 (DD2R), and DopEcR) in MNSc cells and monitored the developmental outcomes.

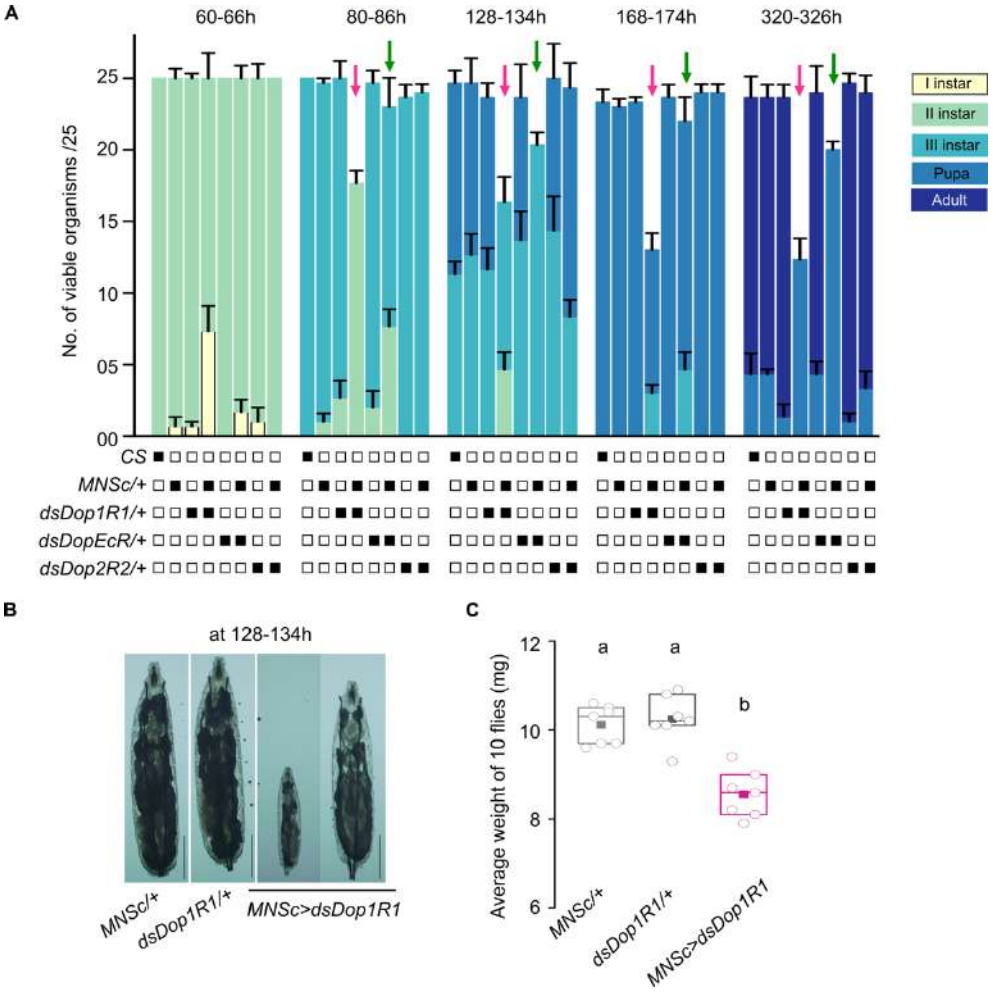

Figure 6.4: Distinct developmental impacts are mediated by different dopamine receptors on MNSc cells.

A. Development profiles of larvae with RNAi mediated knockdown of dopamine receptors in the MNSc. Bar graphs represent number of viable organisms and their developmental stages at the specified hours after egg laying for the indicated genotypes (*CS, MNScGAL4/+, dsDop1R1/+, dsDopEcR/+, dsDop2R2/+* (Controls), *MNSc>dsDop1R1, MNSc>dsDopEcR*, and *MNSc>dsDop2R2*). N=3 batches of n=25 larvae for every genotype. P values of all genotypes compared with appropriate controls were calculated by one way ANOVA followed by post-hoc Tukey's test.

B. Representative images of larvae from specified genotypes at 128-134hr. Scale bar = 1mm

C. Quantification of weight of 10 flies from the indicated genotypes. Box plot shows the 25th and 75th percentiles with median (bar) and mean (square). Each circle represents one set of adult flies consisting of 5 females and 5 males, 6-8h post-eclosion. A minimum of 5 sets were measured for each genotype. Alphabets represent distinct statistical groups as calculated by one way ANOVA followed by post-hoc Tukey's test.

Staging experiments confirmed that *MNSc>Dop1R1* animals exhibited delayed development, reduced larval and adult viability (Fig. 6.4A), and impaired growth (Fig. 6.4B and C). Whereas with delayed pupariation with decreased viability, was observed with knockdown of *DopEcR* (Fig. 6.4A), while larvae with *Dop2R2* knockdown appeared normal (Fig. 6.4A).

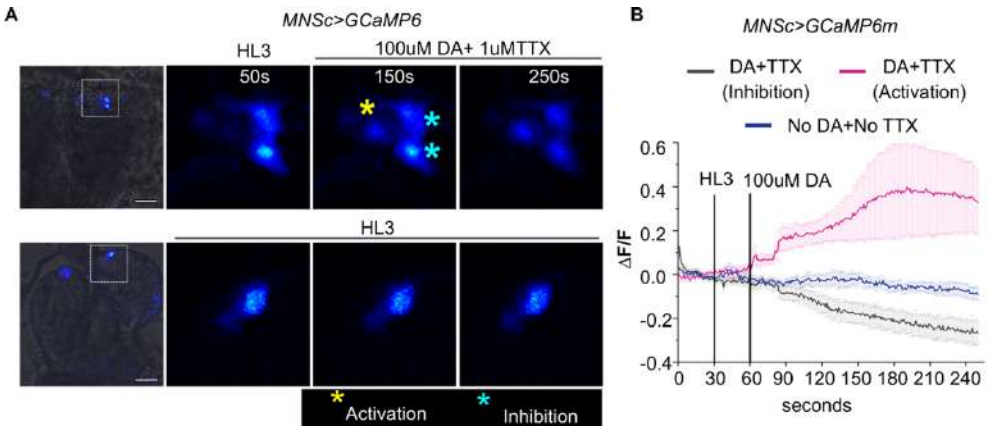

Figure 6.5: Dopamine selectively modulates the activity of MNSc cells.

A. Representative images of larval brains expressing the calcium indicator GCaMP6 in MNSc. Brains were stimulated with either dopamine (DA) in presence of tetrodotoxin (top panel) or a control solution (HL3; lower panel) and imaged over time. Scale bar = 20μm

B. Changes in GCaMP6m fluorescence (mean ± SEM of ΔF/F) from MNSc cells with addition of either dopamine (DA) and Tetrodotoxin (TTX) (7 brains and 12-14 cells) or HL3 (No DA+ No TTX) (5 brains and 14 cells).

To further confirm the involvement of DA signaling in MNSc cells, I investigated the endogenous response of MNSc cells to dopamine stimulation. In this experiment, larval brains (58-62h AEL) expressing a Ca^{2+} sensor in MNSc (*MNSc>GCaMP6m*) were subjected to DA stimulation. Before imaging, larval brains were immersed in HL3 solution containing tetrodotoxin (TTX; Na_v blocker) to effectively block any extraneous neuronal inputs, ensuring that changes in calcium intensity were specifically attributed to the added stimulator. Among the seven targeted MNSc cells in one hemisphere of the larval brain, consistent activation was observed in one cell, while the addition of dopamine inhibited the Ca^{2+} response in three to four cells (Fig 6.5A;First row and quantified in Fig 6.5B). No alterations in the Ca^{2+} responses of MNSc were noted in the absence of dopamine (Fig 6.5A second row and 6.5B)

6.4 Discussion

6.4.1 ilp3 as an anti-growth factor

In *Drosophila*, eight insulin-like peptides (ilps) have been identified, each displaying unique spatial and temporal expression patterns indicative of distinct

roles in the organism's physiology (Nässel & Broeck, 2016; Semaniuk et al., 2021). Among these, ilp2, ilp3, and ilp5 are expressed in a cluster of seven cells known as insulin-producing cells (IPCs), situated symmetrically at the pars intercerebralis of the brain and forming part of the median neurosecretory cells (MNSc) (Brogiolo et al., 2001; Cao & Brown, 2001; Rulifson et al., 2002; Semaniuk et al., 2021).

Despite all seven cells synthesizing all three ilps, there is a distinct temporal regulation in the expression of ilp2, ilp5, and ilp3. Both ilp2 and ilp5 undergo upregulation during the larval growth phase, followed by downregulation as observed with ilp2 during the transition into the wandering stage . In contrast, the expression pattern of ilp3 follows the opposite trajectory, with upregulation as larvae enter the mid-third instar stage (L3 puff stage 1-2) and further increases as the organism reaches its maximum size (L3 puff stage 7-9) (Hu et al., 2017 [DGET]; Okamoto & Nishimura, 2015). In spite of their distinct expression patterns, the release of all ilps (-2, -3, and -5) is dependent on nutrition (Géminard et al., 2009; Ikeya et al., 2002; Kim & Neufeld, 2015).

The characterization of $STIM^{KO}$, where ilp3 is upregulated at the second instar stage, provides insights into the suppression of ilp3 during the growth period (Kasturacharya et al., 2023). The significance of this suppression is reinforced by the partial rescue of $STIM^{KO}$ larval lethality under *ilp3* knockdown (Fig 6.1A-D). Additionally, ilp3 mutants exhibit delayed pupariation (Kim & Neufeld, 2015), a phenotype further confirmed by developmental profile observed with *MNSc>dsilp3* (Fig 6.2A and 6.3A). This delayed pupariation leads to larger pupae and adults (6.3A-C and H), a phenomenon not reported previously. Conversely, overexpression of ilp-3 ($MNSc>ilp3^{+}$) during the growth period results in the opposite phenotype: smaller larvae and partial lethality at the larval stage (Fig 6.2A, 6.3D-F and H). This parallels the phenotype observed when IPCs are ablated or when *ilp5* is knocked down (Okamoto & Nishimura, 2015; Rulifson et al., 2002).

The growth phenotype observed with ilp5 knockdown contrasts sharply with that of ilp3 knockdown. In ilp3 knockdown animals, the growth pattern mirrors that of ilp3 mutants, but with an overall increase in pupal volume. This is the first phenotypic observation made regarding ilp3 function. Additionally,

overexpression of ilp3 results in the opposite phenotype, where larval growth is adversely affected.

In summary, the divergent phenotypes observed through genetic manipulation of ilp3 levels suggest that, unlike ilp2 and ilp5, which are known to be positive growth factors, ilp3 may act as a negative growth regulator. This finding is particularly intriguing, as insulin signaling has traditionally been associated with positive growth regulation, highlighting a unique role for ilp3 in this context.

Additionally, the fact that *Drosophila* possesses a single insulin receptor for all insulin-like peptides (except ilp8, where Lgr3 serves as the receptor for ilp8 (Boulan et al., 2018; Nässel & Broeck, 2016)) further emphasizes the intricate regulation of diverse functions by these peptides. This prompts the need for further investigation into the downstream signaling pathways through which ilp3 acts on cells.

6.4.2 Dopamine influences growth and development by acting on MNSc cells.

Furthermore, the distinct developmental profiles observed among Dopamine receptor knockdowns in MNSc cells, along with the differential calcium responses under both genetically and endogenously induced dopamine stimulation, provide conclusive evidence of the existence of dopamine signaling in these cells. Notably, both Dop1R1 and DopEcR, when compared to their genetic controls, exhibited alterations in developmental patterns, while no such changes were observed with *MNSc>Dop2R2*. Among the utilized dopamine receptors, Dop1R1 and the non-canonical DopEcR function through the activation of adenylate cyclase, stimulating cAMP signaling, whereas DD2R acts as an inhibitory receptor (Karam et al., 2020; Missale et al., 1998).

Supporting evidence from a study by Bjordal et al., 2014 indicates that, within the same cluster of dopaminergic cells, only 3 out of 6 DL1 cells respond to an incomplete diet, leading to the rejection of food by the animal. This aligns with the observed heterogeneous GCaMP responses within the 7 cells of the MNSc IPC cluster, suggesting that different dopamine receptors are enriched across these cells.

In summary, both genetic studies and live imaging confirm the significant role of dopamine (DA) in insulin signaling, as the expression of ilp3 and ilp5 depends on THD' neuronal activity. However, there is no evidence from my data or the literature to suggest that ilp3 acts on dopaminergic neurons to regulate larval growth. Altogether, this study is the first to demonstrate that dopamine signaling regulates the differential transcription of three insulin-like peptides (ilps -2, -3, and -5) within cells, thereby influencing the organism's normal growth. The findings collectively highlight the intricate role of dopamine in orchestrating the transcriptional dynamics of insulin-like peptides, which in turn shape the overall growth and development of the organism.

Chapter 7. Conclusion and future directions

In conclusion, the primary objective of my thesis was to conduct a comprehensive exploration into the cellular underpinnings of Store-Operated Calcium Entry (SOCE) concerning the growth and development of *Drosophila melanogaster*. Focusing on STIM (Stromal Interaction Molecule) as a major molecular player in SOCE, I employed dSTIM (*Drosophila* STIM) as a molecular candidate to unravel the functional aspects of SOCE in the postembryonic development of an organism. The STIM null mutant ($STIM^{KO}$) *Drosophila melanogaster* strain, generated using the CRISPR-*Cas9* gene editing technique, served as a key tool in this investigation.

Throughout this chapter, I aim to encapsulate the key findings and insights gleaned from work done to understand the role of STIM in the context of development. Additionally, I will outline potential avenues for future investigations to build upon the foundation laid by this study.

7.1 STIM and postembryonic development

In summary, the developmental analysis of $STIM^{KO}$ confirms the essential role of STIM in initiating larval growth from the mid-second instar stage. This finding is consistent with observations in mice lacking both STIM1 and STIM2, which exhibit lethality during the perinatal stage of development. Examination of $STIM^{KO}$ feeding patterns at various developmental stages reveals a significant difference: $STIM^{KO}$ larvae fail to increase mouth hook contractions' frequency at 70-74h AEL, equivalent to the 58-62h AEL stage in wild-type (*CS*) larvae. Consequently, systemic growth arrest, as evidenced by measurements of larval length at different time points and NBs cell proliferation lineage, confirms that $STIM^{KO}$ lethality results from an acute nutritional deficit.

Through detailed cellular profiling, cells that are marked by *MNScGAL4*, *THGAL4, THC'GAL4*, and *THD'GAL4* are able to rescue the $STIM^{KO}$ larval lethality to distinct levels. Among these, the rescue of $STIM^{KO}$ under *THD'>STIM*$^{+}$ is sufficient and significantly mitigates $STIM^{KO}$ larval lethality. Subsequent observations made with the staging profiles of $STIM^{KO}$*;THGAL80,THD'>STIM*$^{+}$, *THD'>dsSTIM*, and *THD'>dsTH* confirm the importance of THD' dopaminergic neuronal function for normal larval development.

Even though further analysis of *THD'>GCaMP* at two distinct time points (70-74h and 76-80h AEL) revealed that THD' neuronal activity is required during the mid-second instar stage. The absence of neuronal activity in DL1 and DL2 neurons of THD' in $STIM^{KO}$ larvae at 76-80h AEL was associated with subsequent larval lethality. The restoration of neuronal activity and dopamine release in $STIM^{KO}$ under *THD'>STIM*$^{+}$, as well as altered activity under *THD'>dsSTIM*, further highlights the critical role of STIM in maintaining neuronal function during larval development. Additionally, the observed larval lethality under *THD'>Kir2.1* and *THD'>dsTH*, along with delayed pupariation under *THD'>NaChBaC*, reinforce the importance of dopamine from THD' in maintaining normal larval development.

Despite the lethality resulting from the loss of neuronal activity, the restoration of activity under *THD'>NaChBaC* did not fully rescue the $STIM^{KO}$ phenotype, suggesting additional STIM-dependent cellular functions crucial for sustaining neuronal activity. Notably, research from various groups suggests the potential involvement of STIM in transcriptional regulation. This notion finds support in RNA-seq analysis of $STIM^{KO}$ larval brain tissue, as reported by Kasturacharya et al., 2023, which reveals downregulation of the cellular redox system gene TRX-2. This downregulation correlates with elevated levels of reactive oxygen species (ROS). Based on these findings, it is hypothesized that this dysregulation might disrupt cellular energy homeostasis, subsequently impacting neuronal function. Further investigation is required to elucidate how STIM maintains the cellular redox systems.

Furthermore, the observed CCh-stimulated *THD'>ER-GCaMP* response being effected in $STIM^{KO}$ indicates that IP_3-mediated calcium signaling is impacted. It is well established that IP_3-mediated calcium release is upstream of STIM function. A study by S. Chakraborty et al. (2016) in *Drosophila melanogaster itpr* mutants, where SOCE is affected, and further confirmed by P. Chakraborty et al. (2023), who show that the IP_3 receptor regulates SOCE besides its calcium channel property. However, the observations made in this study shed light on that absence of STIM affects the IP_3-mediated calcium release from the IP_3 receptor. This outlines the intricate relationship between the IP_3 receptor and STIM function and requires further exploration. In addition to this, the inability to achieve complete rescue of $STIM^{KO}$, under

THD'>NaChBac, underscores the complexity of this regulatory network and emphasizes the necessity for continued investigation. In conclusion, these findings contribute valuable insights into the mechanisms governing STIM-mediated neuronal function and the challenges of fully restoring neuronal activity in $STIM^{KO}$ mutants.

7.2 THD' dopaminergic neurons, feeding, and larval development

Dopamine has been predominantly linked with hedonic/reward-based feeding (Boekhoudt et al., 2017; Landayan et al., 2018; Volkow et al., 2011; G.-J. Wang et al., 2011; Wise, 2006), which contrasts with normal feeding patterns regulated by canonical hunger-satiety signals. However, this thesis highlights the role of THD' neuron's dopamine in increasing feeding rates during the mid-second instar stage and sustaining them until larvae enter the wandering stage. Neuropeptide-F is a key foraging neuropeptide in *Drosophila*. Nonetheless, a study by Landayan et al. (2018) uncovers that in adult *Drosophila*, two distinct sets of dopaminergic neuronal circuits govern foraging based on satiation state. The PAM cluster promotes foraging in food-deprived flies, while the PPL1 cluster promotes foraging in well-fed flies. Notably, the DL1 cluster of dopaminergic neurons in larvae corresponds to the PPL1 cluster of adult *Drosophila*. This suggests that the identified 3 cells of DL1 and 2 cells of DL2 clusters in $STIM^{KO}$ may regulate feeding even when nutrients are continuously available. Given the larvae's high demand for nutrition, which supports both energy requirements and growth, with surplus nutrients stored for the non-feeding pupal stage, larvae must counteract satiation signals. To achieve this, the THD' dopaminergic neurons aid in overcoming satiation signals and sustaining feeding until larvae progress into the wandering stage.

The modulation in activity levels of THD' neurons observed at distinct larval feeding stages underscores the significance of THD' dopamine in sustaining feeding throughout larval development. Exploring the mechanisms behind this modulation of the cholinergic signal is both crucial and intriguing. Considering that the cholinergic system computes the internal energy homeostasis, the CCh-stimulated reduced activity of THD' neurons observed at the wandering stage prompts questions: is it due to a lack of cholinergic signaling or are there changes in the availability of respective receptors on THD'

neurons? This aspect warrants further understanding. Additionally, alterations in dopaminergic neuronal activity have been implicated in physiological disorders such as obesity (Low et al., 2021; Volkow et al., 2011). Hence, unravelling this mechanism using *Drosophila* as a model organism holds considerable promise.

Apart from the direct connection with the mushroom body, there are no details of downstream post-synaptic targets of THD' neurons. In this thesis, I demonstrated that during larval development, dopamine differentially regulates the activity of specific neuropeptides present in the MNSc, SEZ, and LNSc regions. Additionally, RNA-seq data from Kasturacharya et al. (2023) indicate that THD' neurons regulate the transcriptional expression of ilps in the MNSc, and through tran-TANGO, I showed physical post-synaptic contact with a subset of serotonergic neurons.

Serotonergic neurons are well known to be part of the gustatory circuit, regulating feeding-related muscle movements by suppressing Hugin neurons in the SEZ (Miroschnikow et al., 2020; Schoofs, Hückesfeld, Schlegel, et al., 2014). Furthermore, optogenetic experiments show that cells from the SEZ respond to THD' neuronal activity. This suggests that there could be a parallel functional effect from both serotonergic and dopaminergic neurons. The physiological and functional relevance between these dopaminergic and serotonergic neurons requires further study. Notably, studies have shown that dopamine regulates feeding preferences in adult Drosophila through specific neuropeptides (Sareen et al., 2021). Genetic and imaging data from my work confirm the role dopamine plays in regulating specific neuropeptides that influence not only feeding but also the organism's growth.

The rescue of ilps (3 and 5) levels in $STIM^{KO}$ by *THD'>STIM*$^{+}$ and the distinct developmental profiles observed under various dopamine receptor knockdowns, the change in GCaMP response in the MNSc region under *THD'>Chrimson, c929>GCaMP6f*, and the responses of *MNSc>GCaMP6m* all together firmly point out the role of dopaminergic signaling in modulating IPC function.

Furthering the partial rescue of $STIM^{KO}$ under *MNSc>dsilp3* and discerning the distinct developmental profiles between *MNSc>dsilp3* and *MNSc>ilp3*$^{+}$*,* I underscored the negative growth regulatory role of ilp3.

Additionally, the observed dynamic changes in THD' neuronal activity across the larval stage were found to be inversely correlated with ilp3 expression profiles.

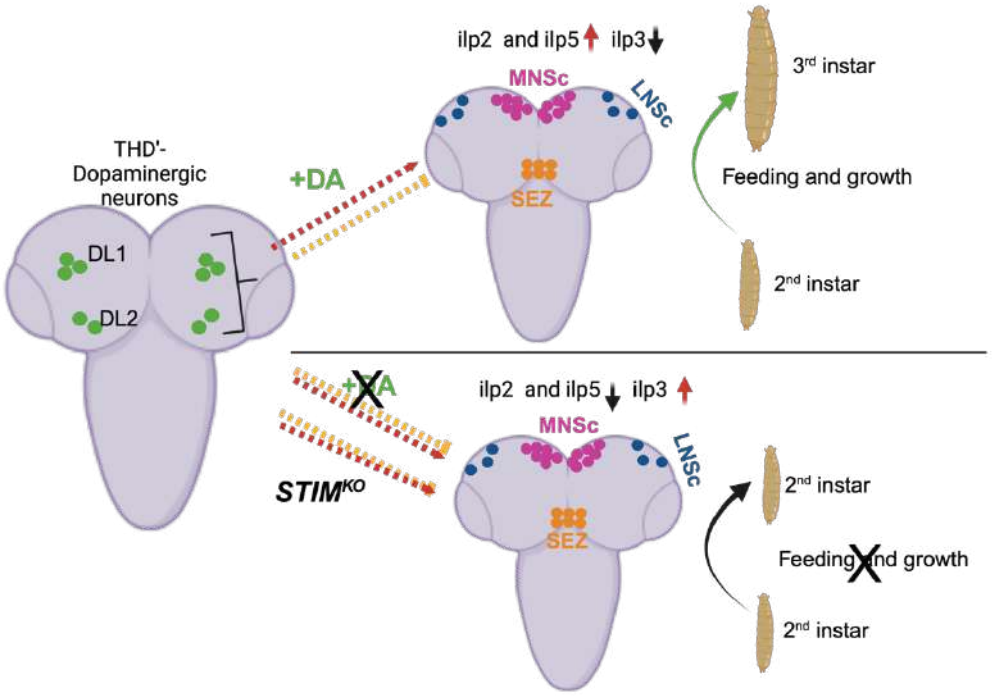

Figure 7.1: Proposed model of STIM function dependent postembryonic development in Drosophila melanogaster

The findings presented in this thesis have raised significant inquiries into the mechanisms governing the transition from the larval stage to pupariation (Fig 7.1). It is widely acknowledged that the pulse of an ecdysteroid regulates developmental timing and (Colombani et al., 2003) demonstrated that insulin signaling enhances ecdysteroid biosynthesis. The timing of ilp3 expression and the onset of the ecdysteroid pulse during the late 3rd instar stage suggest potential involvement of ilp3 in insulin signaling within the PG gland. However, the unchanged mouth hook contraction in *MNSc>ilp3*$^{+}$ larvae suggests that ilp3-dependent insulin signaling may not affect feeding but instead negatively impacts larval growth. Previous studies have shown that ecdysteroid terminates mitotic cell division, as evident in the cessation of neuroblast cell division under ecdysteroid signaling during early pupariation (Homem et al., 2014). This prompts speculation regarding the potential upregulation of ecdysteroid signaling under *MNSc>ilp3*$^{+}$. Furthermore, in conjunction with this, ilp3 expression increases as the activity of THD' neurons reduces (Chapter 4, Fig.

4.9). It is interesting to know what mechanisms are playing a role in complementing each other's functions.

In summary, this study outlines how the phenotypic characterization of the *Drosophila* STIM null mutant led to the discovery of specific subsets of dopaminergic neurons, underscoring the pivotal role of STIM function in these neurons during post-embryonic development. Additionally, this work identified a simple, straight-forward neuronal mechanism where it demonstrated that THD' dopaminergic neurons regulate larval growth by regulating feeding and concurrently influencing ilp3 and ilp5 transcription (Fig 7.1).

References:

Agrawal, N., Padmanabhan, N., & Hasan, G. (2009). Inositol 1,4,5-Trisphosphate Receptor Function in Drosophila Insulin Producing Cells. *PLoS ONE*, *4*(8), e6652.

Amin, T., & Mercer, J. G. (2016). Hunger and Satiety Mechanisms and Their Potential Exploitation in the Regulation of Food Intake. In *Current obesity reports* Vol. 5, Issue 1, pp. 106–112.

Aso, Y., Hattori, D., Yu, Y., Johnston, R. M., Iyer, N. A., Ngo, T.-T., Dionne, H., Abbott, L., Axel, R., Tanimoto, H., & Rubin, G. M. (2014). The neuronal architecture of the mushroom body provides a logic for associative learning. *Elife.*

Bader, R., Colomb, J., Pankratz, B., Schröck, A., Stocker, R. F., & Pankratz, M. J. (2007). Genetic dissection of neural circuit anatomy underlying feeding behavior in *Drosophila* : Distinct classes of *hugin* -expressing neurons. *Journal of Comparative Neurology*, *502*(5), 848–856.

Bagur, R., & Hajnóczky, G. (2017). Intracellular Ca2+ Sensing: Its Role in Calcium Homeostasis and Signaling. In *Molecular Cell* (Vol. 66, Issue 6, pp. 780–788). Cell Press.

Barnstedt, O., Owald, D., Felsenberg, J., Brain, R., Moszynski, J.-P., Talbot, C. B., Perrat, P. N., & Waddell, S. (2016). Memory-Relevant Mushroom Body Output Synapses Are Cholinergic. *Neuron*, *89*(6), 1237–1247.

Berna-Erro, A., Jardin, I., Salido, G. M., & Rosado, J. A. (2017). Role of STIM2 in cell function and physiopathology. *Journal of Physiology*, *595*(10), 3111–3128.

Berridge, M. J. (1998). Neuronal Calcium Signaling. *Neuron*, *21*(1), 13–26.

Berridge, M. J., Lipp, P., & Bootman, M. D. (2000). The versatility and universality of calcium signalling. *Nature Reviews. Molecular Cell Biology*, *1*(1), 11–21.

Birman, S. (2005). Arousal Mechanisms: Speedy Flies Don't Sleep at Night. *Current Biology*, *15*(13), R511–R513.

Bjordal, M., Arquier, N., Kniazeff, J., Pin, J. P., & Léopold, P. (2014). Sensing of Amino Acids in a Dopaminergic Circuitry Promotes Rejection of an Incomplete Diet in Drosophila. *Cell*, *156*(3), 510–521.

Boekhoudt, L., Roelofs, T. J. M., De Jong, J. W., De Leeuw, A. E., Luijendijk, M. C. M., Wolterink-Donselaar, I. G., Van Der Plasse, G., & Adan, R. A. H. (2017). Does activation of midbrain dopamine neurons promote or reduce feeding? *International Journal of Obesity*, *41*(7), 1131–1140.

Bosch, P. S., Ziukaite, R., Alexandre, C., Basler, K., & Vincent, J.-P. (2017). Dpp controls growth and patterning in Drosophila wing precursors through distinct modes of action. *ELife*, *6*.

Boulan, L., Andersen, D., Colombani, J., Boone, E., & Léopold, P. (2018). Inter-organ growth coordination is mediated by the Xrp1/Dilp8 axis in Drosophila. *BioRxiv*, 462473.

Brand, A. H., & Perrimon, N. (1993). Targeted gene expression as a means of altering cell fates and generating dominant phenotypes. *Development*, *118*(2), 401–415.

Britton, J. S., & Edgar, B. A. (1998). Environmental control of the cell cycle in *Drosophila* : nutrition activates mitotic and endoreplicative cells by distinct mechanisms. *Development*, *125*(11), 2149–2158.

Britton, J. S., Lockwood, W. K., Li, L., Cohen, S. M., & Edgar, B. A. (2002). Drosophila's insulin/PI3-kinase pathway coordinates cellular metabolism with nutritional conditions. *Developmental Cell*, *2*(2), 239–249.

Brogiolo, W., Stocker, H., Ikeya, T., Rintelen, F., Fernandez, R., & Hafen, E. (2001). An evolutionarily conserved function of the Drosophila insulin receptor and insulin-like peptides in growth control. *Current Biology*, *11*(4), 213–221.

Budnik, V., Martin-Morris, L., & White, K. (1986). Perturbed pattern of catecholamine-containing neurons in mutant Drosophila deficient in the enzyme dopa decarboxylase. *The Journal of Neuroscience*, *6*(12), 3682–3691.

Buhler, K., Clements, J., Winant, M., Bolckmans, L., Vulsteke, V., & Callaerts, P. (2018). Growth control through regulation of insulin-signaling by nutrition-activated steroid hormone in *Drosophila*. *Development*.

Cameron, N. (2022). Nutrition and growth. In *Human Growth and Development* (pp. 177–201). Elsevier.

Cao, C., & Brown, M. R. (2001). Localization of an insulin-like peptide in brains of two flies. *Cell and Tissue Research*, *304*(2), 317–321.

Carafoli, E., & Krebs, J. (2016). Why Calcium? How Calcium Became the Best Communicator. *Journal of Biological Chemistry*, *291*(40), 20849–20857.

Carlsson, M. A., Enell, L. E., & Nässel, D. R. (2013). Distribution of short neuropeptide F and its receptor in neuronal circuits related to feeding in larval Drosophila. *Cell and Tissue Research*, *353*(3), 511–523.

Cha, G.-H., Kim, S., Park, J., Lee, E., Kim, M., Lee, S. B., Kim, J. M., Chung, J., & Cho, K. S. (2005). Parkin negatively regulates JNK pathway in the dopaminergic neurons of *Drosophila*. *Proceedings of the National Academy of Sciences*, *102*(29), 10345–10350.

Chakraborty, P., Deb, B. K., Arige, V., Musthafa, T., Malik, S., Yule, D. I., Taylor, C. W., & Hasan, G. (2023). Regulation of store-operated Ca2+ entry by IP3 receptors independent of their ability to release Ca2+. *ELife*, *12*.

Chakraborty, S., Deb, B. K., Chorna, T., Konieczny, V., Taylor, C. W., & Hasan, G. (2016). Mutant IP3 receptors attenuate store-operated Ca2+ entry by

destabilizing STIM-Orai interactions in *Drosophila* neurons. *Journal of Cell Science*.

Chatterjee, N., & Perrimon, N. (2021). What fuels the fly: Energy metabolism in *Drosophila* and its application to the study of obesity and diabetes. *Science Advances*, *7*(24), 4336–4345.

Chell, J. M., & Brand, A. H. (2010). Nutrition-Responsive Glia Control Exit of Neural Stem Cells from Quiescence. *Cell*, *143*(7), 1161–1173.

Cheng, L. Y., Bailey, A. P., Leevers, S. J., Ragan, T. J., Driscoll, P. C., & Gould, A. P. (2011). Anaplastic Lymphoma Kinase Spares Organ Growth during Nutrient Restriction in Drosophila. *Cell*, *146*(3), 435–447.

Clapham, D. E. (2007). Calcium Signaling. *Cell*, Vol. 131, Issue 6, pp. 1047–1058. Elsevier B.V.

Colombani, J., Raisin, S., Pantalacci, S., Radimerski, T., Montagne, J., & Léopold, P. (2003). A Nutrient Sensor Mechanism Controls Drosophila Growth. *Cell*, *114*(6), 739–749.

De Moed, G. H., Kruitwagen, C. L. J. J., De Jong, G., & Scharloo, W. (1999). Critical weight for the induction of pupariation in *Drosophila melanogaster*: genetic and environmental variation. *Journal of Evolutionary Biology*, *12*(5), 852–858.

Delanoue, R., & Romero, N. M. (2020). Growth and Maturation in Development: A Fly's Perspective. *International Journal of Molecular Sciences*, *21*(4), 1260.

Delanoue, R., Slaidina, M., & Léopold, P. (2010). The Steroid Hormone Ecdysone Controls Systemic Growth by Repressing dMyc Function in Drosophila Fat Cells. *Developmental Cell*, *18*(6), 1012–1021.

Dhanya, S. K., & Hasan, G. (2021). Purkinje Neurons with Loss of STIM1 Exhibit Age-Dependent Changes in Gene Expression and Synaptic Components. *The Journal of Neuroscience*, *41*(17), 3777–3798.

Edgar, B. A., & Orr-Weaver, T. L. (2001). Endoreplication Cell Cycles. *Cell*, *105*(3), 297–306.

Eichler, K., Li, F., Litwin-Kumar, A., Park, Y., Andrade, I., Schneider-Mizell, et al. (2017). The complete connectome of a learning and memory centre in an insect brain. *Nature*, *548*(7666), 175–182.

Emrich, S. M., Yoast, R. E., & Trebak, M. (2022). Physiological Functions of CRAC Channels. *Annual Review of Physiology*, *84*(1), 355–379.

Erion, R., & Sehgal, A. (2013). Regulation of insect behavior via the insulin-signaling pathway. *Frontiers in Physiology*, *4*(December), 1–6.

Eschbach, C., Fushiki, A., Winding, M., Schneider-Mizell, C. M., Shao, M., Arruda, R., et al. (2020). Recurrent architecture for adaptive regulation of learning in the insect brain. *Nature Neuroscience*, *23*(4), 544–555.

Fahrner, M., Schindl, R., & Romanin, C. (2017). Studies of Structure–Function and Subunit Composition of Orai/STIM Channel. In *Calcium Entry Channels in Non-Excitable Cells* (pp. 25–50). CRC Press.

Falk, S., Lund, C., & Clemmensen, C. (2020). Muscarinic receptors in energy homeostasis: Physiology and pharmacology. *Basic & Clinical Pharmacology & Toxicology*, *126*(S6), 66–76.

Fenno, L., Yizhar, O., & Deisseroth, K. (2011). The Development and Application of Optogenetics. *Annual Review of Neuroscience*, *34*(1), 389–412.

Fingar, D. C., Salama, S., Tsou, C., Harlow, E., & Blenis, J. (2002). Mammalian cell size is controlled by mTOR and its downstream targets S6K1 and 4EBP1/eIF4E. *Genes & Development*, *16*(12), 1472–1487.

Fox, D. T., & Duronio, R. J. (2013). Endoreplication and polyploidy: insights into development and disease. *Development*, *140*(1), 3–12.

Friggi-Grelin, F., Coulom, H., Meller, M., Gomez, D., Hirsh, J., & Birman, S. (2003). Targeted gene expression in Drosophila dopaminergic cells using

regulatory sequences from tyrosine hydroxylase. *Journal of Neurobiology*, *54*(4), 618–627.

Géminard, C., Rulifson, E. J., & Léopold, P. (2009). Remote Control of Insulin Secretion by Fat Cells in Drosophila. *Cell Metabolism*, *10*(3), 199–207.

Gilbert SF. (2000). *Developmental Biology. 6th edition.* (Vol. 6).

Gopurappilly, R., Deb, B. K., Chakraborty, P., & Hasan, G. (2018). Stable STIM1 knockdown in self-renewing human neural precursors promotes premature neural differentiation. *Frontiers in Molecular Neuroscience*, *11*(June), 1–19.

Guertin, D. A., & Sabatini, D. M. (2008). Cell Growth. In *The Molecular Basis of Cancer* (pp. 169–175). Elsevier.

Gwack, Y., Srikanth, S., Oh-hora, M., Hogan, P. G., Lamperti, E. D., Yamashita, et al. (2008). Hair Loss and Defective T- and B-Cell Function in Mice Lacking ORAI1. *Molecular and Cellular Biology*, *28*(17), 5209–5222.

Hartenstein, V., Cruz, L., Lovick, J. K., & Guo, M. (2017). Developmental analysis of the dopamine-containing neurons of the Drosophila brain. *Journal of Comparative Neurology*, *525*(2), 363–379.

Hietakangas, V., & Cohen, S. M. (2009). Regulation of Tissue Growth through Nutrient Sensing. *Annual Review of Genetics*, *43*(1), 389–410.

Hogan, P. G., Hogan, P. G., Chen, L., & Chen, L. (2003). Transcriptional regulation by calcium, calcineurin and NFAT. *Genes Dev.*, *17*(18), 2205–2232.

Homem, C. C. F., & Knoblich, J. A. (2012). *Drosophila* neuroblasts: a model for stem cell biology. *Development*, *139*(23), 4297–4310.

Homem, C. C. F., Steinmann, V., Burkard, T. R., Jais, A., Esterbauer, H., & Knoblich, J. A. (2014). Ecdysone and Mediator Change Energy Metabolism to Terminate Proliferation in Drosophila Neural Stem Cells. *Cell*, *158*(4), 874–888.

Hoth, M., & Penner, R. (1992). Depletion of intracellular calcium stores activates a calcium current in mast cells. *Nature*, *355*(6358), 353–356.

Hu, Y., Comjean, A., Perrimon, N., & Mohr, S. E. (2017). The Drosophila Gene Expression Tool (DGET) for expression analyses. *BMC Bioinformatics*, *18*(1).

Hückesfeld, S., Peters, M., & Pankratz, M. J. (2016). Central relay of bitter taste to the protocerebrum by peptidergic interneurons in the Drosophila brain. *Nature Communications*, *7*(1), 12796.

Ikeya, T., Galic, M., Belawat, P., Nairz, K., & Hafen, E. (2002). Nutrient-Dependent Expression of Insulin-like Peptides from Neuroendocrine Cells in the CNS Contributes to Growth Regulation in Drosophila. *Current Biology*, *12*(15), 1293–1300.

Inzaghi, E., Pampanini, V., Deodati, A., & Cianfarani, S. (2022). The Effects of Nutrition on Linear Growth. *Nutrients*, *14*(9), 1752.

Jacobs, H. T., George, J., & Kemppainen, E. (2020). Regulation of growth in Drosophila melanogaster: the roles of mitochondrial metabolism. *The Journal of Biochemistry*, *167*(3), 267–277.

Jayakumar, S., Richhariya, S., Reddy, O. V., Texada, M. J., & Hasan, G. (2016a). Drosophila larval to pupal switch under nutrient stress requires IP3R/Ca2+ signalling in glutamatergic interneurons. *ELife*, *5*.

Joshi, R., Venkatesh, K., Srinivas, R., Nair, S., & Hasan, G. (2004). Genetic Dissection of *itpr* Gene Function Reveals a Vital Requirement in Aminergic Cells of Drosophila Larvae. *Genetics*, *166*(1), 225–236.

Karam, C. S., Jones, S. K., & Javitch, J. A. (2020). Come Fly with Me: An overview of dopamine receptors in *Drosophila melanogaster*. *Basic & Clinical Pharmacology & Toxicology*, *126*(S6), 56–65.

Kasturacharya, N., Dhall, J. K., & Hasan, G. (2023). A STIM dependent dopamine-neuropeptide axis maintains the larval drive to feed and grow in Drosophila. *PLOS Genetics*, *19*(6), e1010435.

Kim, J., & Neufeld, T. P. (2015). Dietary sugar promotes systemic TOR activation in Drosophila through AKH-dependent selective secretion of Dilp3. *Nature Communications*, *6*(1), 6846.

Klapoetke, N. C., Murata, Y., Kim, S. S., Pulver, S. R., Birdsey-Benson, A., Cho, Y. et al. (2014). Independent optical excitation of distinct neural populations. *Nature Methods*, *11*(3), 338–346.

Kleinridders, A., & Pothos, E. N. (2019). Impact of Brain Insulin Signaling on Dopamine Function, Food Intake, Reward, and Emotional Behavior. *Current Nutrition Reports*, *8*(2), 83–91.

Koyama, T., Texada, M. J., Halberg, K. A., & Rewitz, K. (2020). Metabolism and growth adaptation to environmental conditions in Drosophila. *Cellular and Molecular Life Sciences*, *77*(22), 4523–4551.

Landayan, D., Feldman, D. S., & Wolf, F. W. (2018). Satiation state-dependent dopaminergic control of foraging in Drosophila. *Scientific Reports*, *8*(1), 5777.

Lee, K. S., You, K. H., Choo, J. K., Han, Y. M., & Yu, K. (2004). Drosophila short neuropeptide F regulates food intake and body size. *Journal of Biological Chemistry*, *279*(49), 50781–50789.

Lewis, R. S. (2001). Calcium Signaling Mechanisms in T Lymphocytes. *Annual Review of Immunology*, *19*(1), 497–521.

Lin, S., Senapati, B., & Tsao, C.-H. (2019). Neural basis of hunger-driven behaviour in *Drosophila*. *Open Biology*, *9*(3).

Liou, J., Fivaz, M., Inoue, T., & Meyer, T. (2007). Live-cell imaging reveals sequential oligomerization and local plasma membrane targeting of stromal interaction molecule 1 after Ca^{2+} store depletion. Proc Natl Acad Sci U S A 2007 May 29;104(22):9301-6.

Low, A. Y. T., Goldstein, N., Gaunt, J. R., Huang, K.-P., Zainolabidin, N., Yip, A. K. K., et al. (2021). Reverse-translational identification of a cerebellar satiation network. *Nature*, *600*(7888), 269–273.

Luo, D., Broad, L. M., Bird, G. S. J., & Putney, J. W. (2001). Signaling Pathways Underlying Muscarinic Receptor-induced $[Ca^{2+}]_i$ Oscillations in HEK293 Cells. *Journal of Biological Chemistry*, *276*(8), 5613–5621.

Mancarella, S., Potireddy, S., Wang, Y., Gao, H., Gandhirajan, R. K., Autieri, M., et al . (2013). Targeted STIM deletion impairs calcium homeostasis, NFAT activation, and growth of smooth muscle. *FASEB Journal*, *27*(3), 893–906.

Maus, M., Cuk, M., Patel, B., Lian, J., Ouimet, M., Kaufmann, U., et al. (2017a). Store-Operated Ca2+ Entry Controls Induction of Lipolysis and the Transcriptional Reprogramming to Lipid Metabolism. *Cell Metabolism*, *25*(3), 698–712.

May, C. M., Doroszuk, A., & Zwaan, B. J. (2015). The effect of developmental nutrition on life span and fecundity depends on the adult reproductive environment in Drosophila melanogaster. *Ecology and Evolution*, *5*(6), 1156–1168.

Miroschnikow, A., Schlegel, P., & Pankratz, M. J. (2020). Making Feeding Decisions in the Drosophila Nervous System. In *Current Biology* (Vol. 30, Issue 14, pp. R831–R840). Cell Press.

Missale, C., Nash, S. R., Robinson, S. W., Jaber, M., & Caron, M. G. (1998). Dopamine Receptors: From Structure to Function. In *Physiological Reviews* (Vol. 78, Issue 1).

Nakamura, K., & Nakamura, Y. (2018). Hunger and Satiety Signaling: Modeling Two Hypothalamomedullary Pathways for Energy Homeostasis. *BioEssays*, *40*(8).

Nässel, D. R., & Broeck, J. Vanden. (2016). Insulin/IGF signaling in Drosophila and other insects: factors that regulate production, release and post-release action of the insulin-like peptides. *Cellular and Molecular Life Sciences*, *73*(2), 271–290.

Nässel, D. R., & Zandawala, M. (2019). Recent advances in neuropeptide signaling in Drosophila, from genes to physiology and behavior. In *Progress in Neurobiology* (Vol. 179). Elsevier Ltd.

Nässel, D. R., & Zandawala, M. (2020). Hormonal axes in Drosophila: regulation of hormone release and multiplicity of actions. In *Cell and Tissue Research* (Vol. 382, Issue 2). Cell and Tissue Research.

Newton, A. C., Bootman, M. D., & Scott, J. D. (2016). Second Messengers. *Cold Spring Harbor Perspectives in Biology*, *8*(8), a005926.

Nitabach, M. N., Blau, J., & Holmes, T. C. (2002). Electrical Silencing of Drosophila Pacemaker Neurons Stops the Free-Running Circadian Clock An important area of circadian rhythm research is the relationship between the function of the molecular clock in pacemaker neurons and the central physiological. *Cell*, *109*, 485–495.

Nitabach, M. N., Wu, Y., Sheeba, V., Lemon, W. C., Strumbos, J., Zelensky, et al. (2006). Electrical hyperexcitation of lateral ventral pacemaker neurons desynchronizes downstream circadian oscillators in the fly circadian circuit and induces multiple behavioral periods. *Journal of Neuroscience*, *26*(2), 479–489.

Oh-hora, M., Yamashita, M., Hogan, P. G., Sharma, S., Lamperti, E., Chung, W., Prakriya, M., Feske, S., & Rao, A. (2008). Dual functions for the endoplasmic reticulum calcium sensors STIM1 and STIM2 in T cell activation and tolerance. *Nature Immunology*, *9*(4), 432–443.

Okamoto, N., & Nishimura, T. (2015). Signaling from Glia and Cholinergic Neurons Controls Nutrient-Dependent Production of an Insulin-like Peptide for Drosophila Body Growth. *Developmental Cell*, *35*(3), 295–310.

Okamoto, N., Yamanaka, N., Yagi, Y., Nishida, Y., Kataoka, H., O'Connor, M. B., & Mizoguchi, A. (2009). A Fat Body-Derived IGF-like Peptide Regulates Postfeeding Growth in Drosophila. *Developmental Cell*, *17*(6), 885–891.

Oliva, M. K., Pérez-Moreno, J. J., O'Shaughnessy, J., Wardill, T. J., & O'Kane, C. J. (2020). Endoplasmic Reticulum Lumenal Indicators in Drosophila Reveal Effects of HSP-Related Mutations on Endoplasmic Reticulum Calcium Dynamics. *Frontiers in Neuroscience*, *14*(August), 1–10.

Park, D., Veenstra, J. A., Park, J. H., & Taghert, P. H. (2008). Mapping peptidergic cells in Drosophila: Where DIMM fits in. *PLoS ONE*, *3*(3).

Pathak, T., Trivedi, D., & Hasan, G. (2017). CRISPR-Cas-Induced Mutants Identify a Requirement for dSTIM in Larval Dopaminergic Cells of *Drosophila melanogaster*. *G3 Genes|Genomes|Genetics*, *7*(3), 923–933.

Paudel, S., Sindelar, R., & Saha, M. (2018). Calcium signaling in vertebrate development and its role in disease. In *International Journal of Molecular Sciences* (Vol. 19, Issue 11). MDPI AG.

Pauls, D., Selcho, M., Gendre, N., Stocker, R. F., & Thum, A. S. (2010). *Drosophila* Larvae Establish Appetitive Olfactory Memories via Mushroom Body Neurons of Embryonic Origin. *The Journal of Neuroscience*, *30*(32), 10655–10666.

Peper, J. S., & Dahl, R. E. (2015). Diseases caused by mutations in ORAI1 and STIM1. *Annals of the New York Academy of Sciences*, *22*(2), 134–139.

Pool, A.-H., & Scott, K. (2014). Feeding regulation in Drosophila. *Current Opinion in Neurobiology*, *29*, 57–63.

Prakriya, M., & Lewis, R. S. (2015). Store-Operated Calcium Channels. *Physiological Reviews*, *95*(4), 1383–1436.

Pu, Y., Zhang, Y., Zhang, Y., & Shen, P. (2018). Two Drosophila Neuropeptide Y-like Neurons Define a Reward Module for Transforming Appetitive Odor Representations to Motivation. *Scientific Reports*, *8*(1), 11658.

Putney, J. W., Steinckwich-Besançon, N., Numaga-Tomita, T., Davis, F. M., Desai, P. N., D'Agostin, D. M., Wu, S., & Bird, G. S. (2017). The functions of store-operated calcium channels. *Biochimica et Biophysica Acta (BBA) - Molecular Cell Research*, *1864*(6), 900–906.

Richhariya, S., Jayakumar, S., Abruzzi, K., Rosbash, M., & Hasan, G. (2017). A pupal transcriptomic screen identifies Ral as a target of store-operated calcium entry in Drosophila neurons. *Scientific Reports*, *7*(February), 1–12.

Robert B. Church, F. W. R. (1966). Church RB, Robertson FW. A biochemical study of the growth of Drosophila melanogaster. J. Exp. Zool. 1966;162:337–351. *Wiley Online*, *162*(3), 337–351.

Rosenberg, S. S., & Spitzer, N. C. (2011). Calcium Signaling in Neuronal Development. *Cold Spring Harbor Perspectives in Biology*, *3*(10), a004259–a004259.

Rulifson, E. J., Kim, S. K., & Nusse, R. (2002). Ablation of Insulin-Producing Neurons in Flies: Growth and Diabetic Phenotypes. *Science*, *296*(5570), 1118–1120.

Sabbioni, S., Barbanti-Brodano, G., Croce, C. M., & Negrini, M. (1997). GOK: a gene at 11p15 involved in rhabdomyosarcoma and rhabdoid tumor development. *Cancer Research*, *57*(20), 4493–4497.

Sareen, P. F., McCurdy, L. Y., & Nitabach, M. N. (2021). A neuronal ensemble encoding adaptive choice during sensory conflict in Drosophila. *Nature Communications*, *12*(1), 4131.

Saumweber, T., Rohwedder, A., Schleyer, M., Eichler, K., Chen, Y. C., Aso, Y., et al. (2018). Functional architecture of reward learning in mushroom body extrinsic neurons of larval Drosophila. *Nature Communications*, *9*(1).

Schoofs, A., Hückesfeld, S., & Pankratz, M. J. (2018). Serotonergic network in the subesophageal zone modulates the motor pattern for food intake in Drosophila. *Journal of Insect Physiology*, *106* (March 2017), 36–46.

Schoofs, A., Hückesfeld, S., Schlegel, P., Miroschnikow, A., Peters, M., Zeymer, M., Spieß, R., Chiang, A.-S., & Pankratz, M. J. (2014). Selection of Motor Programs for Suppressing Food Intake and Inducing Locomotion in the Drosophila Brain. *PLoS Biology*, *12*(6), e1001893.

Schoofs, A., Hückesfeld, S., Surendran, S., & Pankratz, M. J. (2014). Serotonergic pathways in the Drosophila larval enteric nervous system. *Journal of Insect Physiology*, *69*(C), 118–125.

Selcho, M., Pauls, D., Han, K.-A., Stocker, R. F., & Thum, A. S. (2009). The Role of Dopamine in Drosophila Larval Classical Olfactory Conditioning. *PLoS ONE*, *4*(6), e5897.

Semaniuk, U., Piskovatska, V., Strilbytska, O., Strutynska, T., Burdyliuk, N., Vaiserman, A., Bubalo, V., Storey, K. B., & Lushchak, O. (2021). *Drosophila* insulin-like peptides: from expression to functions – a review. *Entomologia Experimentalis et Applicata*, *169*(2), 195–208.

Sharma, A., & Hasan, G. (2020). Modulation of flight and feeding behaviours requires presynaptic IP3Rs in dopaminergic neurons. *ELife*, *9*, 1–25.

Shim, J., Gururaja-Rao, S., & Banerjee, U. (2013). Nutritional regulation of stem and progenitor cells in Drosophila. *Development*, *140*(23), 4647–4656.

Silva-Rojas, R., Laporte, J., & Böhm, J. (2020). STIM1/ORAI1 Loss-of-Function and Gain-of-Function Mutations Inversely Impact on SOCE and Calcium Homeostasis and Cause Multi-Systemic Mirror Diseases. *Frontiers in Physiology*, *11*(November).

Sitaraman, D., Zars, M., LaFerriere, H., Chen, Y.-C., Sable-Smith, A., Kitamoto, T., Rottinghaus, G. E., & Zars, T. (2008). Serotonin is necessary for place memory in *Drosophila*. *Proceedings of the National Academy of Sciences*, *105*(14), 5579–5584.

Somasundaram, A., Shum, A. K., McBride, H. J., Kessler, J. A., Feske, S., Miller, R. J., & Prakriya, M. (2014). Store-Operated CRAC Channels Regulate Gene Expression and Proliferation in Neural Progenitor Cells. *Journal of Neuroscience*, *34*(27), 9107–9123.

Sousa-Nunes, R., Cheng, L. Y., & Gould, A. P. (2010). Regulating neural proliferation in the Drosophila CNS. *Current Opinion in Neurobiology*, *20*(1), 50–57.

Sousa-Nunes, R., Yee, L. L., & Gould, A. P. (2011). Fat cells reactivate quiescent neuroblasts via TOR and glial insulin relays in Drosophila. *Nature*, *471*(7339), 508–512.

Steinhart, Z., & Angers, S. (2018). Wnt signaling in development and tissue homeostasis. *Development*, *145*(11).

Sun, F., Zeng, J., Jing, M., Zhou, J., Feng, J., Owen, S. F., Luo, Y., et al. (2018). A Genetically Encoded Fluorescent Sensor Enables Rapid and Specific Detection of Dopamine in Flies, Fish, and Mice. *Cell*, *174*(2), 481-496.e19.

Szczypka, M. S., Rainey, M. A., Kim, D. S., Alaynick, W. A., Marck, B. T., Matsumoto, A. M., & Palmiter, R. D. (1999). Feeding behavior in dopamine-deficient mice. *Proceedings of the National Academy of Sciences*, *96*(21), 12138–12143.

Talay, M., Richman, E. B., Snell, N. J., Hartmann, G. G., Fisher, J. D., Sorkaç, A., Santoyo, J. F., Chou-Freed, C., Nair, N., Johnson, M., Szymanski, J. R., & Barnea, G. (2017). Transsynaptic Mapping of Second-Order Taste Neurons in Flies by trans-Tango. *Neuron*, *96*(4), 783-795.e4.

Tennessen, J. M., & Thummel, C. S. (2011). Coordinating growth and maturation - Insights from drosophila. *Current Biology*, *21*(18), R750–R757.

Toth, A. B., Shum, A. K., & Prakriya, M. (2016). Regulation of neurogenesis by calcium signaling. *Cell Calcium*, *59*(2–3), 124–134.

Tsao, C.-H., Chen, C.-C., Lin, C.-H., Yang, H.-Y., & Lin, S. (2018). Drosophila mushroom bodies integrate hunger and satiety signals to control innate food-seeking behavior. *ELife*, *7*, 1–35.

Tyson, J. J., Monshizadeh, A., Shvartsman, S. Y., & Shingleton, A. W. (2023). A dynamical model of growth and maturation in *Drosophila*. *Proceedings of the National Academy of Sciences*, *120*(49).

Venkiteswaran, G., & Hasan, G. (2009). Intracellular Ca2+ signaling and store-operated Ca2+ entry are required in Drosophila neurons for flight. *Proceedings of the National Academy of Sciences of the USA*, *106*(25), 10326–10331.

Volkow, N. D., Wang, G. J., & Baler, R. D. (2011). Reward, dopamine and the control of food intake: Implications for obesity. *Trends in Cognitive Sciences*, *15*(1), 37–46.

Wang, G.-J., Geliebter, A., Volkow, N. D., Telang, F. W., Logan, J., Jayne, M. C., et al. (2011). Enhanced striatal dopamine release during food stimulation in binge eating disorder. *Obesity (Silver Spring, Md.)*, *19*(8), 1601–1608.

Wang, Y., Pu, Y., & Shen, P. (2013). Neuropeptide-Gated Perception of Appetitive Olfactory Inputs in Drosophila Larvae. *Cell Reports*, *3*(3), 820–830.

Wiencke, K., Horstmann, A., Mathar, D., Villringer, A., & Neumann, J. (2020). Dopamine release, diffusion and uptake: A computational model for synaptic and volume transmission. *PLoS Computational Biology*, *16*(11).

Wilinski, D., Winzeler, J., Duren, W., Persons, J. L., Holme, K. J., Mosquera, J., et al. (2019). Rapid metabolic shifts occur during the transition between hunger and satiety in Drosophila melanogaster. *Nature Communications*, *10*(1), 4052.

Winding, M., Pedigo, B. D., Barnes, C. L., Patsolic, H. G., Park, Y., Kazimiers, T., et al. (2023). The connectome of an insect brain. *Science*, *379*(6636).

Wise, R. A. (2006). Role of brain dopamine in food reward and reinforcement. *Philosophical Transactions of the Royal Society B: Biological Sciences*, *361*(1471), 1149–1158.

Wu, Q., Wen, T., Lee, G., Park, J. H., Cai, H. N., & Shen, P. (2003). Developmental Control of Foraging and Social Behavior by the Drosophila Neuropeptide Y-like System. *Neuron*, *39*(1), 147–161.

Xie, T., Ho, M. C. W., Liu, Q., Horiuchi, W., Lin, C. C., Task, D., Luan, H., White, B. H., Potter, C. J., & Wu, M. N. (2018). A Genetic Toolkit for Dissecting Dopamine Circuit Function in Drosophila. *Cell Reports*, *23*(2), 652–665.

Xu, Y., Borcherding, A. F., Heier, C., Tian, G., Roeder, T., & Kühnlein, R. P. (2019). Chronic dysfunction of Stromal interaction molecule by pulsed RNAi induction in fat tissue impairs organismal energy homeostasis in Drosophila. *Scientific Reports*, *9*(1), 1–15.

Yamamoto, S., & Seto, E. S. (2014). Dopamine Dynamics and Signaling in Drosophila: An Overview of Genes, Drugs and Behavioral Paradigms. *Experimental Animals*, *63*(2), 107–119.

Zhang, I., & Hu, H. (2020). Store-Operated Calcium Channels in Physiological and Pathological States of the Nervous System. *Frontiers in Cellular Neuroscience*, *14*.

Zhang, S. L., Yu, Y., Roos, J., Kozak, J. A., Deerinck, T. J., Ellisman, M. H., Stauderman, K. A., & Cahalan, M. D. (2005). STIM1 is a Ca2+ sensor that activates CRAC channels and migrates from the Ca2+ store to the plasma membrane. *Nature*, *437*(7060), 902–905.

Zhang, T., Branch, A., & Shen, P. (2013). Octopamine-mediated circuit mechanism underlying controlled appetite for palatable food in *Drosophila*. *Proceedings of the National Academy of Sciences*, *110*(38), 15431–15436.

Zhang, W., & Liu, H. T. (2002). MAPK signal pathways in the regulation of cell proliferation in mammalian cells. *Cell Research*, *12*(1), 9–18.

Zhao, X. L., & Campos, A. R. (2012). Insulin signalling in mushroom body neurons regulates feeding behaviour in *Drosophila* larvae. *Journal of Experimental Biology*, *215*(15), 2696–2702.

Zielke, N., Edgar, B. A., & DePamphilis, M. L. (2013). Endoreplication. In *Cold Spring Harbor Perspectives in Biology* (Vol. 5, Issue 1).

Zielke, N., Korzelius, J., Straaten, M. Van, Bender, K., Schuhknecht, G. F. P., Dutta, D., Xiang, J., & Edgar, B. A. (2014). Resource Fly-FUCCI : A Versatile Tool for Studying Cell Proliferation in Complex Tissues. *Cell Reports*, *7*(2), 588–598.

.